Ignition, Charring and Structural Performance of Laminated Veneer Lumber

By

Warren Peter Lane

Supervised by

Professor Andrew H. Buchanan
&
Associate Professor Peter J Moss

Fire Engineering Research Report 05/3
October 2005

A project submitted in partial fulfilment of the requirements for the degree of Master of Engineering in Fire Engineering

Department of Civil Engineering
University of Canterbury
Private Bag 4800
Christchurch, New Zealand

Abstract

This report describes the results of an investigation into the fire performance of laminated veneer lumber (LVL), considering both the early fire hazard and the structural fire performance as well as to develop design methods for the structural performance of LVL beams and columns exposed to post flashover fires.

To determine ignition properties cone calorimeter tests were undertaken at heat fluxes varying from 10 to 50 kW/m^2, the time to ignition was recorded for each heat flux and for the orientation of the grain being exposed.

To determine charring rates cone calorimeter tests were carried out on blocks of LVL with a number of grain orientations, each for a range of heat flux exposures. Instrumented samples incorporating embedded thermocouples were used to locate the char front within the sample. Char rates found from the instrumented tests were confirmed on subsequent tests of un-instrumented samples that were subjected to the same heat fluxes but for selected exposure times.

Charring experiments were also carried out on three LVL beams, approximately 100 x 300 mm in cross section and 2 m long, tested in a pilot scale furnace following the ISO 834 standard fire curve. Embedded thermocouples were used to record layer temperatures, which were then used to calculate the residual cross section for prediction of structural behaviour in fire conditions.

A load-bearing fire resistance test was carried out on a larger LVL beam spanning 4 m in a full size furnace, following the ISO 834 standard fire curve.

The report concludes by including design recommendations for a simple method for predicting the fire performance of radiata pine LVL exposed to post-flashover fires.

Acknowledgements

First I would like to thank my supervisors, Professor Andy Buchanan and Associate Professor Peter Moss for their enthusiasm for the topic, encouragement, ideas and guidance. Thank you to all of the ME fire lecturing staff that supplied challenging lectures and topics for discussion during 2002.

To the technical staff of the Civil Engineering faculty at Canterbury University who provided support and guidance for use of equipment, special thanks to Grant Dunlop for providing technical support on the operation of the Cone Calorimeter and construction of a specific sample holder.

Thanks to Peter Collier from BRANZ and the fire laboratory staff at BRANZ who assisted greatly in the set up and operation of the Pilot Furnace Tests and the load test in the Full Scale Furnace on the LVL beams.

To the fire engineering class of 2002, who were a compatible group, worked well together, shared information, supported each other and were interested in each others progress and experiences at university and in life in general.

Finally, thank you to Sonja whose love and support was and still is much needed, to my children who sacrificed time with their Dad and to my parents for their interest and the many values that they have installed into my life.

Table of Contents Page

List of Figures

List of Tables

Chapter 1: Introduction

Fire is one of the most unpredictable and dangerous accidents that may occur in our environment, especially in residential buildings. The excellent fire endurance of buildings constructed with heavy timber for columns, beams, floors and joists has long been recognized and proven. A slow rate of charring and a slow loss of strength of wood under fire exposure allow large members to perform their intended function despite the intense heat and fire. However, designing wood members for a specific degree of fire endurance has been quite empirical. To remain competitive with other construction materials more precise data should be obtained upon which to design and predict fire endurance of wood assemblies.

Fires development, behaviour and effects are very complex. In order for a fire to occur, flammable materials need to be ignited. Ignitability is defined in ISO 3261 as the capability of a material to be ignited. Ignition is one of the essential fire properties, which must or always be considered in any assessment of fire hazard.

Ignition depends on various interrelated factors. As the surface is exposed to heat flux, initially most of the heat is transferred into the interior of the specimen. The rate of this heat transfer is dependent on the thermal properties of the material including ignition temperature, T_{ig}; ambient temperature, T_{amb}; material thermal conductivity, k; material specific heat, c; and the density of the material, ρ. The ignition of wood is more complex than other materials, especially when a layer of char is formed. It also depends on the species, moisture content, inherent variability of wood as a natural material, the orientation of the specimen when exposed to the incident heat flux and the grain orientation (along or across the grain).

Once the surface temperature of the wood is above 350 – 360 ^{o}C, ignition usually occurs in the presence of a small pilot flame or spark, and then the char layer begins to form. After ignition the rate of heat release is high because volatiles diffuse easily through the surface layer. Later the growing char layer acts as an insulator for the un-charred wood beneath, resulting in a lower heat exposure for the un-charred wood than previously. Consequently the rate of heat release decreases from its maximum and after some time

reaches a constant value when the thickness of the char layer remains practically constant. The boundary between the char layer and the un-burnt wood is quite distinct, corresponding to a temperature of 300 ^{o}C. The commonly accepted charring temperature in North America is 288 ^{o}C, and Mikkola (1990) defines the char front in his research as 360 ^{o}C, because there is still some strength left in the wood until this temperature is reached. However the precise temperature is not important due to the steepness of the temperature gradient.

1.1 Objectives

The objective of this project is to:

- Determine ignition properties of Laminated Veneered Lumber (LVL), manufactured from New Zealand Radiata pine using simple thermal models.
- Determine representative char rates for Laminated Veneered Lumber (LVL) to be used in design models.
- And the recommendation of a simple method for predicting the fire performance of radiata pine LVL exposed to post-flashover fires.

1.2 Methodology

1.2.1 Ignition Properties

Two simple thermal correlations developed by various researchers will be used and compared to find out the best way to predict the ignition time. This project will also determine another important ignition property of a material known as the minimum heat flux, $\dot{q}''_{min}$, which is the lowest incident heat flux that can ignite LVL . (i.e. Ignition of LVL will not occur, lower than the minimum flux, $\dot{q}''_{min.}$)

The methodology of the ignition tests used in this project is based on the British Standard BS 476: Part 13 (1987); also called the ISO Ignitability Test. The LVL samples are exposed to 8 levels of constant irradiances, 5 levels from 10 – 30 kW/m^2, will be perform specifically on 50 mm samples for ignition testing solely and the remaining 3 levels 35, 50 & 65 kW/m^2 results obtained whilst testing thicker (85 mm) instrumented LVL samples to obtain char depths/temperature gradients at specific depths. The

experimental method and equipment used with respect to BS 476: Part 13 is discussed in detail in Chapter 2.

The duration of the ignition test influences the determination of the minimum heat flux. According to BS 476: Part 13, each test should be terminated if no sustained surface ignition occurs within 15 minutes. However, in this research the specimens were given a period of 20 minutes to be ignited. A specimen is ignited if it has a continuous flame at its surface for an uninterrupted period of at least 10 seconds. For the ignitions recorded during the char test at higher the heat fluxes, all times to ignition occurred in a time less than 1-2 minutes.

1.2.2 Cone Calorimeter Char Rate

Char depths were determined in instrumented tests, where thermocouples located the 300^{o}C isotherm, which depicts the char front within the samples, at constant irradiances or heat fluxes of 35, 50 & 65 kW/m^2. The results from the instrumented tests were then compared to un-instrumented tests performed on similar sized samples. The un-instrumented samples were exposed to the same corresponding heat fluxes for specific time periods, then removed from the constant irradiance, extinguished immediately and the char removed so that the un-charred LVL residual thickness measured to determine the char depth.

1.2.3 Pilot Furnace Char Rate

Char rates determined from the instrumented and un-instrumented char tests were then compared to three instrumented tests that also obtained char rates in larger LVL sections, exposed to the standard ISO 834 design fire in the Pilot Furnace at the BRANZ research facility at Porirua in New Zealand. The aim from these tests and comparisons is to determine an appropriate char rate to be used in the recommended design method for the structural performance of LVL beams and columns exposed to post flashover fires

1.2.4 Load Test – Full Scale Furnace

Finally the char rate determined for the recommended design method for LVL was to be put to the test in the full size furnace where a loaded beam was exposed to the ISO 834 design fire and the time to failure and the corresponding deflections of the beam measured.

1.3 Outline of Project Report

The scope of this project report covered the following:

1.3.1 Chapter 2: Description of Testing Equipment

Chapter two describes the testing equipment used for the testing undertaken for this research project, the conditions the equipment was used under and the specific setup required for testing.

1.3.2 Chapter 3: Literature review

Chapter three reviews publications that are applicable to this project. Papers and publications include topics discussing the thermal and ignition properties of wood and the charring of wood and wood products. Review of information on the fire and mechanical properties of the parent timbers used in the manufacture of LVL. Review of tests and relevant literature on fire testing of natural solid timber, glulam beams and columns and drawing any comparisons or expectations for the fire testing proposed for LVL in this project.

1.3.3 Chapter 4: Ignition Properties

Chapter four describes the ignition tests carried out at five different levels of heat flux and two main grain orientations, with three replications of each test. The ignition tests utilised the Cone Calorimeter to obtain the LVL ignition data. This included a series of tests at reducing heat fluxes for a minimum duration of 30 minutes, or until ignition, to determine the critical heat flux. Times were taken to ignition, glowing and flaming or flaming directly.

1.3.4 Chapter 5: Cone Calorimeter Char Tests

Chapter five describes the series of instrumented and un-instrumented char tests performed using the Cone Calorimeter to obtain char rates at various heat fluxes for several durations.

Initially a series of instrumented tests were undertaken for the maximum duration of 90 minutes at heat fluxes of 35, 50 and 65 kW's to be able to detect the char front by the measurement of the temperature gradient through the sample. Previous testing and

literature studies have indicated that the char front occurs at 300 ^{O}C in solid natural wood. These tests were performed in both the principal directions. (i.e. normal to the veneers and in plane to the veneers)

Once these test were completed then un-instrumented char tests were performed on similar sized specimens to confirm the instrumented char depth results. The un-instrumented tests were undertaken at target heat fluxes and fixed durations to confirm the char depth predictions obtained from the instrumented test results.

1.3.5 Chapter 6: Pilot Furnace Char Tests

Chapter six describes and discusses the results of three pilot furnace tests undertaken on instrumented LVL beams exposed to the standard ISO 834 design fire curve were completed at the BRANZ Fire Research facility.

Testing in the Pilot furnace at BRANZ was completed on LVL beam assemblies (2200 mm long) using medium size LVL sections measuring 300 x 105 mm and a composite section measuring 360 x 133 mm. The beams were exposed to the standard ISO fire at various durations. Theses test were exposed to the fire on three faces and the samples were instrumented at two sections along the beams to record temperatures, thermal gradients and the location of the char front.

Comparison to similar testing completed on Glulam Beams by Collier (1992) may be significant and it may be prudent to replicate his thermocouple layout in the section on at least one test. Char rates obtained from the pilot furnace tests were compared to the cone calorimeter char test results.

1.3.6 Chapter 7: Full Scale Fire Test

Chapter seven describes the full scale test performed at the BRANZ testing facility on a loaded section of Laminated Veneer Lumber to confirm the recommended char rate obtained from Cone Calorimeter and Pilot Furnace testing.

The test in the full size furnace at BRANZ was used to confirm the performance of the LVL section (300 x 105 x 4000 mm long) under loaded conditions and using the recommended char rate mentioned above in the design of the test. The beam was loaded

with a central point load, with a load cell monitoring the load to maintain it as constant as possible whilst recording the time to failure and the deflection. This test cannot be instrumented due to the loading applied.

1.3.7 Chapter 8: Summary & Recommendations

Chapter eight provides a summary of the test results found in this project, confirm and/or discuss further those results and comparisons and where appropriate provide recommendations.

1.3.8 Chapter 9: Conclusions

Chapter nine provides conclusions in relation to the objectives of this report.

Chapter 2: Description of Testing Equipment and Testing Setup

This chapter describes the testing equipment used for the testing undertaken for this research project, the conditions the equipment was used under and the specific setup required for testing.

2.1 The Cone Calorimeter – University of Canterbury

The cone calorimeter is a bench scale apparatus used to measure heat release rates and associated fire properties of a small product sample. This section describes the instrument, discusses its components and back grounds the theoretical considerations behind the development of the cone calorimeter.

The cone calorimeter is so named due to the shape of its heater; it was developed at the National Institute of Standards and technology (NIST), previous known as the National Bureau of Standards (NBS), in the 1980's (Babrauskas 1982). Its purpose is to measure the properties on a bench-scale of a product sample size subjected to heat and/or fire. The properties of interest were identified at the conception being:

- Ignition properties.
- Flame spread behaviour.
- Heat release rate per unit area.
- Smoke release rate per unit area

The prime function of a cone calorimeter in determining these properties, is the measurement of the heat release rate of a product sample and hence an estimation of that product's contribution to the fire. This allows approximations of the product's properties to be made, independent of knowledge of the exact combustion chemistry.

The American Society for Testing Materials (ASTM) approved a cone calorimeter standard in 1990. This was given the designation ASTM E 1354 1990, and titled: Standard Test method for Heat and Visible Smoke Release Rates for Materials and products using an Oxygen Consumption Calorimeter. A similar standard was published by the International Standards Organisation (ISO), designated ISO 5660 1992. The National Fire Protection Association (NFPA) issued a parallel standard to both of these in

1990. It targets the specific application of testing upholstered furniture composites, NFPA 264A. As a result of the development of the cone calorimeter NIST was awarded an 'R&D 100' award 1988. This recognition in the field of research and development is additionally significant in that this is the first such award for a reaction to fire test.

2.1.1 Description of the Apparatus

Figure 2.1 is an overall view of the apparatus showing the position of all the main components.

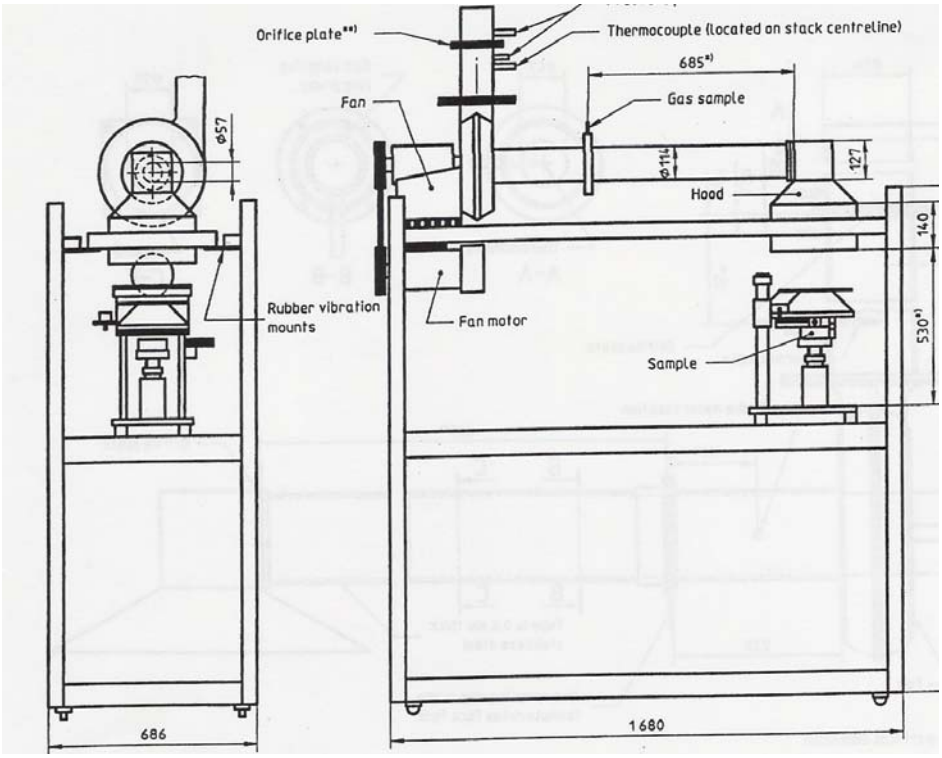

Figure 2.1 Overall view of Cone Calorimeter Apparatus from BS 476: Part 15: 1993 / ISO 5660-1: 1993.

The cone calorimeter apparatus consists of many components and systems. The general properties of theses components are prescribed in ASTM E 1354. For simplicity, in a review such as this it is convenient to group these components and systems into the following items.

Conical Heater: The heater is similar to that used in the ignitability test ISO 5657, except for a greater heat flux capacity of up to 100 kW/m^2, from a maximum operating level of 5 kW at 240V.

The 8 mm diameter and 3.4 m long element consists of heating wire packed in MgO refractory and swaged in a high temperature alloy sheath. The element is wound into a cone shape and inserted in a double walled steel truncated cone.

Electronic control is affected by fixed thermocouples in contact with the heater element. The element should be able to be maintained at a steady temperature to within +/- 2^oC.

The cone and sample can be arranged both vertically and horizontally; however the cone will be in the vertical orientation for all testing in this project.

Exhaust System: The hood is of dimensions adequate to ensure test products are removed. The ducting is designed to enhance mixing and flow development via a restrictive orifice. An orifice flow plate, a centre-line bi-directional probe and a centre-line thermocouple provides data for mass flow rate calculations. The exhaust gases are driven by a high temperature centrifugal fan in the range of 0.012m^3/s to 0.035m^3/s.

Figure 2.2: Cone Calorimeter, University of Canterbury

2.1.2 Sample Mounting and Load Cell

Samples are normally cut to 100 x 100 mm in size, generally are up to 50 mm thick but in this study will be used with sample thicknesses up to 85 mm thick. The samples are contained in a robust stainless steel mounting. The sample is exposed to the heat flux on the upper surface in a square pattern approximately 98 x 98 mm.

For the instrumented charring test to be carried out under the cone calorimeter, a special sample holder was made to allow the thermocouples to be inserted into the necessary locations to measure internal temperatures within the LVL sample and identify the char front as exposed to varying heat fluxes. Figure 2.3 shows the layout of the thermocouples for the instrumented test and Figure 2.4 shows the LVL sample holder constructed that allows the insertion of the thermocouples.

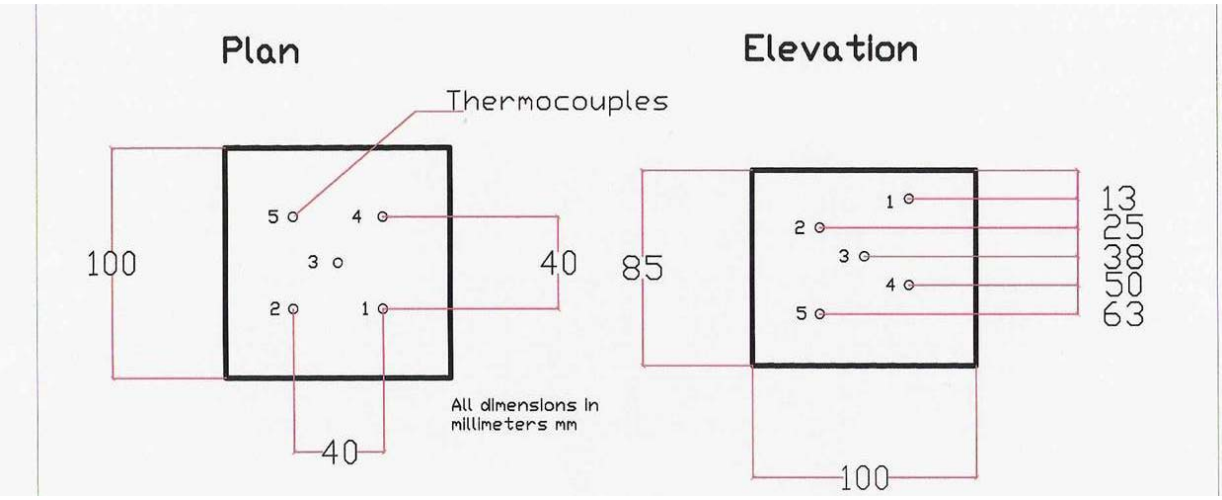

Figure 2.3 Thermocouples Layout for Instrumented Tests

Figure 2.4 Sample holder allowing Thermocouple Instrumentation

2.2 Pilot Furnace – BRANZ fire testing laboratory Porirua

The Pilot furnace is a 1.1 metre by 2.2 metre by 0.5 metre deep fire box fuelled by 8 diesel injection burners, but additional specimen frames may be added to make the depth of the furnace greater if required. The furnace allows complete assemblies, such as doors, windows or mechanical smoke handling equipment etc. to be constructed within a concrete framed specimen holder and fitted to the furnace thus completing the sealed fire box to the furnace. Refer to Figure 2.5, this photo is looking into the furnace in an upright position; the furnace may be rotated back into the horizontal position.

Figure 2.5 Pilot Furnace, BRANZ Fire Research Facility

The furnace is fitted with four thermocouples which monitor the furnace temperature during the test, allowing the operator to control the furnace temperature to meet the time temperature curve of the design fire; in these tests that is ISO 834 Design Fire. Control of

the fuel to each of the diesel injection burners can be controlled independently allowing the temperature within the furnace to be adjusted to provide as even a temperature as possible throughout the furnace.

Figure 2.6 shows the operator with the computer monitoring the thermocouple temperatures within the furnace and on the panel behind are the hand operated control valves controlling the flow of fuel to the burners.

Figure 2.6 Pilot Furnace Control Panel & BRANZ Operator.

In Figure 2.7 below is the ISO 834 design fire curve is shown with the recommended upper and lower limits to the temperature range.

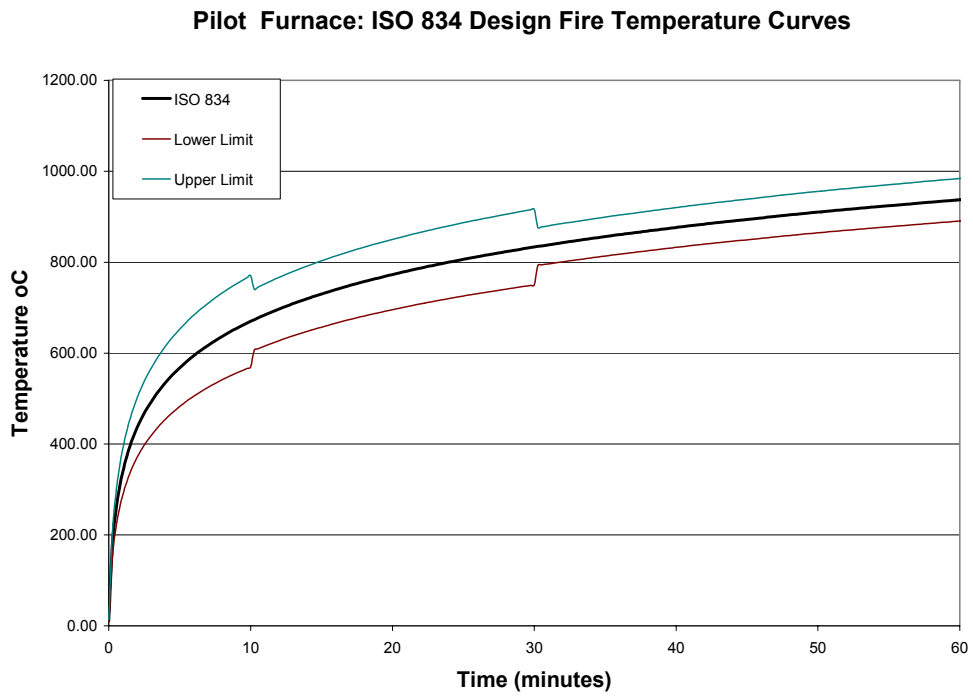

Figure 2.7 ISO 834 Design Fire Curve used in the Pilot Tests

2.3 Full Scale Furnace – BRANZ fire testing laboratory Porirua

The Full Scale furnace measures 4.0 metre by 3.0 metre fire box with variable depth, depending on the number of perimeter frames that can be added (refer Figure 2.8). The furnace is fuelled by diesel injection burners and additional specimen frames may be added to make the depth of the furnace greater depending on the assembly requirements of the test. The furnace allows complete assemblies, such as walls, structural elements or larger mechanical smoke handling equipment etc. to be constructed within a concrete framed specimen holder, which is fitted to the furnace and completes the sealed fire box.

Figure 2.8 Full Scale Furnace – BRANZ Fire Research Facility

The furnace may be in the horizontal or vertical position for tests.

The furnace is fitted with twelve thermocouples which monitor the furnace temperature during the test, allowing the operator to control the furnace temperature to meet the time temperature curve of the design fire, in these tests that is ISO 834 Design Fire. As for the pilot furnace, control of the fuel to each of the diesel injection burners can be controlled independently allowing the temperature within the furnace to be adjusted to provide as even as temperature as possible throughout the furnace. Another thermocouple measures the ambient temperature outside the furnace.

2.3.1 Load Test Setup

The set up for the load test required the LVL beam to be built into a specimen holder with the beam enclosed inside a perimeter timber framed enclosure that was clad with 2 layers of 13mm Winstones Fyreline Gibraltar Board, giving the assembly a minimum fire rating of 60 minutes. Refer Figures 2.9 & 2.10.

Figure 2.9 Beam fixed to Specimen Frame prior to enclosing Assemble

Figure 2.10 Completed Assemble Prior to Lifting onto Furnace

2.3.2 Load Test Reaction Frame

To apply the load to the LVL beam positioned over the furnace, a very strong steel fabricated reaction frame was constructed over the furnace to enable the load to be applied and monitored. Refer Figure 2.11

Figure 2.11 Steel Reaction Frame constructed over Completed Assembly

During the load test on the LVL beam data logging of the load applied on the beam was kept constant as possible by manual control of the pressure on a hydraulic jack, which was monitored by a load cell fitted between the hydraulic jack and the steel stub that imparted the load to the LVL Beam.

Figure 2.12
Load Test Monitoring Equipment.

Refer Figure 2.12 which shows the Hydraulic Jack, Load Cell & Potentiometer attached to Full Scale Furnace – BRANZ Fire Research Facility. The deflection was monitored during the test with the use of a potentiometer.

Chapter 3: Literature Review

This chapter reviews the prior literature and links it into this research project.

3.1 Thermal Properties of Wood

The thermal properties of wood are not well defined and vary considerably with temperature as moisture is driven off at 100^{o} C and as wood turns to char at 300^{o}C Jannsens (1994).

The density of wood varies significantly between species, between trees of the same species and within individual trees. The density drops to approximately 90% of its original value when the temperature exceeds 100 ^{o}C, and to approximately 20% of its original value when the wood is converted to char above 300^{o}C. There are also various definitions of wood density and Collins (1983) describes the various definitions used at the Forest Research Institute in Rotorua, New Zealand for radiate pine. These definitions; along with well established relationships between basic density and shrinkage for radiata pine, allowed Collins (1983) to derive expressions to permit conversions amongst the various definitions of wood density. This is of value not only for solid wood, but also for other wood products.

The thermal conductivity of wood varies greatly between various studies by various authors; Figure 3.1 shows the variation of thermal conductivity with temperature as proposed by Knudson and Schneiwind (1975) which is a representation of other published values.

Konig and Walleij (1999) found that they had to increase the thermal conductivity to much higher values at temperatures over 500 ^{o}C in order to give good predictions of measured behaviour. Konig and Walleij (1999) established the relationship between variations of specific heat with temperature shown in Figure 3.2. The large spike at 100^{o}C represents the heat required to evaporate the moisture in the wood.

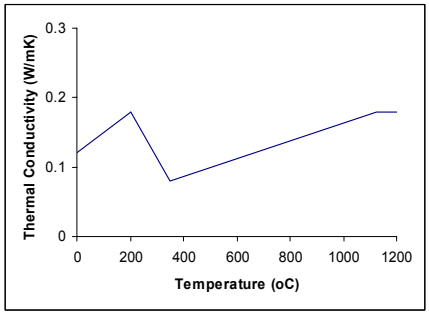

Figure 3.1 Variation of thermal Conductivity of Wood with Temperature, Konig and Walleij (1999).

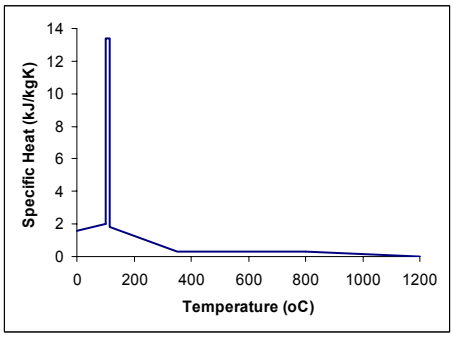

Figure 3.2 Variation of Specific heat of Wood with Temperature, Konig and Walleij (1999).

3.2 Ignition Properties

The literature researched considers only the ignition of timber caused by piloted ignition. Piloted ignition occurs when a material is heated with an ignition source present. The ignition source can be a small flame, a spark, an electric arc, a burning ember and so on. When the material is heated, it decomposes and releases mass in the form of pyrolyzates. Ignition then occurs when the concentration of the gases released (pyrolysis) exceeds the lower flammable limit in the presence of an ignition source close to the irradiated surface.

In his thesis NGU (2001) reviewed seven ignition time/Irradiance correlations and concluded that although there is no perfect method, his recommendation was that best

were Mikkola & Wichman (1981) and Delichatsios, Panagiotou & Kiley (1991). These two correlations shall be used in determining the ignition properties of LVL in this study.

Research of the various correlations have one thing in common; that is, the inclusion of a critical heat flux, q''_{cr}. Critical heat flux is a theoretical lower limit for the incident flux necessary to create the conditions for ignition. The critical heat flux should not be confused with minimum heat flux, q''_{min} . According to Janssens (1991), these two terms have the same meanings, except that q''_{cr} is an estimate of q''_{min} derived from a correlation of experimental data. The q''_{cr} is extrapolated from experimental correlation by making the time to ignition equal to infinity. Therefore q''_{cr} is dependent on the type of model used for correlating the ignition data. As a result, q''_{cr} is not the best way to estimate the minimum safe radiation level. The q''_{min} is more reliable and is obtained experimentally from a series of decreasing flux levels until ignition does not occur, and it depends on the decision of the researcher as to how long the test should be run. Thus the minimum heat flux is somewhere between the lowest incident heat flux at which ignition occurred and highest incident heat flux at which ignition did not occur. Therefore q''_{min} should be greater than q''_{cr} ($q''_{min} > q''_{cr}$) Shields, Silcock Murray, (1994).

Note that all the specimens tested in this research are physically thermally thick. According to Mikkola and Wichman (1989), wood specimens with a thickness greater than 15-20 mm may be considered as thermally thick. To say that a sample is thermally thick, means that the temperature on the unexposed surface, T_s, has not begun to rise.

Babrauskus (2002) in his review of practical and experimental data on the ignition of solid wood found that panel products such as plywood and particleboard have ignition properties very similar to wood so results on solid wood will generally be applicable to them. LVL is a processed panel product and ignition properties should also have ignition properties similar to that of solid wood.

3.3 Charring of Wood

.

White (2002) in Section 4/Chapter 11 of the SPFE Handbook, state's that "When attention is given to all the details, the fire endurance of a wood member or an assembly depends three items:

1. Performance of its protective membrane (if any),
2. Extent of charring of the structural wood element, and
3. Load carrying capacity of the remaining un-charred portions of the structural wood elements."

The investigations for this report do not include any testing with membranes protecting the LVL. Therefore the testing and results shall be targeted at establishing the extent or rate of charring of the LVL beam and the load carrying capacity of the remaining un-charred LVL.

Wood undergoes thermal degradation (pyrolysis) when exposed to fire. (Refer to Figure 3.3). By converting the wood to char and gas, pyrolysis results in the reduction in the woods density. The pyrolysis gas undergoes flaming combustion as it leaves the charred wood surface. Glowing combustion and mechanical disintegration of the char eventually erode the outer char layer.

The charring rate generally refers to the linear rate at which wood is converted to char. Under standard fire exposure the charring rate tends to be fairly constant after a higher initial char rate.

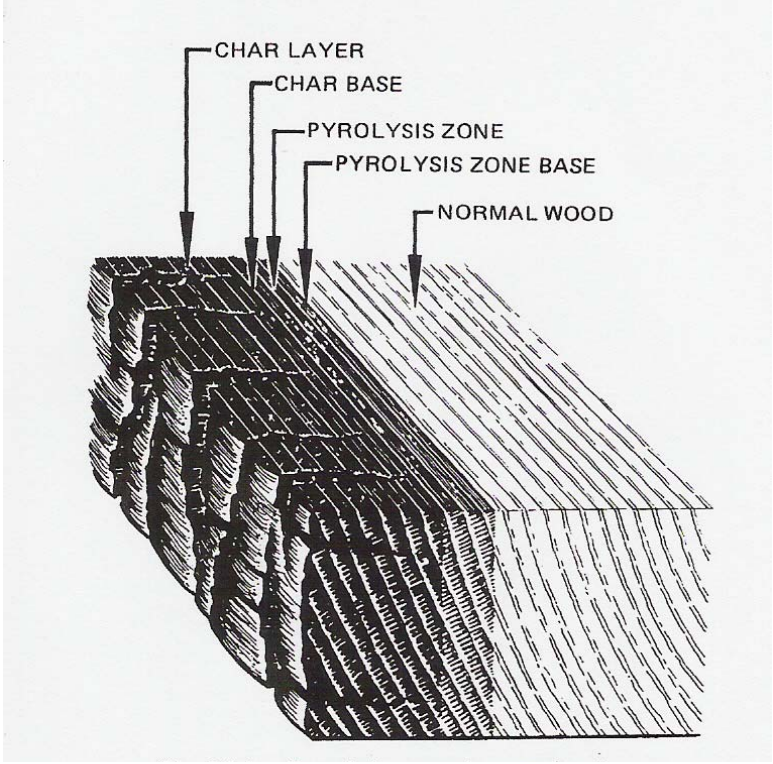

Figure 3.3 Degradation zones in a charring wood section, White (2002).

Establishing the charring rate is critical to evaluating fire resistance because char has virtually no load bearing capacity. There is a fairly distinct demarcation between char and un-charred wood. White (2002) states that the base of the char layers is wood reaching 290 ^{O}C. However as discussed already above there appears to be quite a range of temperatures from 288 – 360 ^{O}C.

Collier (1992) indicated from his results that a revision of the methods used to design timber structures for fire resistance was warranted. Collier found that the current practice of assuming a charring rate of 0.6 mm/min was found to be valid only for higher density timber (ρ = 600 kg/m3 at 12% moisture content). Collier found that the selection of a charring rate based on timber density would be more reliable especially for lower density timbers. After several models were evaluated Collier used White's Model (1988) for the basis for his experimental programme. White's Model provided a means of readily comparing the results of practical charring tests. This model has been used to evaluate the charring influences and used as a comparison for the char test results achieved in this project.

Buchanan (2002) in his overview of structural design for fire in New Zealand states that many test have confirmed that heavy timber exposed to a standard fire tends to char at a constant rate, with the nominal charring rate adopted in NZS 3603 (1993) being 0.65 mm/min. This rate was taken from Colliers (1992) results and modified in the code to account for density definitions and conversions given by Collins (1983)

White (2003) tested rim boards made from Laminated Veneer Lumber LVL. Rim boards are the boundary joist or ribbon plate as known in New Zealand, in a flooring system between upper and lower floors and are especially relevant in floor wall connections between in inter-tenancy walls. In testing single layer 32 mm thick LVL rim board samples White found that the linear charring rate for the LVL samples exposed to the fire exposure specified in ASTM E 119 (2000) in a small vertical furnace, varied from 1.35 – 1.26 min/mm or 0.74 – 0.79 mm/min. White also tested double layers of 32 mm thick LVL rim boards and here he found a linear char rate of 1.52 min/mm or 0.69 mm/min. As shown and discussed further in this report, Whites results appear to be very similar.

Njankouo, Dotreppe and Franssen (2004) undertook a study of the charring rate of tropical hardwoods, their results indicate that their method could be used for assessing the charring rate of timber both softwood and hardwood species. The test methodology used a gas fired furnace with the specimens exposed to the standard ISO 834 fire. Seven different tropical hardwood species with densities ranging from 400 to 1000 kg/m^3 were tested; the char front was identified as the corresponding time for each thermocouple to reach 300 ^{o}C. Although LVL is not produced from tropical hardwoods the lower densities tested in this study compare with the density range for pinus radiata grown in NZ and used for the production of LVL. The resulting charring rates of 0.36 mm/min to 0.71 mm/min were recorded and again very similar to the results of this report. The test results also showed that the density of wood significantly affects the charring rate and that the values recommended in Eurocode 5 for high density timber are conservative.

Mikkola (1990) describes a model for charring of wood as well as summarising experimental charring rates for some wood species and wood products. He found that the charring rate is affected by density and moisture content of wood, external heat flux and oxygen concentration of the surrounding air. LVL samples with a density of 520 kg/m^3

and 37 mm thick, were included in the wood products that Mikkola tested. In his study he defined the char front as the location of the 360 ^{O}C temperature isotherm. Looking more closely at the LVL experimental results Mikkola found that the charring rate of LVL exposed to 50 kW/m^2, varied from 0.68 – 0.82 mm/min with corresponding moisture contents of 20 – 10% respectively. Mikkola concludes that the results of his study can be applied to composites, if the composite components are all wood with about the same thermal properties. Mikkola also concludes that the relationship between the standard fire test (ISO 834) and the cone calorimeter test for charring can be used to estimate large-scale charring rates from small-scale experiments. Later in this report, comments on the suitability and the appropriate heat flux to be used with the cone calorimeter and its relationship to the ISO 834 standard fire test will be stated and a recommendation given for its use.

Chapter 4: Ignition Tests on LVL Specimens

Ignition tests were carried out at five different levels of heat flux and two main grain orientations, with three replications of each test. The grain orientations were on the exterior veneer face (face grain) and on the edges of the cut veneers parallel to the grain of the veneers. The ignition tests on the LVL samples were are based on the British Standard BS 476: Part 13 (1987), Method of measuring the ignitability of products subjected to thermal irradiance. This part of BS 476 is similar to ISO 5657. 1986: .Fire Tests. Reaction to Fire. Ignitability of Building Products. The units of irradiance are given in kW/m^2.

4.1 Principles of the Test

The specimens are mounted with the exposed surface horizontal in the sample holder during the test. Their upper surface of each sample is exposed to a constant thermal irradiance released by the radiator cone heater, within the range of 10 - 50 kW/m^2. Refer Figure 4.1 which shows the sample holder used in the cone calorimeter tests for the 50 mm thick ignition samples.

Figure 4.1 Standard size Ignition Test sample Holder

In this project research, the levels of irradiance ranged from 10 - 30 kW/m^2, using 50 mm thick samples of LVL. The ignition times recorded in the instrumented char tests at irradiances of 35, 50 & 65 kW/m^2 using 85 mm thick have been included with the specific ignition tests to provide another series of tests at the upper irradiance range.

A pilot flame or intermittent spark is then applied to a position 10 mm above the centre of each specimen to ignite any volatile gases that are given off near the surface of the specimens. Refer Figure 4.2 which shows the ignition sample in the holder under the cone with the pilot spark ignition device in position.

Figure 4.2 Ignition Sample in Holder with Spark Ignition device in Place.

The pilot flame is widely used due to its simplicity. The time at which sustained surface ignition occurs is recorded. The test does not measure the ignition temperature, T_{ig}.

4.2 Specimen Preparation

Three specimens of each grain orientation are tested at each level of irradiance. The orientation of grain Face Surface and Edge Surface of the LVL is as shown on the following sketch in Figure 4.3.

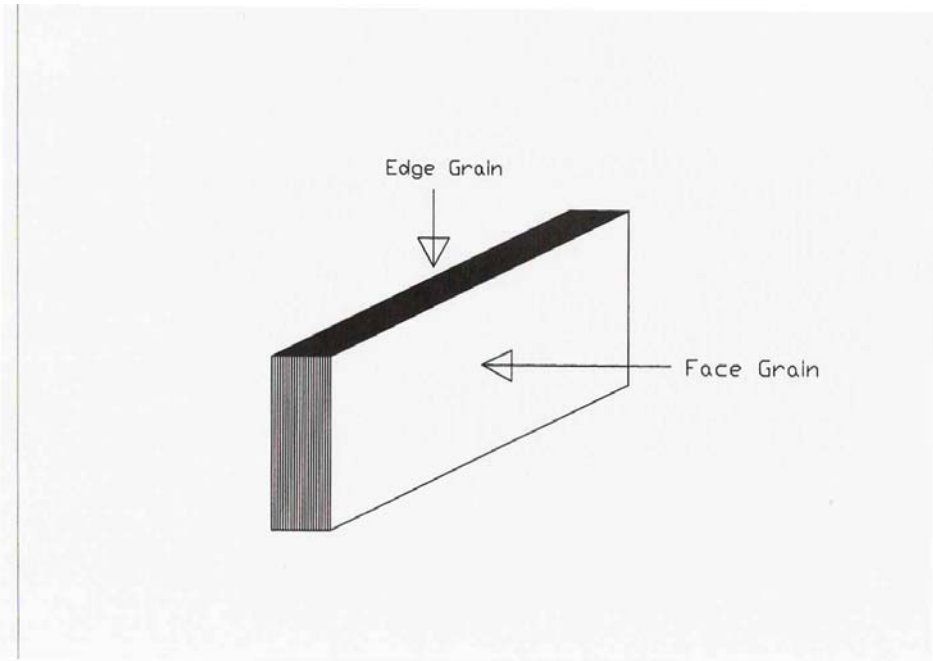

Figure 4.3: LVL Grain Orientation

For the study of the ignition properties 8 levels of incremental heat fluxes were used (10, 15, 20, 25, 30, 35, 50 & 65 kW/m^2).

The specimens shall have a size of 100 × 100 mm squares according to BS 476: Part 13, with thicknesses of 50 mm and 85 mm as already discussed. The 50 mm thick samples will fit in the standard specimen holders whereas a deeper specimen holder has been made to accommodate the thicker samples as well as allow thermocouples to be inserted at the depths required for the charring rate instrumented tests to follow.

A more detailed description and photograph of this sample holder is supplied in the instrumented charring rate test procedure. Refer Figure 2.4, for a picture of the instrumented sample holder fabricated for the instrumented char tests.

4.3 Test Apparatus

The cone calorimeter constructed in accordance with the requirements of clause 6 of ISO 5660-1:1993 (E) which includes:

Cone shaped radiant heater
Temperature controller
Specimen holders
Exhaust gas system
Gas sampling apparatus
Ignition circuit
Ignition timer
Oxygen analyser
Heat flux meter
Calibration burner
Data collection and analysis system

The general arrangement of the apparatus is shown in Figure 5 BS 476: Part 15: 1993**,** ISO 5660 – 1: 1993, this overall view of the cone calorimeter apparatus has been reproduced in this report in Figure 2.1.

The tests were carried out in at the fire laboratory at University of Canterbury with controlled airflows over the specimen, with the apparatus shielded. The airflow must be less than 0.02 m/s to satisfy this condition. This is because if the induced airflow is more than 0.02 m/s, it may disturb the natural airflow near the surface of the specimen and hence cause excessive unwanted convection cooling.

4.4 Calibration

4.4.1 Heater calibration

The heater calibration required the adjustment of the temperature controller so that the conical heater producers the required irradiance, as measured by the heat flux meter, at the start of each test day, when changing to a new irradiance or when the conical heater orientation is changed. Note in this project no change of heater orientation was required.

For the ignition testing using the cone calorimeter heat calibration was the only calibration required. Oxygen analyzer and the heat release rate calibration were not necessary in order for the ignition tests to be performed.

4.5 Test Procedure

The following procedure is basically similar to BS 476, with some modifications. These modifications include deleting the necessary procedures to use the oxygen analyzer and the heat release rate as heat release rates are not required for this test. As the cone heater was used in the horizontal position only, procedures outlined in BS 476 for the use of the cone heater in the vertical position were followed and included in the steps taken below.

4.5.1 Steps taken just before the test:

a) Once the specimens have reach constant mass, remove the specimens from conditioning cabinet, measure them, record the moisture content using the hand held moisture meter and weigh them.
b) Record the mass, and other relevant information.

4.5.2 Steps taken during the test:

a) Turn on the fan of the fume cupboard.
b) Set up and check the apparatus.
c) Before starting check the following equipment is in the lab and readily available:
    1. CO2 fire extinguisher.
    2. Safety glass.
    3. Stop watch.
    4. Insertion and location tray (Sample holder).
    5. Dummy specimen board (Insulation board) for cone calorimeter.
    6. Specimen screening plate (Cone shield).
    7. Metal bucket half full of water.
d) Get ready with the prepared specimen-baseboard combination and make sure it has been weighed.

e) Turn on the power to the cone calorimeter.

f) On the apparatus front panel, turn on the main power to the apparatus.

g) Then turn on the power to the cone heater on the apparatus front panel as well.

h) Place the dummy specimen board on the pressing plate.

i) Adjust the temperature setting of the controller to the appropriate value established by heat calibration procedure to correspond to 400 ^{O}C or other heat flux required.

j) Allow the apparatus to heat up to equilibrium. When the heater has attained the required temperature equilibrium, a further 5 minutes should be allowed to elapse before commencing the test and exposure of a specimen.

k) Remove a prepared specimen from conditioning cabinet and place the prepared specimen in the holder for insertion under the cone heater.

l) The adjustable height mounting that the specimen holder slides onto shall be checked to ensure that the correct distance from the bottom surface of the cone heater and the top surface of the specimen is 25 mm.

m) After the radiator cone is preheated, set the cone to the desired irradiance level.

n) Once the cone has reached the desired temperature and reached equilibrium, conduct the next steps in rapid succession (15 seconds) wearing safety glass and gloves:

    1. Place the specimen screening plate on top of the masking plate.
    2. Place the specimen in the specimen holder and location tray onto the mounting plate.
    3. Remove the specimen screening plate and start timer (stopwatch).
    4. Turn on the spark igniter.

o) Record the time to ignition.

p) Turn off the spark igniter.

q) Remove the specimen holder from under the cone heater.

r) Place the dummy specimen board on the plate.

s) Remove the specimen from the insertion and location tray and cool the specimen in water.

t) Operations m) to s) should be repeated for the remaining specimens.

4.5.3 Repeatability and End of Test:

a) A further set of three specimens are tested at the next lower level of irradiance.
b) If no sustained surface ignition occurs with all three specimens at a given irradiance, then tests are not carried out at another lower irradiance.
c) When adjusting the heater to the next level of irradiance, sufficient time (3 minutes) should be allowed for the apparatus to reach thermal equilibrium following the change in temperature.

4.5.4 Observations during Test:

Several important observations during the test need to be recorded are:

- Time, position and nature of ignition.
- Glowing decomposition of the specimen.
- Any form of melting, foaming, spalling, cracking, expansion or shrinkage of the exposed surface of the specimen.

4.5.5 When finished the Test:

a) When finished with all testing, reduce the cone temperature to 400 degrees Celsius and let it cool for 5 minutes
b) Turn off the power to the cone heater.
c) Turn off the main power on the wall.
d) Check all of the equipment is left in a neat and orderly fashion.
e) Turn off fan.

4.6 Observations During Ignition Tests

4.6.1 Ignition of Instrumented Samples

Ignition in the instrumented samples at the higher heat fluxes of 50 & 65 kW/m^2 all occurred within 30 seconds of the start of the test, with ignition indicated by direct sustained flaming across the exposed surface. Ignition of the instrumented samples at 35 kW/m^2, were a little slower to ignite with the time to ignition generally varying from 40 – 50 seconds, with ignition of one face grain exposed LVL sample and the end grain sample igniting in 1 minute 14seconds, after flickering several times after 50 seconds.

All the instrumented samples were on LVL sample sizes of 100 x 100 x 85 mm thick, compared to the ignition test on the samples at heat fluxes of 30kW/m^2 and lower, where LVL sample sizes were 100 x 100 x 50 mm thick.

4.6.2 Ignition of samples at 30 kW/m^2.

Ignition on samples exposed to 30 kW/m^2 heat flux occurred within a time range of 1 minute 15 seconds to 1 minute 32 seconds, with no real difference whether it was face grain exposed or the edge grain. Very little flickering (flashing or transitory flaming) occurred with only two samples exhibiting minor flickering only seconds before sustained flaming occurred.

Figure 4.4 shows the sustained surface ignition of a sample exposed to 30 kW/m^2 heat flux, immediately after ignition occurring.

Note: Sustained flaming is defined as the existence of flame on or over the surface of the sample for periods over 4 seconds. Transitory flaming is defined as the existence of flame on or over the surface of the sample for periods between 1 and 4 seconds.

Figure 4.4 Sustained surface Ignition at 30 kW/m^2 Heat Flux

Using a straight edge across the surface of the samples immediately after the sample was removed from the test and cooled; the surface shrinkage/char depth was measured. If the space between the straight edge and the sample surface was less than 1.0 mm then the space was probed with a feeler gauge. For the 30 kW/m2 series of tests the surface shrinkage was measured at less than 0.25 mm for all the face grain samples, however one edge exposed sample measured 0.5 mm surface shrinkage /char depth, with the other two edge exposed samples measuring less than 0.25 mm.

4.6.3 Ignition of samples at 25 kW/m^2.

Ignition on samples exposed to 25 kW/m^2 heat flux occurred within a time range of 2 minute 15 seconds to 6 minute 39 seconds, and again their was no real difference whether it was face grain exposed or the edge grain. The longest sample time in this series was face grain exposed with the surface starting to glow after 5 minutes and 57 seconds before sustained flaming occurring at 6 minutes and 39 seconds. From the edge grain exposure one sample commenced flickering after 3 minutes and 49 seconds, glowing after 4 minutes and 10 seconds before sustained flaming occurred at 5 minutes and 12 seconds. The other samples tested at this heat flux all sustained flaming in a time range from 2 minutes and 14 seconds to 4 minutes and 17 seconds, and all these samples exhibited flickering up to 1 minute prior to sustained flaming occurring.

For the 25 kW/m2, series of tests the surface shrinkage/char depth was again less than 0.25 mm for all the face grain samples, however two of the edge grain exposed samples, measured between 0.5 mm and 1.0 mm for surface shrinkage/char depth, with the other measuring between 0.25 and 0.50 mm.

4.6.4 Ignition of samples at 20 kW/m^2.

Ignition on samples exposed to 20 kW/m^2 heat flux occurred within a time range of 5 minute 11 seconds to 11 minute 09 seconds.

The time range for the face grain exposed samples at this heat flux was significantly different to edge grain exposure. The range for the face grain exposure was from 5 minute 11 seconds to 6 minute 29 seconds, whereas for the edge grain exposure the time range was from 8 minute 14 seconds to 11 minutes 09 seconds. Most sample's exhibited glowing and intermittent flickering prior to sustained flaming, with the glowing and intermittent flickering period being shorter (up to 10 seconds) for the face grain samples, whereas for the edge grain exposure this glowing and intermittent flicker period could occur for 2 - 3 minutes before sustained flaming occurred.

For the 20 kW/m2, series of tests the surface shrinkage/char depth was again less than 0.25 mm for all the face grain samples, however for the edge grain exposed samples measurements of between 1.0 mm and 3.0 mm for surface shrinkage/char depth were found.

4.6.5 Ignition of samples at 15 kW/m^2.

Ignition on all samples exposed to 15 kW/m^2 heat flux occurred within a time range of 11 minute 54 seconds to 31 minute 38 seconds.

The time range for the face grain exposed samples at this heat flux was again significantly different to that of edge grain exposure. The range for the face grain exposure was from 11 minute 54 seconds to 14 minute 16 seconds, whereas for the edge grain exposure the time range was from 28 minute 52 seconds to 31 minutes 38 seconds.

Most samples exhibited glowing and intermittent flickering prior to sustained flaming with the glowing and intermittent flickering period being shorter (up to 2 minutes) for the face grain samples, whereas for the edge grain exposure this glowing and intermittent flicker period occurred from 7 – 12 minutes before sustained flaming occurring.

Figure 4.5 Surface shrinkage or char depth; edge grain exposed sample at 15 kW/m^2.

For the 15 kW/m^2 series of tests the surface shrinkage/char depth was less than 0.25 mm for two of the face grain samples, with the other face grain exposed sample measuring 0.5 mm, however for the edge grain exposed samples, measurements of between 3.0 mm and 9.0 mm for surface shrinkage or char depth were found. Refer to Figure 4.5 above showing surface shrinkage/char depth to an edge grain exposed sample at 15 kW/m^2.

4.6.6 Ignition of samples at 10 kW/m^2.

For all tests at this heat flux on both face and edge grain exposed samples, ignition did not occur within 30 minutes of the test commencing and no signs that ignition might occur were observed.

For the 10 kW/m2 series of tests; there was no measurable surface shrinkage for the face grain samples, however for the edge exposed samples surface shrinkage/char depth of up to 0.50 mm was measured.

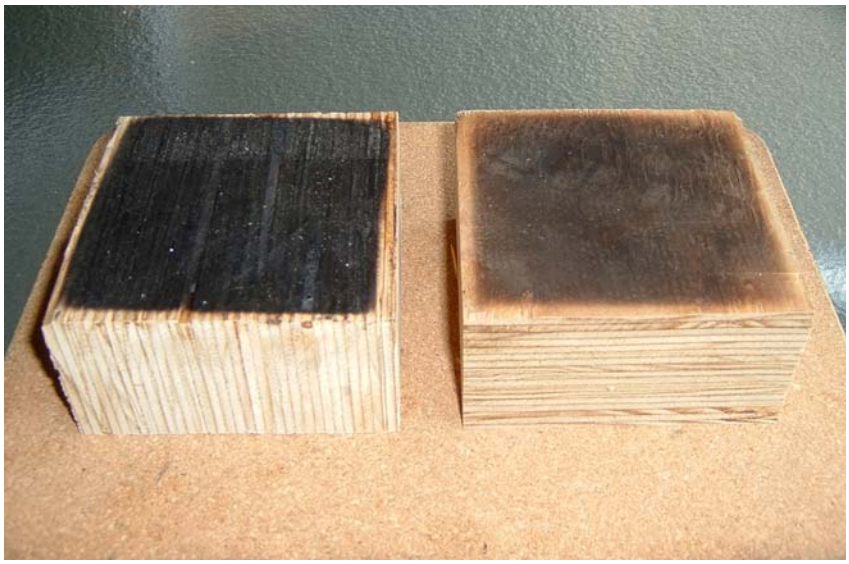

Figure 4.6 Surfaces face & edge grain exposed sample at 10 kW/m^2.

Refer to Appendix G for photos of the surfaces of ignition samples for heat fluxes 30 – 10 kW/m^2.

4.7 Ignition Results

The results of these tests are shown in Figure 4.7 for the face grain and Figure 4.8 for the edge grain, where the inverse of the square root of the temperature has been plotted against the incident heat flux, together with the line of best fit.

Two methods were used to estimate the ignition properties of the LVL. The first method is that of Mikkola & Wichman (1989) and the second one is by Delichatsios, Panagiotou & Kiley (1991). These methods were recommended by Ngu (2001) as having the best correlations based on his testing of the ignition properties of New Zealand timbers. The resulting values for the surface ignition temperature (T_{ig}) and the thermal inertia ($k\rho c$) of the LVL samples, along with the estimate of the critical heat flux (q_{cr}) are shown in Table 4.1.

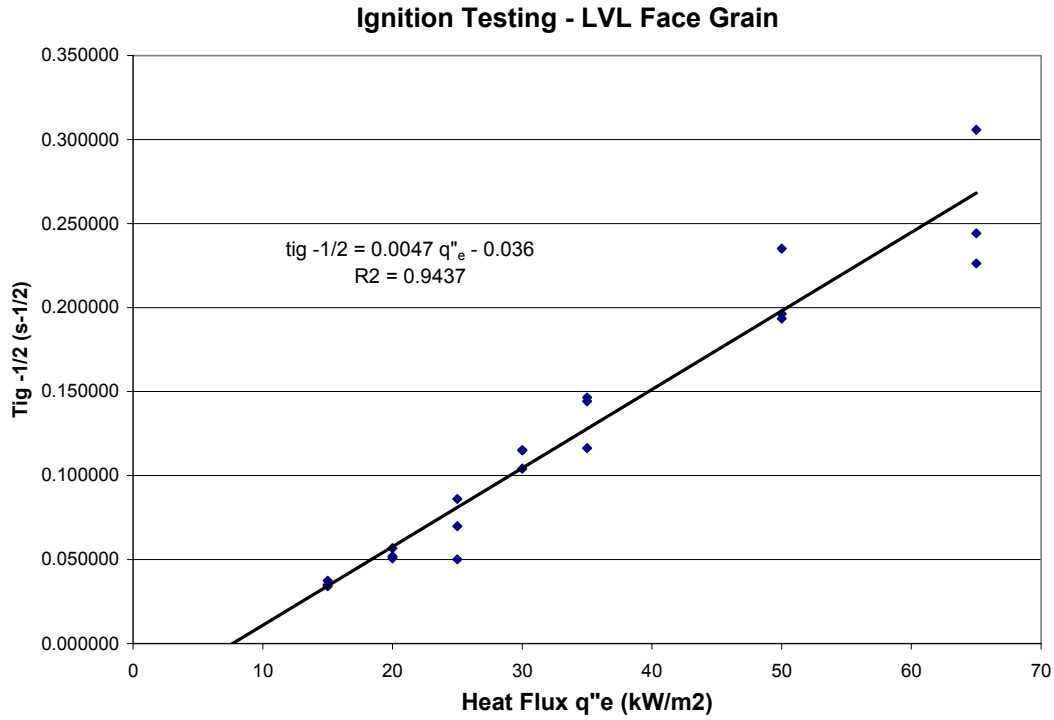

Figure 4.7 Ignition Data LVL – Face Grain

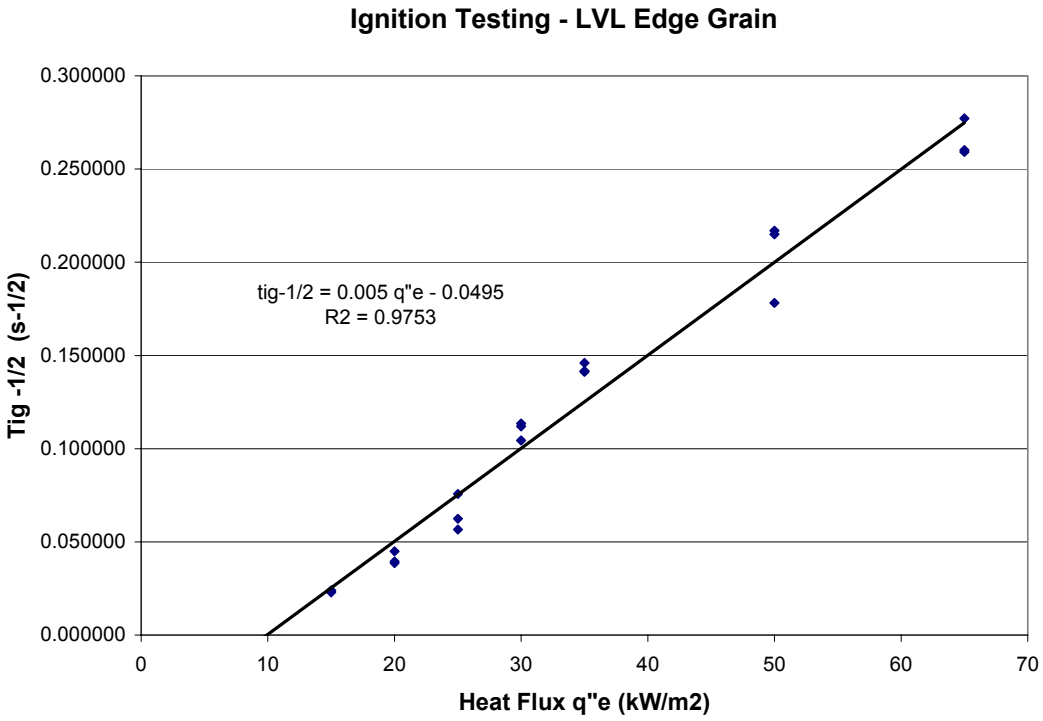

Figure 4.8 Ignition Data LVL – Edge Grain

The critical heat flux, q''_{cr}, for the Mikkola & Wichman (1989) correlation is obtained as the intercept of the best-fit regression line (see Figures 4.7 & 4.8) on the q''_e axis whereas for the Delichatsios, Panagiotou & Kiley (1991) correlation q''_{cr} is obtained as the intercept on the q''_e axis divided by 0.64. The ignition temperature can be estimated by solving the equation:

$$\varepsilon \dot{q}''_{cr} = h_c\left(T_{ig} - T_\infty\right) + \varepsilon\sigma\left(T_{ig}^4 - T_\infty^4\right)$$

Where h_c = convective heat transfer coefficient

ε = emmissivity or absorptivity of the surface, and

σ = Stefan Boltzmann coefficient (= 5.67 x 10^{-11} kW/m^2K^4)

The thermal inertia, kρc, is determined from the slope of the regression line as

$$slope = \frac{2}{\sqrt{\pi k\rho c}.\left(T_{ig} - T_\infty\right)}$$

which can be rearranged to give:

$$k\rho c = \frac{4}{\pi}\left[\frac{1}{slope\left(T_{ig} - T_\infty\right)}\right]^2$$

Ignition Properties	**Units**	**Face grain**		**Edge grain**	
		MW [18]	DPK [19]	MW [18]	DPK [19]
Critical heat flux	$\mathbf{q_{cr}}$ (kW/m^2)	7.66	11.97	9.90	15.47
Surface ignition temperature	$\mathbf{T_{ig}}$ (^{o}C)	251	341	294	380
Thermal inertia	**kρc** (kW/m2)^{2}s	1.080	0.558	0.678	0.393

Table 4.1 Estimated ignition properties, MW – Mikkola & Wichman (1989), DPK – Delichatsios, Panagiotou & Kiley (1991)

Chapter 5 Char Rate

Two types of testing were undertaken to determine the char rate for LVL. Firstly, char rates were established from instrumented tests on samples over a 90 minute period, where the progress of the char front was determined from LVL temperatures obtained from thermocouples placed in each sample.

Secondly, once the char depths were established from the instrumented tests for the various heat fluxes, then un-instrumented tests on similar LVL samples where performed for specified periods of time at the same heat fluxes and the resulting char depths measured and compared to the instrumented results obtained.

5.1 Instrumented Char Tests

The instrumented tests required the samples to be instrumented with thermocouples to determine the char front traveling through each sample when it was exposed to a constant heat flux using the Cone Calorimeter.

In his various studies of literature covered in Chapter 2, many authors defined the char front as the location of the 300 ^{O}C temperature isotherm, with a range from 288 – 360 ^{O}C. The range is not particularly significant as the temperature gradient is very steep at around this temperature range and the time difference small. Therefore the temperatures were recorded at various depths in 18 samples of LVL measuring 100 x 100 x 85 mm deep, at constant irradiances or heat fluxes of 35, 50 & 65 kW/m^2, in order to located the 300 ^{O}C temperature isotherm.

Thermocouples were placed in the central region of the instrumented LVL blocks at depths of 13, 25, 38, 50 & 63 mm, as shown in Figure 5.1.

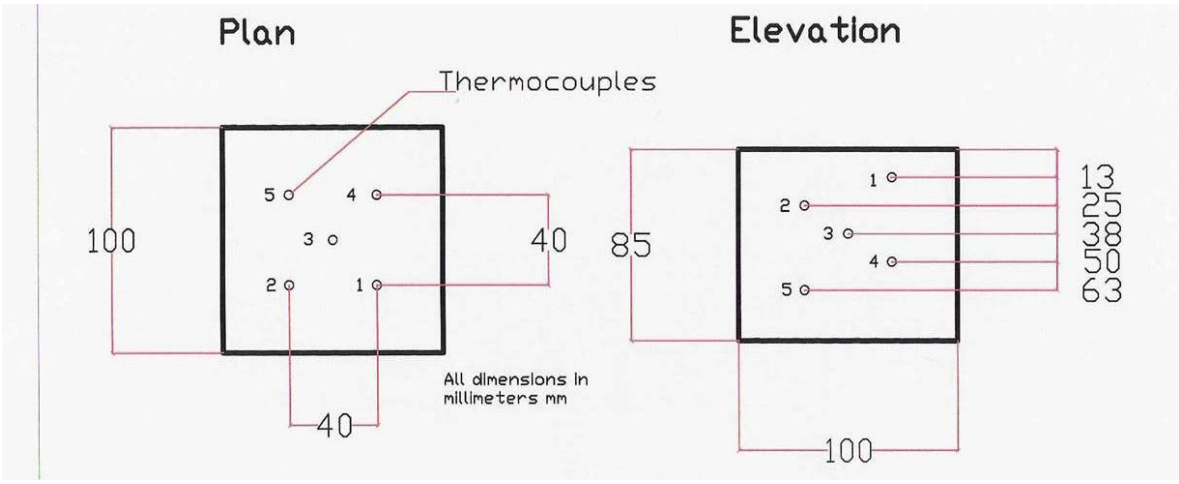

Figure 5.1: Layout and depth of thermocouples

From the results of these tests (refer Appendix B) the time for each thermocouple to reach 300°C was extrapolated for each thermocouple depth, the results averaged and then char depth plotted against time for each grain orientation and for each heat flux (Refer to appendix C for the individual heat flux and grain orientation graphs). In Figure 5.2 all char depths against time curves are shown for all heat flux levels and grain orientations.

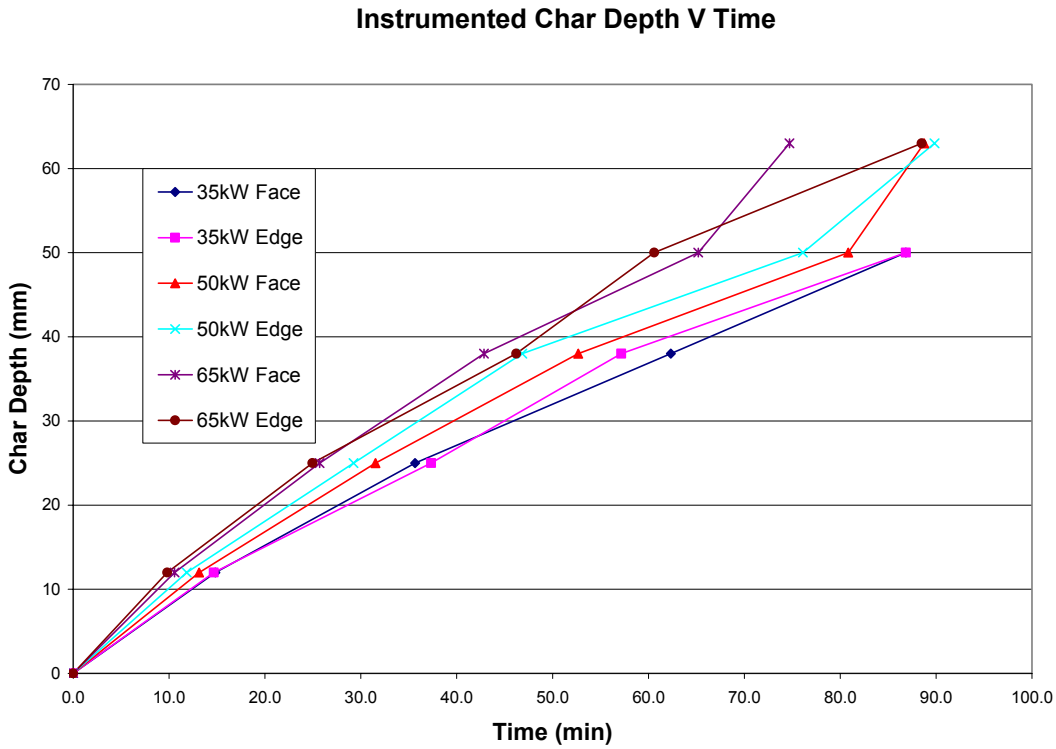

Figure 5.2: Instrumented char depth results

5.2 Un-instrumented Char Tests

Un-instrumented LVL blocks of the same dimensions were exposed to the same constant heat fluxes as used for the instrumented tests in the Cone Calorimeter, however for these series of tests the time period of exposure was limited to 20, 40 and 60 minutes.

Three tests were completed for each time period and for each grain orientation. The residual sample thickness of the instrumented tests has been included in the results, with the instrumented test durations varying in time from 80 – 95 minutes. This should not be a problem as the corresponding time has been graphed against the char thickness for the corresponding time.

Once the exposure to the heat flux was completed for the specified time the samples were removed from the heat source immediately, the char removed and the remaining solid LVL measured and the char depth recorded.

The un-instrumented results for each of the heat fluxes and the different grain orientations are shown on Figure 5.3. Very good correlations between the instrumented and the un-instrumented results were obtained.

However the results towards the longer durations from 80 to 95 minutes shows a wider spread when comparing the instrumented results from the thermocouple temperature and the actual char thickness calculated by measuring the residual timber at the end of the tests.

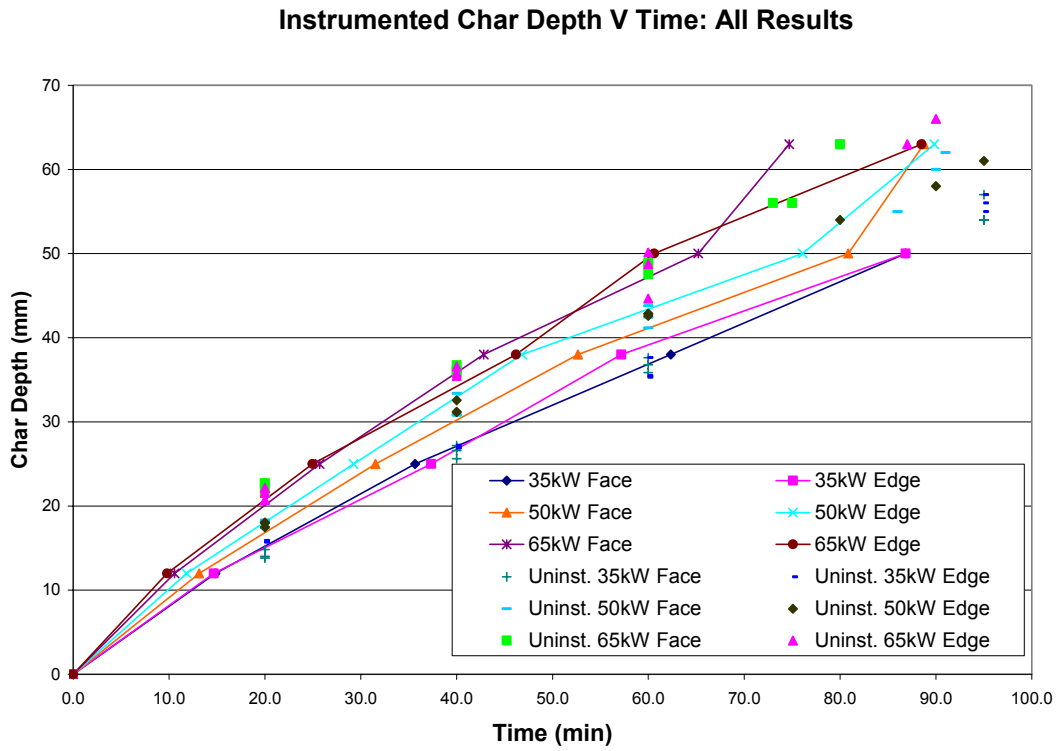

Figure 5.3: Instrumented & un-instrumented char depth results

Figures 5.4 to 5.9 show the char depths found for both the instrumented and the un-instrumented char tests for each particular heat flux and for each grain orientation of the LVL samples.

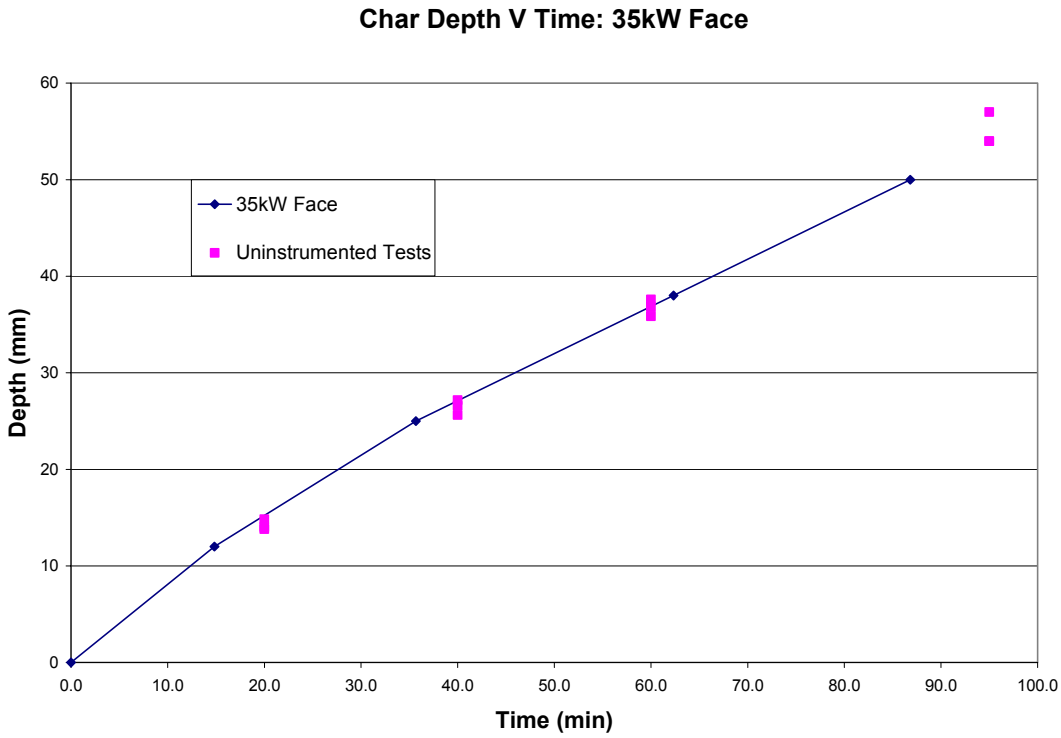

Figure 5.4 Instrumented & un-instrumented char depths: 35 kW/m^2 Face.

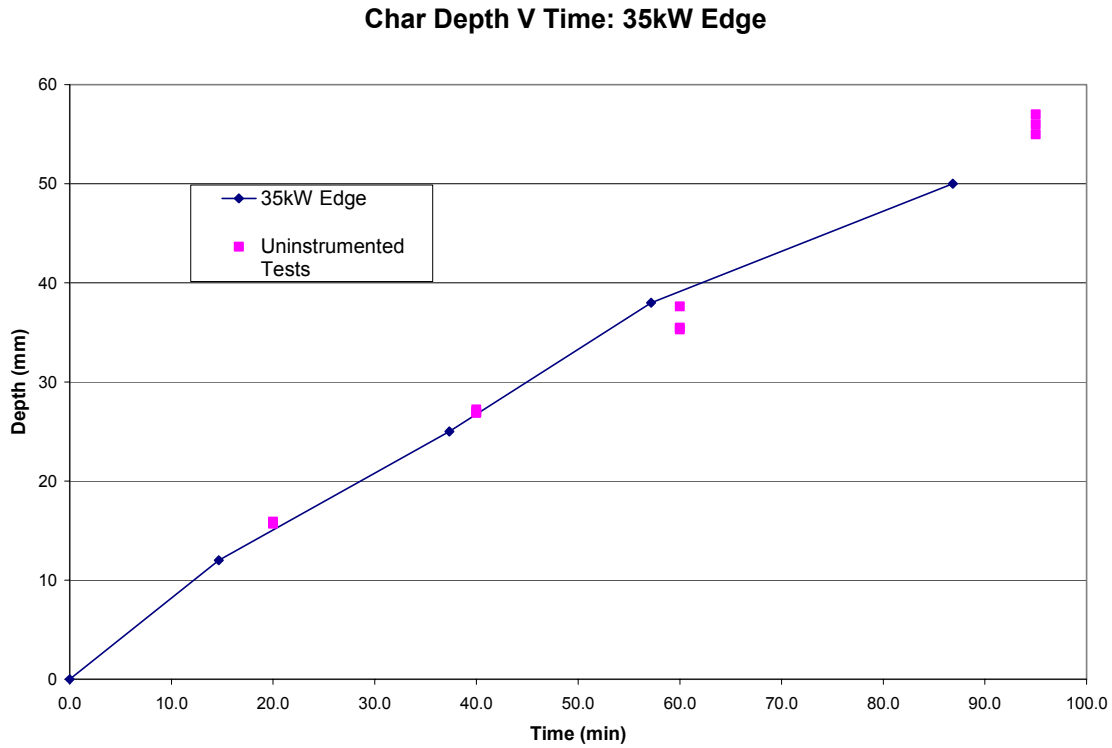

Figure 5.5 Instrumented & un-instrumented char depths: 35 kW/m^2 Edge

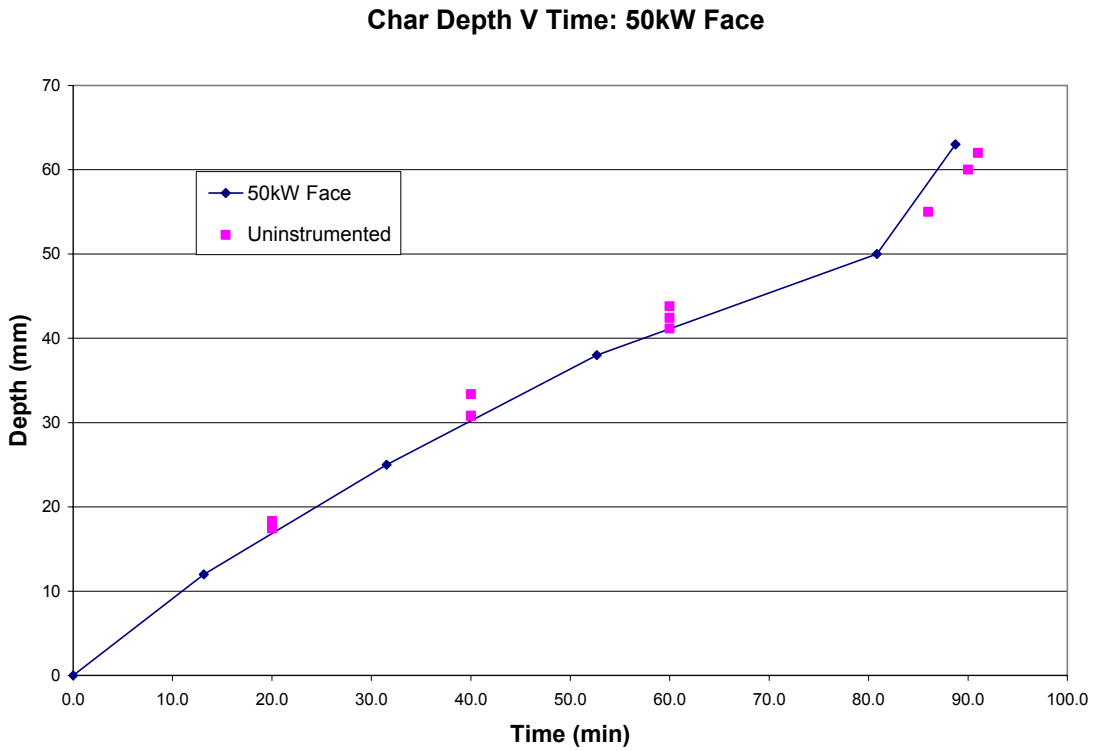

Figure 5.6 Instrumented & un-instrumented char depths: 50 kW/m^2 Face.

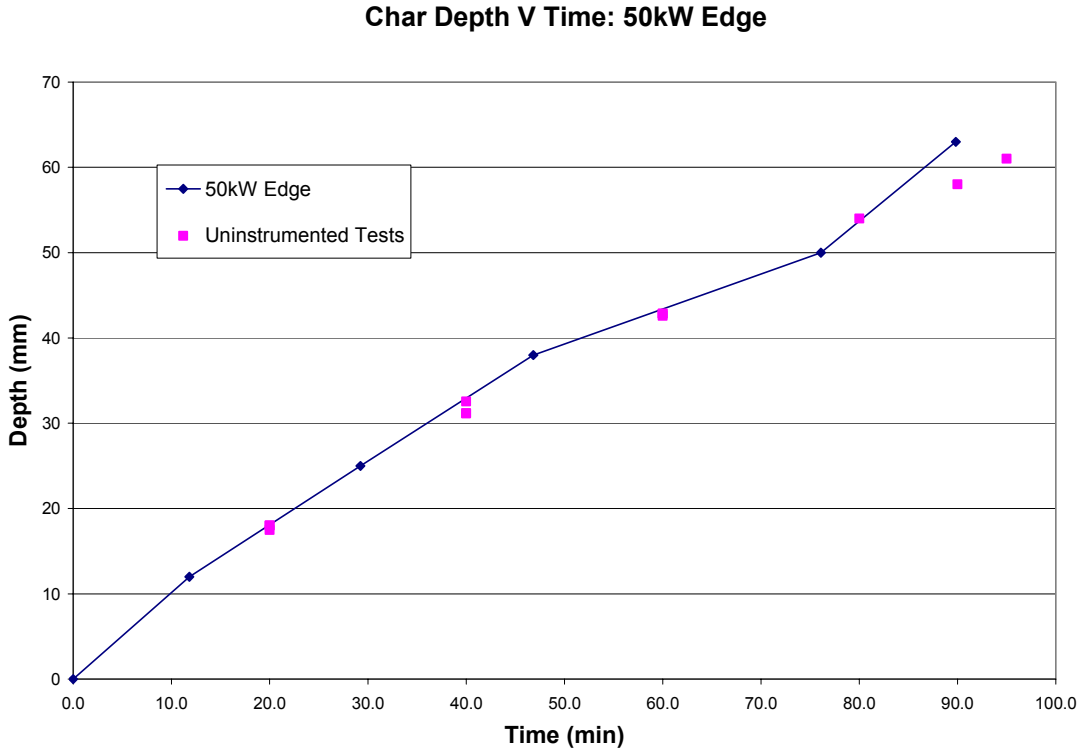

Figure 5.7 Instrumented & un-instrumented char depths: 50 kW/m^2 Edge

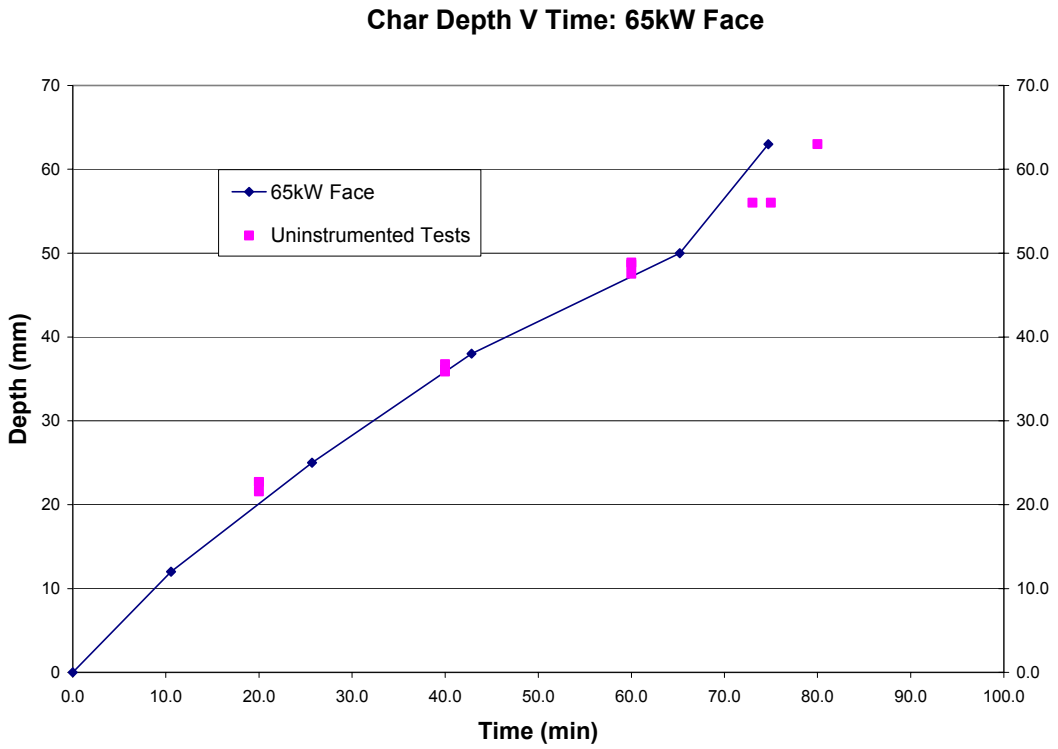

Figure 5.8 Instrumented & un-instrumented char depths: 65 kW/m^2 Face.

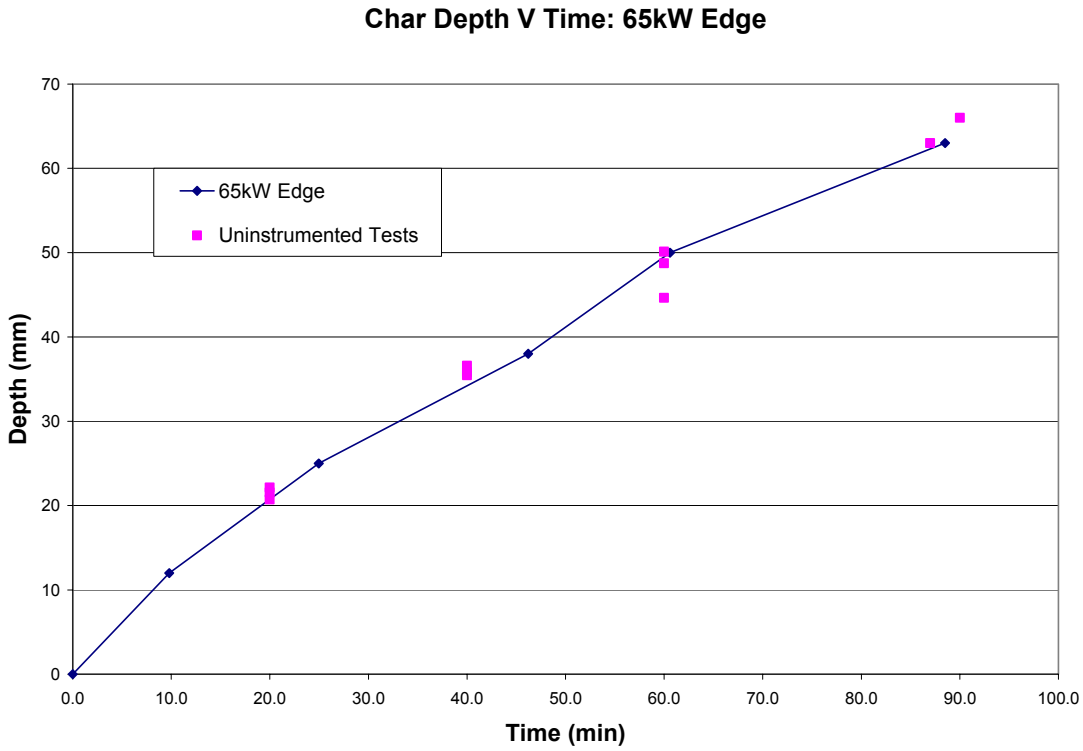

Figure 5.9 Instrumented & un-instrumented char depths: 65 kW/m^2 Edge.

5.3 White's Char Model

White (1988) & (2002) discusses empirical models for expressing the charring rate in the standard ASTM E-119 test, on charring rates of different wood species. In his thesis White developed a model for estimating the char depth with time, charring rate and the cumulative charring rate. The model allowed for differing density of timber, moisture content and a factor for the hardness of the timber. Refer to Appendix F for notes and calculations using White's model.

White's Model Formulae: A time location model expressed as:

$$t = mx_c^{1.23}$$

Using the oven dried test density of 555 kg/m3, moisture content of 13.7%, penetration depth CCA of 20 mm for Ratiata Pine (a transport factor), and a factor c = 1, for hardness of the softwood Radiata Pine, into R H White Char Model we get the following curve for the LVL which we have superimposed onto figure 5.3, as shown in figure 5.10.

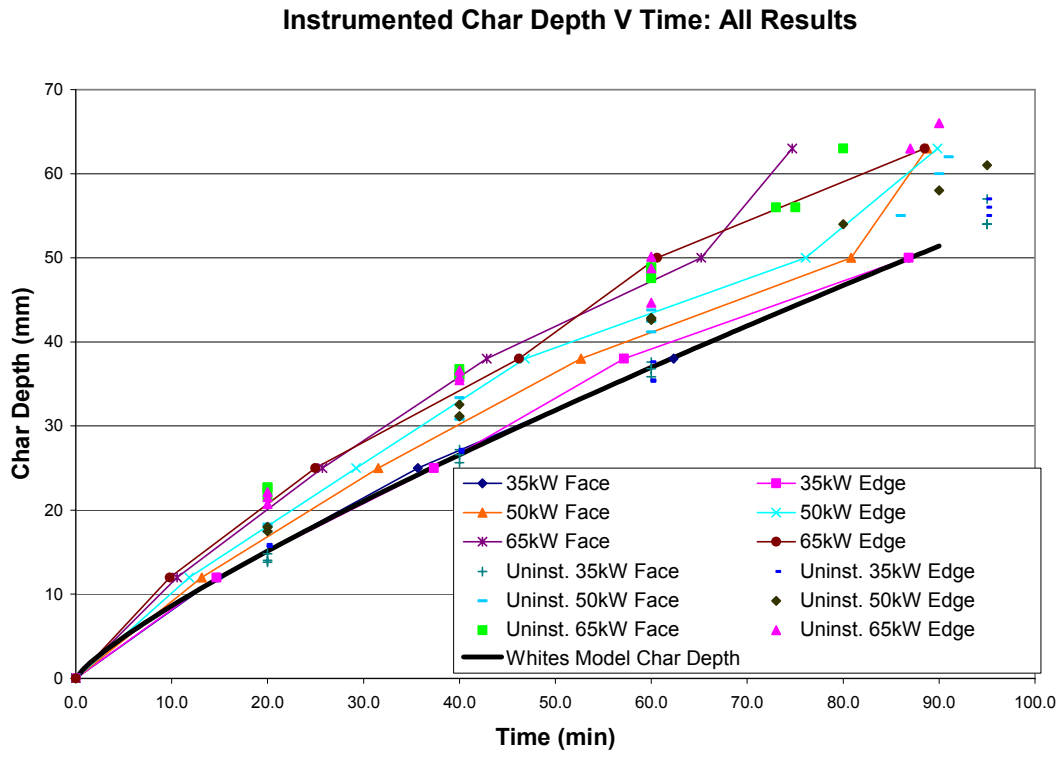

Figure 5.10 Whites model superimposed on instrumented & un-instrumented char depth results.

5.4 Char Rate Un-Instrumented Tests

From the 18 un-instrumented test results, cumulative charring rates for each test was calculated, and the average for each heat flux including both grain orientations was collated into Table 5.1 and graphed against time as shown in Figure 5.11.

Time (min)	35kW/m^2	50kW/m^2	65kW/m^2
20	0.75	0.89	1.09
40	0.67	0.79	0.90
60	0.61	0.71	0.80

Table 5.1 Average Char Rate for all Un-Instrumented Test

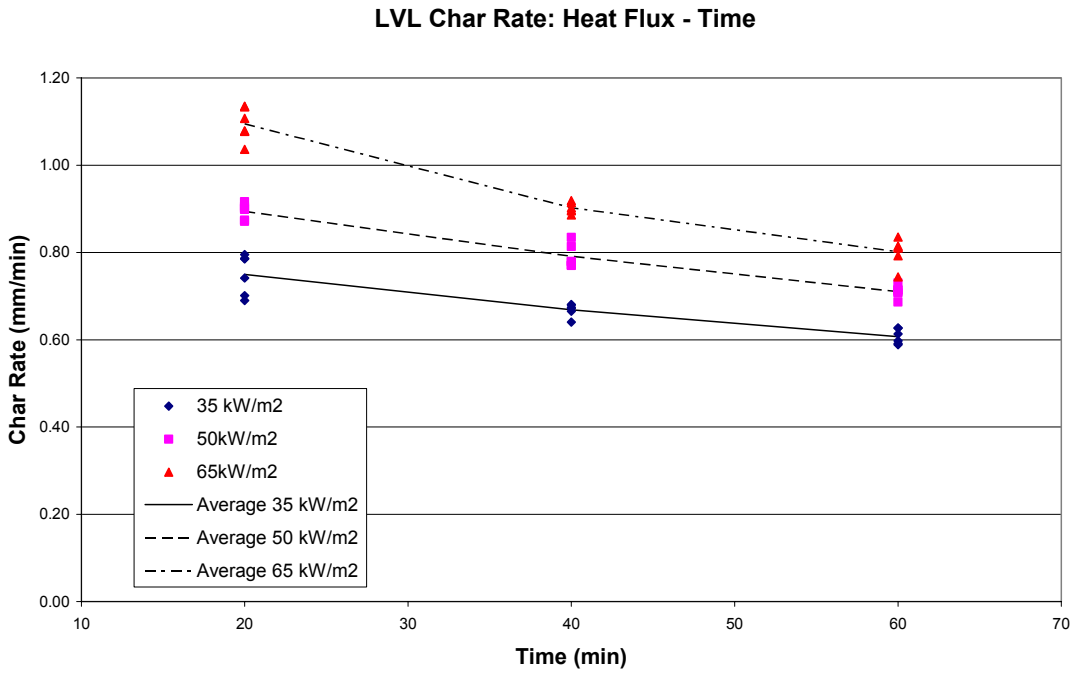

Figure 5.11: LVL Char Rate from un-instrumented cone calorimeter tests

Whites model was used for calculating the cumulative charring rate as described above in section 5.3, this was superimposed on the LVL char rate graph above and is shown Figure 5.12.

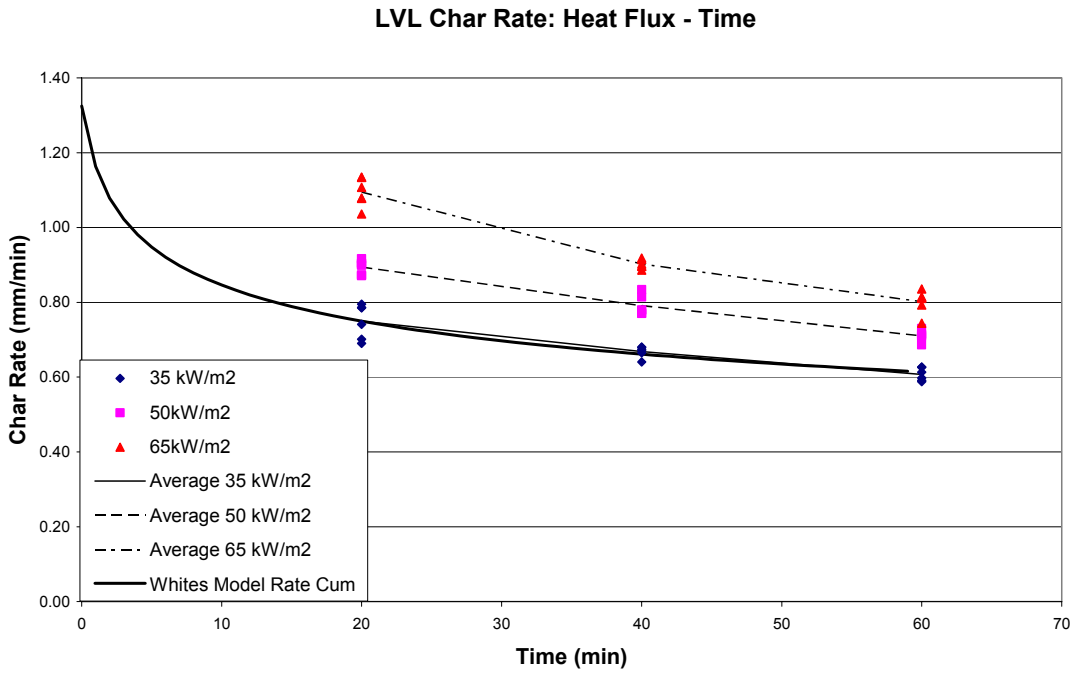

Figure 5.12: White's cumulative char rate superimposed on LVL Char Rate from un-instrumented cone calorimeter tests

As can be seen from Figure 5.12, White's model used with the appropriate densities and factors for the LVL tested, produces a curve for the cumulative charring rate that compared remarkably well to the charring rate found from tests performed at a heat flux of 35kW/m2 in the cone calorimeter.

5.5 Transverse Char Rate

The proposed testing of the charring rates for LVL involved testing the samples exposed in the cone calorimeter to face and edge grain, both of these directions are in fact still testing the charring rate parallel to the grain of the timber veneers within the LVL, as that is the most common form of member exposure in fire conditions. End grain exposure to fire and the resulting charring, is charring transverse to the grain, and is not usually considered in design methods as the ends of timber beams, columns, floors and joists are not as vulnerable to exposure. The ends of timber elements are normally enclosed or are protected by other timber members or claddings. However if fire exposure is a problem at the ends of timber members, then design aspects of beam column junctions, connections and beam seating requirements may be need specific design consideration under fire conditions.

Whilst performing the instrumented char tests on the edge grain samples at 35kW/m^2 heat flux exposure, one sample was inadvertently was end grain exposed. The sample had been cut out of the LVL with the wrong grain orientation. The charring was in fact transverse to the grain and not parallel to the grain. Refer Figure 5.13 which shows the end grain sample with the char not removed, note the significant shrinkage laterally.

It became very obvious that it was exposure to the end grain as ignition was equally the slowest tested at 1 minute and 14 seconds for this heat flux and after 4 minutes 50 seconds the flaming extinguished itself and the spark igniter was repositioned. With the ignition spark in place the surface began to flicker with flame from 6 minutes and 50 seconds, with an extreme glow appearing from 11 minutes 10 seconds and sustained flaming again being achieved from 11 minutes 40 seconds. The ignition spark was removed after 12 minutes. The strength of the surface flaming throughout the test was weaker in comparison to all other tests.

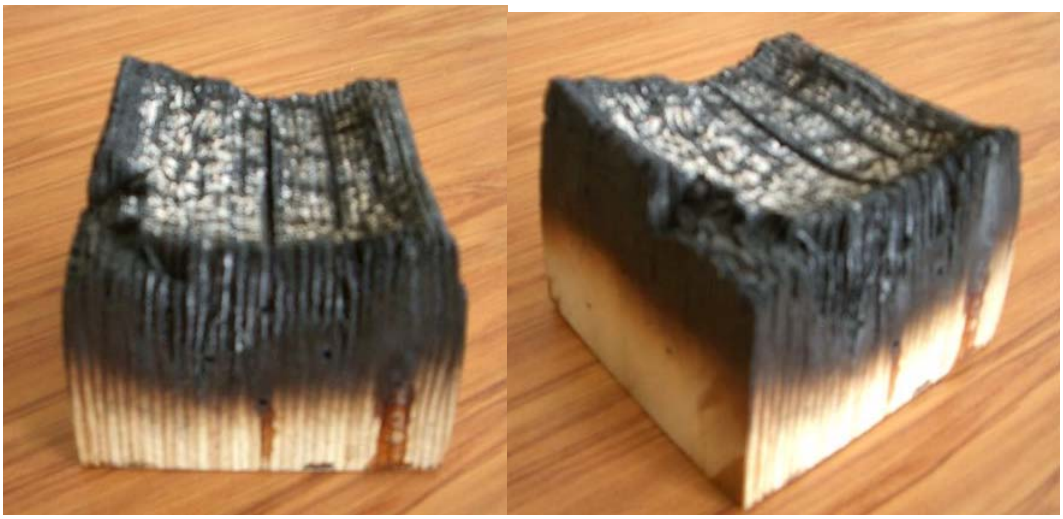

Figure 5.13: Two views: End grain sample exposed to 35kW/m^2 heat flux

5.5.1 Instrumented Temperatures for End Grain Sample

The graph shown in Figure 5.14 is the recorded temperatures for the 5 thermocouples in the end grain sample tested.

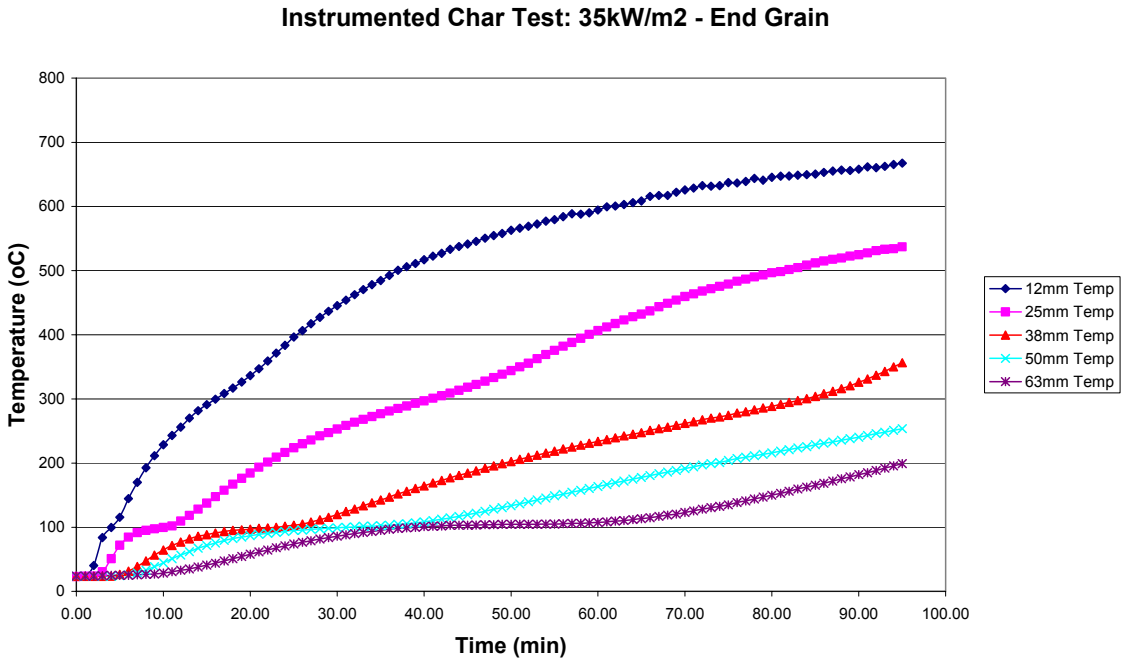

Figure 5.14 Instrumented Char Test 5 - 35 kW/m^2, End Grain

In comparison to both the face grain and the edge grain samples tested (Refer to Figures B1 – B6 in Appendix B), it can be seen that the gradients of the curves for temperature against time for each thermocouple position is far flatter.

It also can be seen that the length of the plateau regions of each curve corresponding to 100 ^{O}C is longer indicating that with this grain orientation it appears to be more difficult to drive off the excess moisture within the sample.

5.5.2 Instrumented Char Results for End Grain Sample

From the results of this test shown in Figure 5.14 the time for each thermocouple to reach 300^{o}C was extrapolated for each thermocouple depth and then the char depth plotted against time for the end grain at 35 kW/m^2, see Figure 5.15. The linear best fit regression line is also shown on figure 5.15. The slope of the regression line is the "best fit" charring rate for the end grain of LVL considering that only one test was performed.

End Grain Charring Rate = 0.44 mm/min.

This end grain charring rate is 65% of the mean cumulative charring rate found from the instrumented and un-instrumented tests, exposed to 35 kW/m2 heat flux.

Figure 5.16 shows the end grain instrumented char depth curve compared to all other instrumented face and edge grain results.

Note that the end grain char depth versus exposure time is significantly less than all other char depth results, and more significantly less than the face and edge grain results at the same heat flux of 35 kW/m^2.

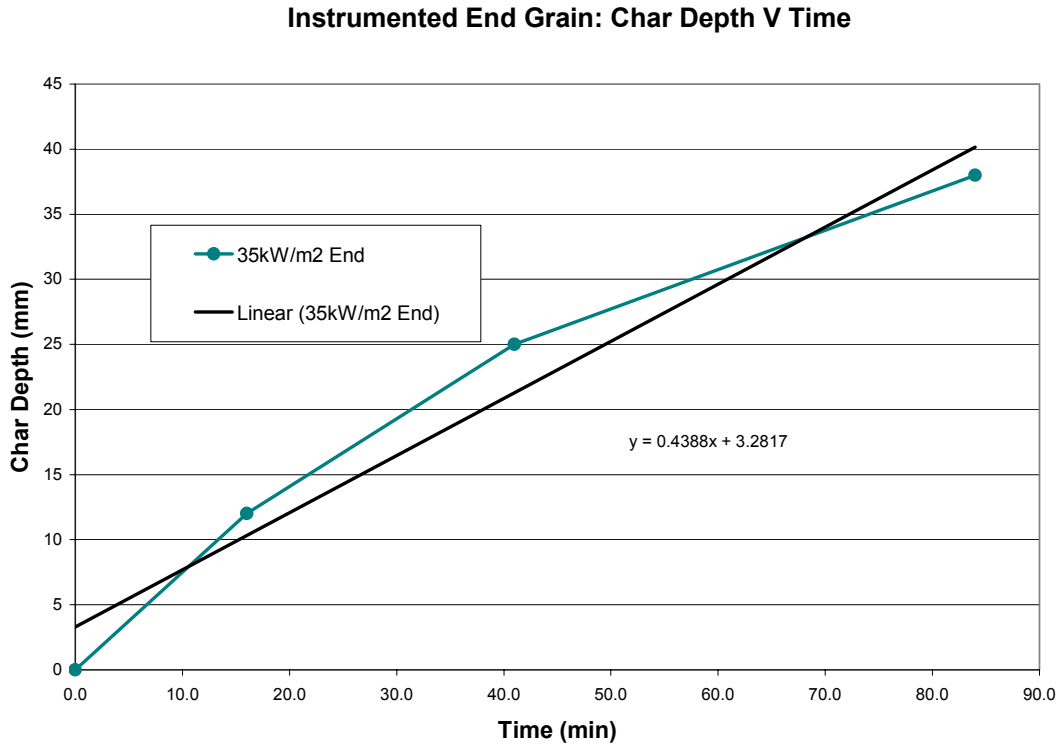

Figure 5.15 Instrumented char depths: 35 kW/m^2 - End Grain.

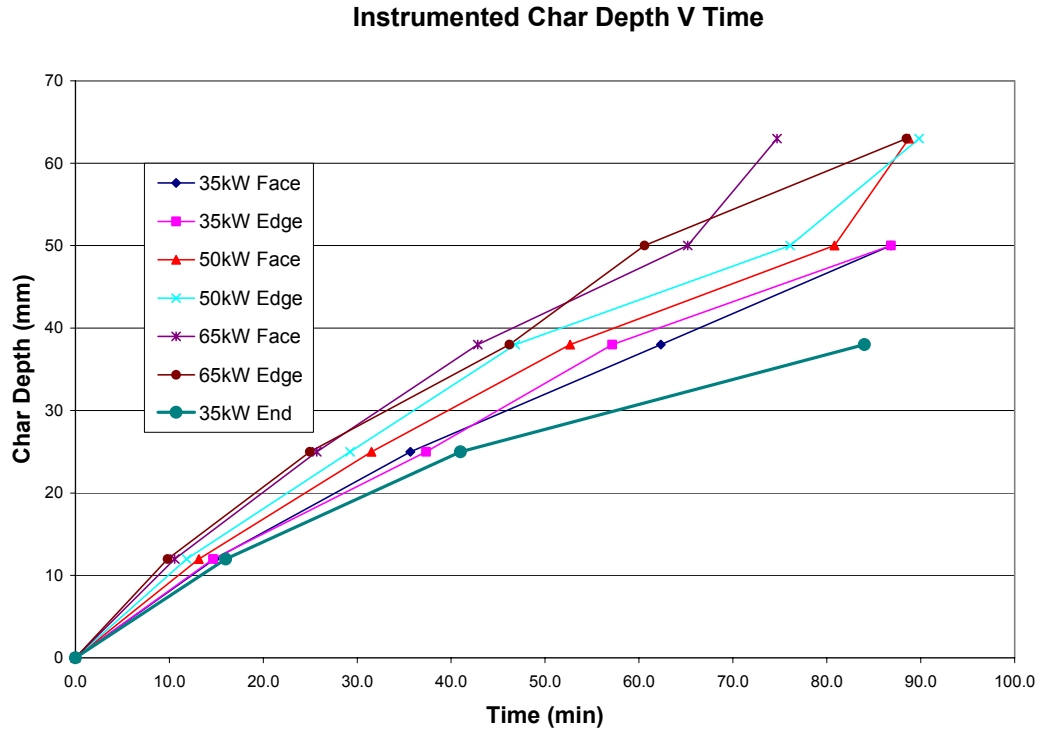

Figure 5.16: Instrumented Char Depth Results, including End Grain Test.

Chapter 6 Pilot Furnace Tests

This chapter describes the test and results of three pilot furnace tests on instrumented LVL beams exposed to the standard ISO 834 design fire curve were completed at the BRANZ Fire Research facility.

6.3 Test Procedure

In each of the tests the LVL beams were instrumented at sections located at third points along the beam with 12 thermocouples installed at depths of 18 mm and 36 mm. Refer to Appendix D for thermocouple layout and dimensions.

The thermocouples at the corners were exposed to the fire on two faces, whereas all other thermocouples essentially had single face exposure.

The layout of thermocouples replicates char rate tests carried out on glulam beams by Collier (1992): Charring Rates of Timber.

A typical instrumented section of LVL used in the pilot furnace tests is shown in the Figure 6.1

Figure 6.1 Thermocouple layout

Once the sections were instrumented the three sections of LVL where then glued back together using heat resistant resorcinol glue and cured for 24 hours. Refer Figure 6.2.

Density samples were taken from the off cuts of the LVL and stored with the beams whilst curing.

Figure 6.2 Resorcinol Glued Joint after thermocouples installed

The beams where then installed into a concrete specimen holder with an opening measuring 2.2 x 1.0 metres. A perimeter frame using LVL was required to pack the edges of the specimen holder so as the edges of the LVL framing and the top of the beam surfaces were flush allowing a true fit with no gaps.

Figure 6.3 shows the beam fixed into the specimen holder without any kao wool protection. A layer of fire resistant kao wool was placed between the concrete specimen holder and the LVL packing frame.

Note also the thermocouple wires extending from the instrumented sections of the beam at third points.

The exposed edges of the LVL packing frame where protected with kao wool (Refer Figure 6.4). The kao wool was glued to the exposed LVL edges to ensure that irradiance from the blackened surface of the charring LVL framing would not influence the charring rate of the LVL beam and that the exposure to the ISO 834 fire curve would be as true as possible.

Figure 6.3 Pilot Furnace Specimen Holder with LVL Beam installed in position

Figure 6.4 Base of LVL beam positioned in specimen holder with kao wool protecting exposed edge framing.

Figure 6.5 Assembled LVL beam installed in frame and clad with two layer of 12.5 mm Fyreline.

Two layers of 12.5 mm Fyreline Gibraltar Board was used to give a minimum of 60 minutes fire protection. The two layers of Gibraltar Board were nailed into position with an intumescent sealant between the Gibraltar Board and the LVL packing frame (Refer Figure 6.5).

The specimen holder was now orientated into a vertical position and fixed onto the pilot furnace using a specimen carriage that was pulled in against the furnace and bolted into position (Refer Figure 6.6).

Prior to the testing commencing the density samples where measured and weighed with dimensions and weights recorded. The samples where then placed in the oven for drying for density calculations (Refer Appendix A.2).

Each thermocouple was then attached to the electronic data recorder and the thermocouple numbers checked for position and recorded.

Figure 6.5 Specimen Holder in position to be attached to Pilot furnace.

6.4 Pilot Test No 1 & 2.

The LVL beams used in tests No1 & 2 were Hy-span with a section size measuring 300 x 105 mm. The beams were was instrumented at third points as already discussed and it was the aim of the test to last at least 60 minutes or longer until all thermocouple temperatures exceeded 300^{O}C.

6.2.1 Furnace Temperature

The furnace was started and controlled by hand operated valves varying the flow of fuel oil to the burners to expose the LVL beam to the fire design curve ISO 834. The following graph Figure 6.6 shows the temperatures of the individual thermocouples located within the furnace. (Refer to Appendix D for similar graphs for Tests 2 & 3.)

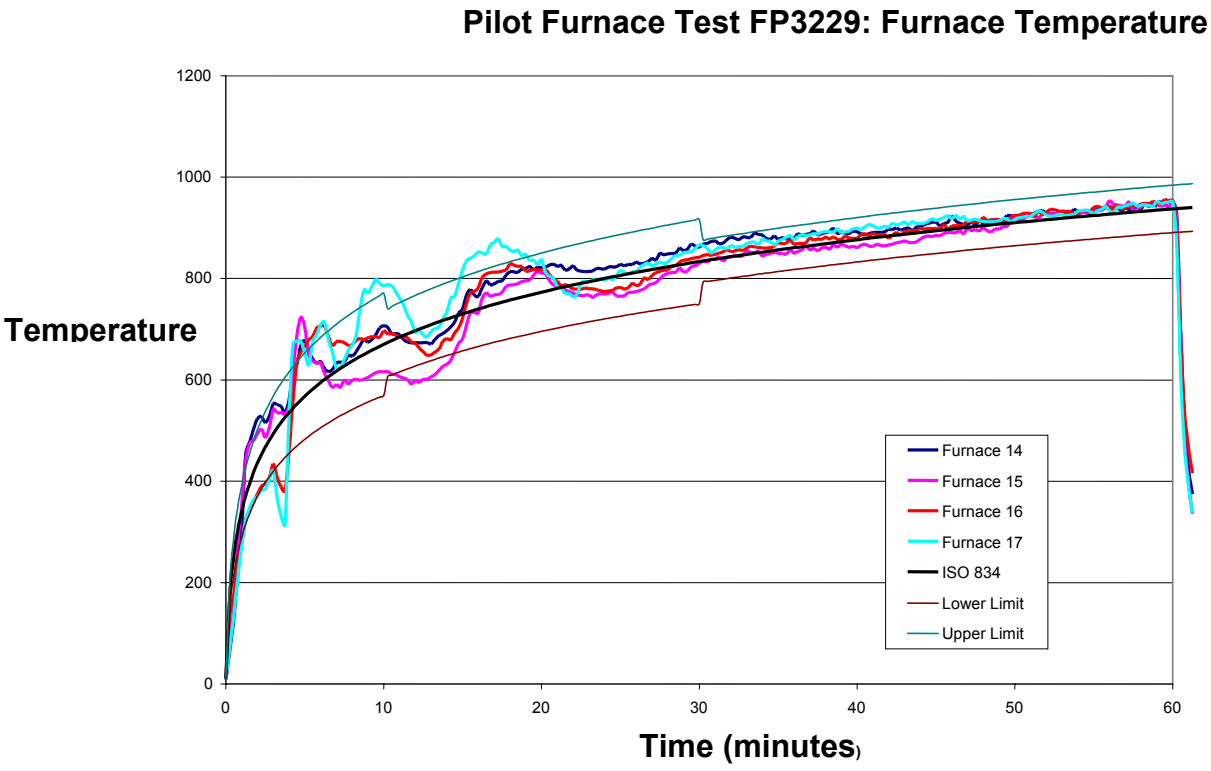

Figure 6.6 Furnace Thermocouple Temperatures for Test No: 1

The average temperature within the furnace is shown in figure Figure 6.7, where it can be seen that the average temperature is contained within the limits for the test procedure except for a minute around 5 minutes after test commenced.

Regulating the furnace temperature in the initial stages is difficult due to the initial combustion of the LVL beam itself, and the unknown contribution to the fuel source within the furnace. However, later in the test compensation for temperature variation within the furnace is easier to handle as shown by the more consistent results in the average furnace temperature recorded beyond 20 minutes (Refer Figure 6.7).

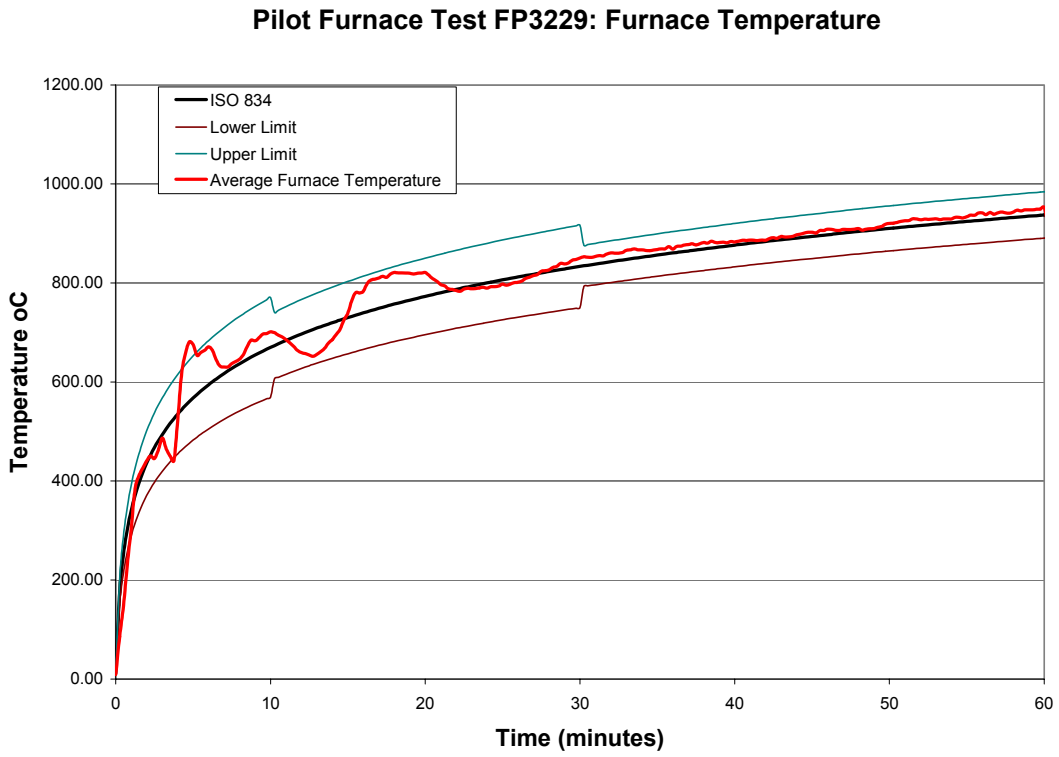

Figure 6.7 Average Furnace Thermocouple Temperature for Test No: 1

6.2.2 Observations Pilot Test No 1 & 2.

Once the furnace was lit and the test commenced the burning of the LVL beam within the furnace was observed through the small observation ports on each side of the furnace and to the rear, the following photos and comments were recorded. Pilot test 2, which benefited from the experience of test No 1, has the more complete record and will be discussed first.

The photo record for Test No 1 was not as complete during the test due to poor vision through the observation ports.

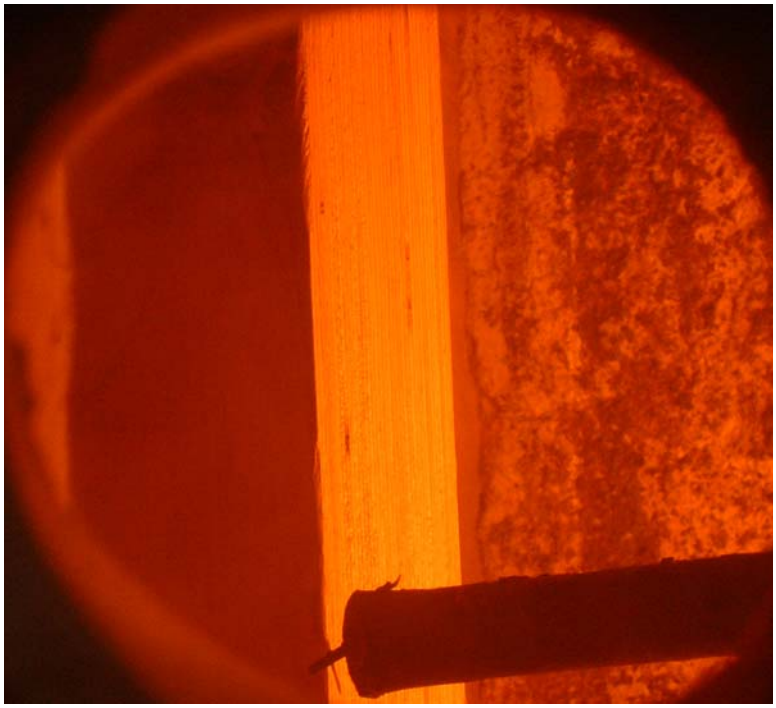

The initial photo through the upper observation port 1 of Test 2, see Figure 6.8, shows that the after 34 seconds of exposure that the beam has not started to blacken.

The tube like object in the bottom of Figure 6.8 is the tubular sheath that protects the furnace thermocouple.

Figure 6.8 LVL beam after 34 seconds after furnace ignited. Photo viewed from upper observation port 1.

This Figure above poses a very good question which is explained latter in the report and that is: When does the charring start in relationship to the start of the furnace and in reality the start of the fire?

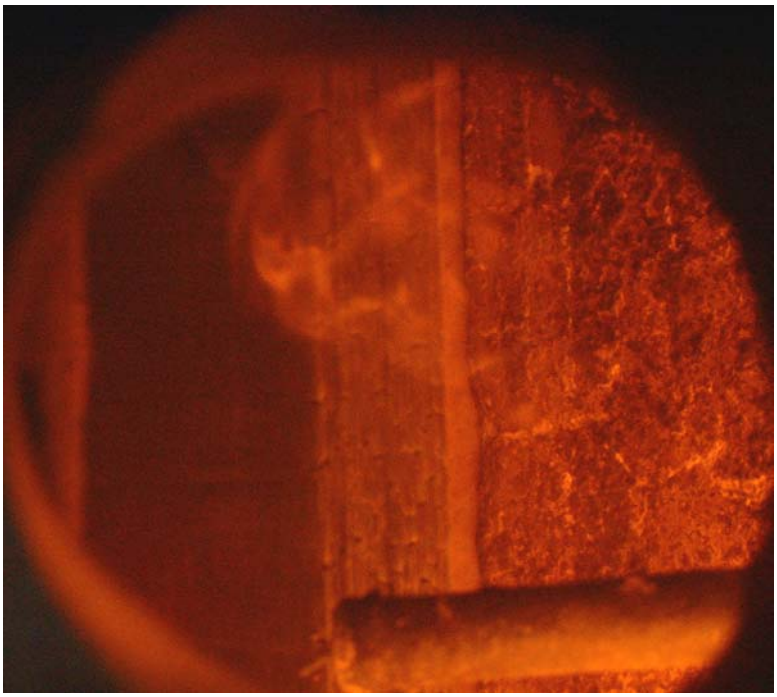

Figure 6.9 is a view from the same observation port 1 as in Figure 6.8 with a lapsed time of 3 minutes & 44 seconds. The beam has blackened significantly although surface ignition has not occurred.

Figure 6.9 LVL beam 3 minutes 44 seconds after furnace ignition. Photo viewed from upper observation port 1.

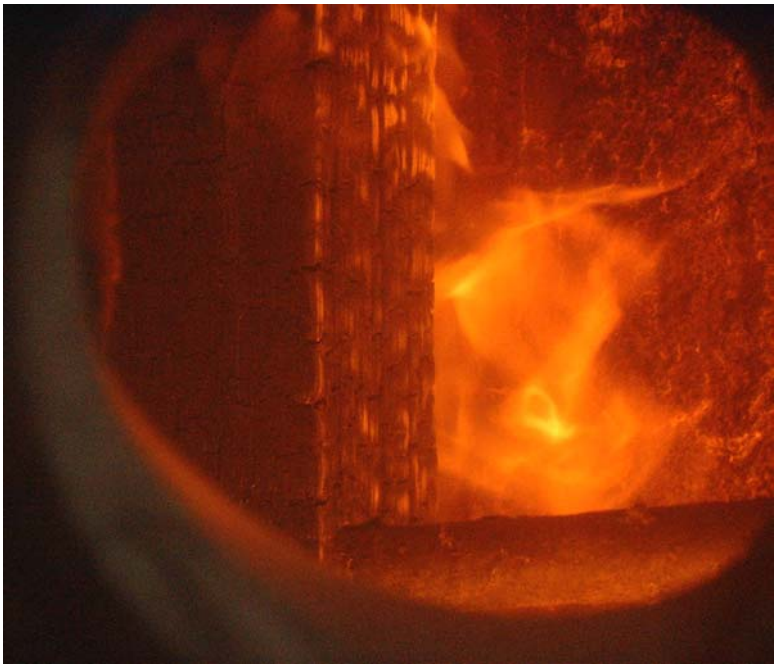

Figure 6.10 observation port 1 viewed after 8 minutes, shows the beam burning, with surface ignition and white ash forming on the underside surface of the charring beam.

Figure 6.10 LVL beam 8 minutes 0 seconds after furnace ignition Photo viewed from upper observation port 1.

Figure 6.11 shows the beam observed from upper central observation port 3, after 9 minutes & 16 seconds. Currently the beams surface is not ignited, but it has been. The presence of a reasonable quantity of white ash on the underside of the beam indicates that charring is well established, with significant shrinkage cracking developing.

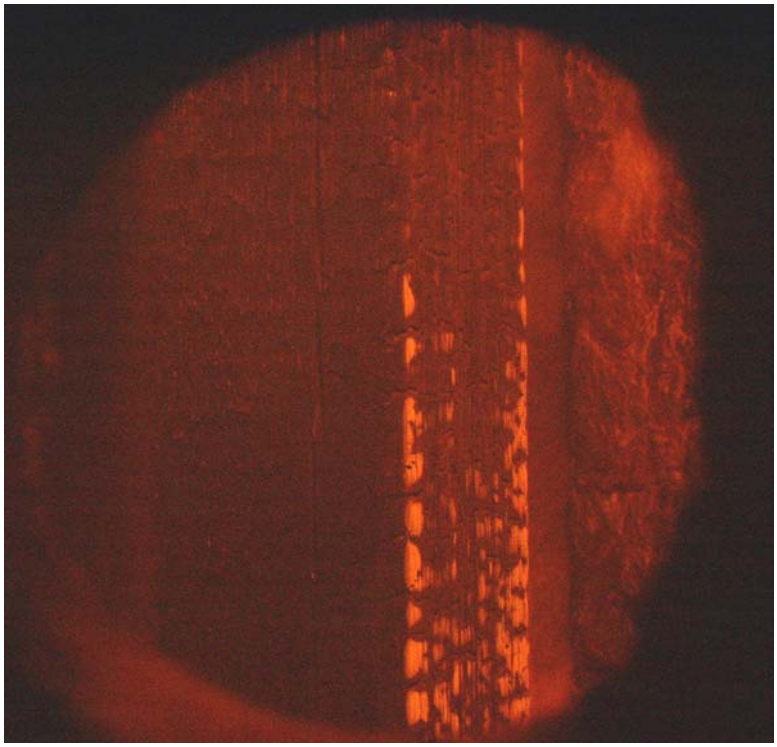

Figure 6.11 LVL beam 9 minutes 16 seconds after furnace ignition, Photo viewed from central observation port 3.

Figure 6.12 shows a view of the beam from the lower observation port 2, located on the opposite side of the furnace from previous photos.

This photo taken 25 minutes 14 seconds after furnace ignition shows the side of the beam, the Gibraltar Board Fyreline cladding and another furnace thermocouple. The side of the beam shows the crazed shrinkage cracking of the charring to the LVL beam.

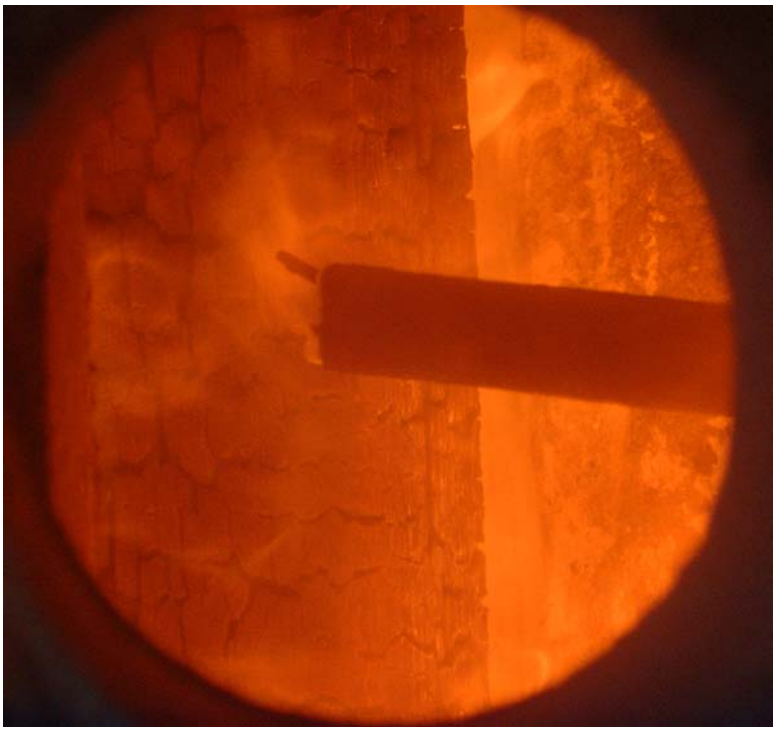

Figure 6.12 LVL beam 25 minutes 14 seconds after furnace ignition, Photo viewed from the lower observation port 2.

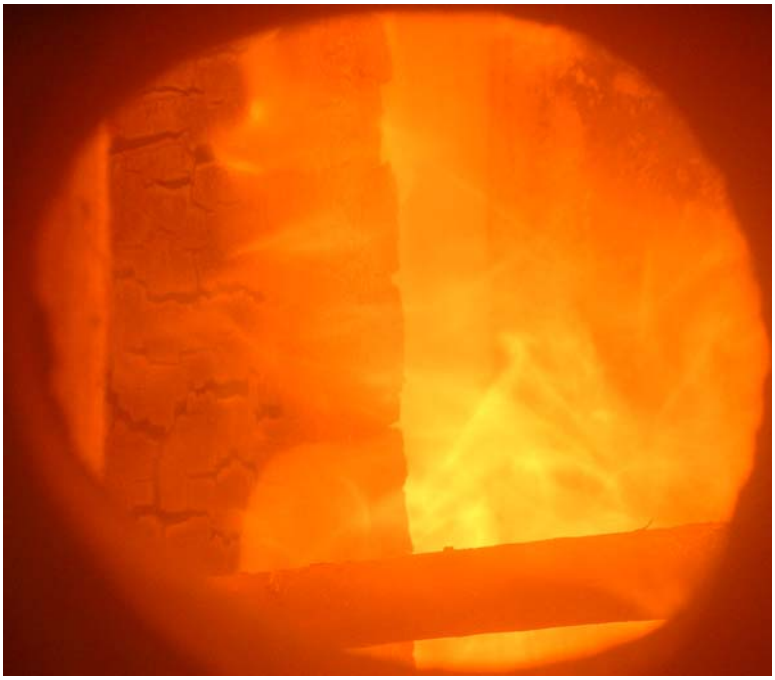

Figure 6.13 taken 55 minutes and 50 seconds after the furnace ignited and viewed from observation port 1 shows that a section of the LVL beam adjacent to the portal had collapsed with 2/3rds of the beam fallen away.

Photo 6.13 LVL beam 55 minutes 50 seconds after furnace ignition, Photo viewed from the upper observation port 1.

Figure 6.14 taken 56 minutes and 40 seconds after the furnace ignited and viewed from observation port 2, shows that a section of the LVL beam adjacent to the port is still in place whereas in Figure 6.13 a photo taken only a minute earlier, a section of the LVL beam had collapsed and fallen away.

The side and bottom of the beam exhibits the crazed shrinkage cracking of the advanced charring to the LVL beam.

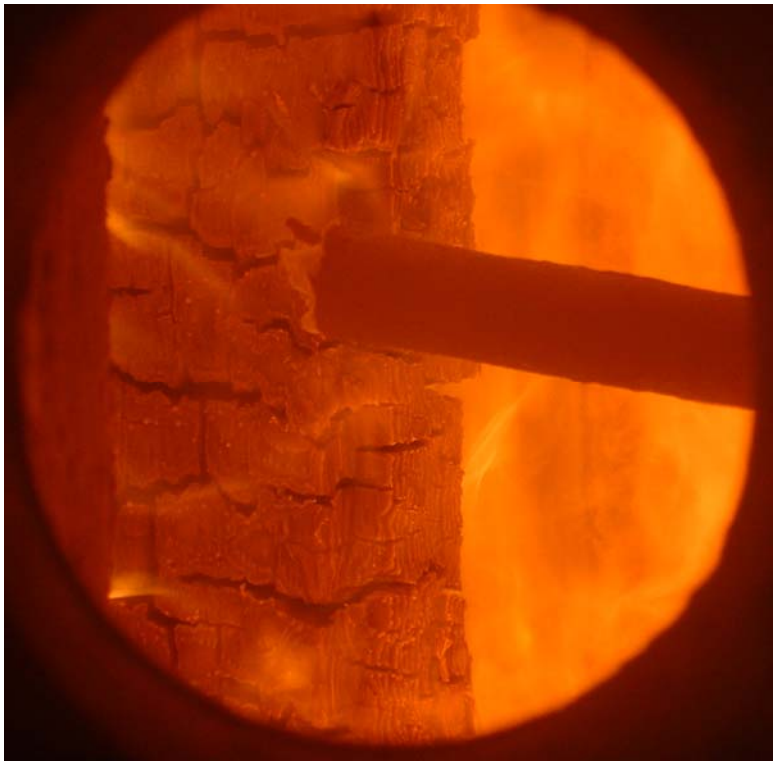

Figure 6.14 LVL beam 56 minutes 40 seconds after furnace ignition, Photo viewed from the upper observation port 2.

Figure 6.15 taken 1 hour 13 minutes and 32 seconds after the furnace ignited and viewed from observation port 2, shows the beam ready to collapse as the fire can be seen through the beam in the lower section of this photo. Soon after the section of the beam also collapsed and the test was stopped.

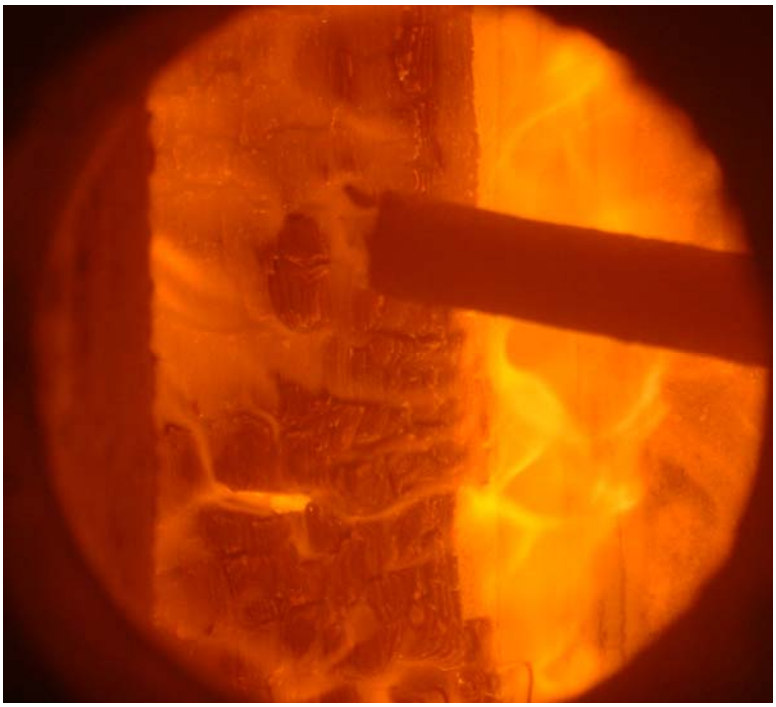

Figure 6.15 LVL beam 1 hour 13 minutes 32 seconds after furnace ignition, Photo viewed from the upper observation port 2.

Figure 6.16 shows what was left of the LVL beam after the test had ceased and the specimen holder released from the furnace. The duration of test no 2, lasted 1 hour 21 minutes and 30 seconds. This was longer than anticipated due to several of the thermocouples being connected in parallel with unused ambient thermocouples, which affected the temperatures displayed and recorded. Hence on the video display several of the thermocouples did not attain the 300 ^{O}C as planned, whereas in fact they had attain this temperature far earlier. This problem was easily corrected with the data modified to allow for the low temperatures recorded.

Figure 6.16 LVL beam test No2: 1 hour 23 minutes 20 seconds after furnace ignition, data logging stopped at 1 hour 21 minutes and 30 seconds.

.

Figure 6.17 LVL beam test No1: 1 hour 00 minutes 27 seconds after furnace ignition, data logging stopped at 60 minutes.

Figure 6.17 shows the LVL beam in test No1, which had test duration of 60 minutes, in comparison to the remains shown above for test No 2, the beam in test No1 had some residual section remaining.

The beam was immediately extinguished and the charring stopped. See photos in Figures 6.18 – 6.23 below

Figure 6.18 shows a close up view of the charred surface of the LVL beam in test No 1, immediately after the beam had been extinguished.
The beam was still in the pilot furnace specimen holder. Note the exposed thermocouples in the bottom of the photo.

Figure 6.18 Charred Surface Pilot Test No 1

Figure 6.19 shows a close up view of the charred surface with the beam removed from the specimen holder and cooled off enough to handle comfortably. Note the crazed pattern of the shrinkage cracking of the surface of the char, and the residual section remaining at the top of the beam.

Figure 6.19 Close View Charred Surface Test No: 1

Figure 6.20 shows the glued joint where the thermocouples were installed, the corner thermocouples exposed and the wires exiting the top of the LVL beam.

Figure 6.20 Charred Joint Pilot Test No 1

Figure 6.21shows the 12 thermocouple wires exiting the top LVL beam, and again the residual section remaining at the top of the beam.

Figure 6.21 Thermocouple Wire Top of Beam

Figure 6.22 shows the bottom of the charred LVL beam section, char is not removed and the two corner thermocouples were exposed.

Figure 6.22 Thermocouples Bottom of Beam

Figure 6.23 shows an oblique view of a section of the residual beam from Test No 1, against the original section tested.

Figure 6.23
Oblique View of Charred & Un-charred Section

6.2 Observations Pilot Test No 3

After the experiences of Pilot furnace tests 1 & 2, it was decided that a larger section would be an advantage to test a thicker LVL beam. Consequently two LVL Hy90 sections measuring 360 mm deep and 66 & 67 mm thick respectively, were glued together using a heat resistant resorcinol glue to provide a final section size of 360 x 133 mm, 2200 mm long. Refer Figure 6.24 showing the fabricated beam being installed into the pilot furnace specimen holder.

Figure 6.24 Shows fabricated LVL beam set up for Pilot Test No 3.

Note that for this test one instrumented section was moved from the 1/3rd point along the beam to the centre. This change to the location of the instrumented section was to test whether there were as any effects to the charring rate, due to temperature variation within the pilot furnace, by positioning the one instrumented section further away from the burner ports and position it in the centre. As a result it was concluded that the effects from possible temperature variation within the furnace were insignificant and did not appear to be a problem. It will be shown later in this section that the charred section was

visually uniform along the section and there was no significant differences in the recorded temperatures between the instrumented sections. The thermocouple layout in each instrumented section is as shown in Figure Figure 6.1 above, and as dimensioned in Appendix D.

Figure 6.25 shows a view of the glued joint in the LVL beam in specimen in Test No 3, between the two sections of Hy90 LVL and the slice cut to instrument the beam.

Figure 6.25 Glued Joint in Beam Test No 3.

Figure 6.26 shows the LVL beam for Test No 3 installed in the specimen frame ready to be fixed in position against the furnace.

Figure 6.26 LVL Beam Pilot Test No 3 in Specimen Frame

Photos taken through the observation ports during pilot Test No 3 were again not very clear and add little to the photos taken during Test No 2. The following Photos in Figures 6.27 – 6.3?, show the results of Test No 3.

Figure 6.27 LVL Beam still in specimen holder with Gibraltar Board cladding removed

Figure 6.28 shows the charred section of Test No 3 at the instrumented section located at the upper 1/3rd point on the beam. Note corner thermocouples are exposed.

Figure 6.28
Upper Joint Test No 3

Figure 6.29 shows central instrumented section from under the beam.
Note that here the thermocouples in the corners are just showing through the char.

Figure 6.29 Central Joint Pilot Test No 3.

Figure 6.30 shows the upper instrumented section of the beam with all the char removed, note the thermocouples have been placed back in approximately their true positions. Note also the charred section is very uniform along the beam.

Figure 6.30 Upper Instrumented Section of the Beam Char Removed

Figure 6.31 Shows a face on view of the section shown in photo 6.30.

Note that the performance of the glued joint was good for the duration of this test and no perceptible cupping or opening of the transverse joint occurred.

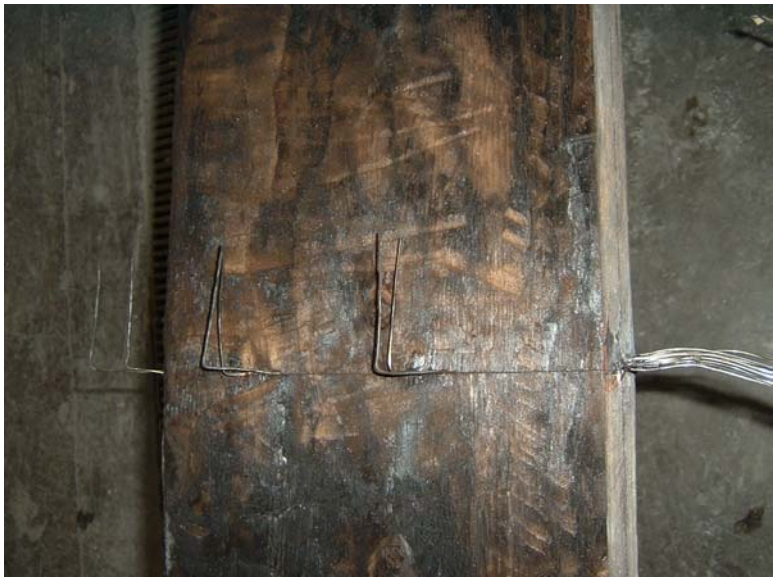

Figure 6.31 Face of Beam Section at Joint, Char Removed.

Figure 6.32 shows the central instrumented section viewed from below with the thermocouples placed approximately in their original position.

Figure 6.32 Central Joint Thermocouples Exposed.

This Figure 6.32 gives a good indication of the char depth in relation to the thermocouple positions. Note also that the longitudinal glued joint performed very well and is almost imperceptible.

Figure 6.33 shows the central instrumented section broken on the glued joint line. Grooves cut for the sheathed thermocouple can be seen.

Figure 6.33 Glued Joint Test No 3, Broken on Glue Line.

Figure 6.34 Residual Sections Test No 3.

Figure 6.34 shows two slices of the residual section of the LVL beam from pilot Test No 3.

6.4 Pilot Tests Results

6.4.1 Temperature Gradients within LVL Beam Section

The electronic data logging recorded temperatures for each thermocouple at 0.25 minute intervals and from the results the temperature rise was graphed against time for each location. The temperature rise for all the thermocouples shown on a single graph would be very congested and meaningless, so thermocouples in similar positions within the LVL beam have been grouped together to provide a more meaningful result.

For pilot furnace test No 1 the following graphs, Figures 6.35 – 38 show thermocouple temperatures plotted against time in positions according to depth of the thermocouple and also whether it was on a corner having double face exposure, of along the side of the LVL beam essentially having only single face exposure.

In Figures 6.35 – 38, it can be seen that in all thermocouple positions there is a plateau in the temperature – time lines at 100 ^{O}C, this is explained above by the moisture within the LVL beam sections being driven off as steam.

The densities of two samples taken from each pilot test beam have been tabulated and are shown in Appendix A2; Table 6.1 shows a summary of densities and moisture contents.

Pilot Tests	Density of samples						
Test Sample	Weight Un-Dried kg	Density Dg Un-Dried kg/m3	Weight Oven Dry kg	Density Db,x Basic kg/m3	Moisture x Oven Dry %	Volume Oven Dry m3	Density Dod Oven Dry kg/m3
Pilot 1 Sample 1	0.944	611.60	0.844	546.81	11.85%	0.0015	562.74
Pilot 1 Sample 2	1.824	596.96	1.639	536.41	11.29%	0.002983	549.48
Pilot 2 Sample 1	1.824	590.86	1.634	529.32	11.63%	0.003007	543.35
Pilot 2 Sample 2	1.858	591.32	1.661	528.62	11.86%	0.003059	543.05
Pilot 3 Sample 1	1.402	605.48	1.245	537.68	12.61%	0.002266	549.32
Pilot 3 Sample 2	1.46	629.98	1.297	559.65	12.57%	0.002261	573.64

Table 6.1 Summary of Densities and Moisture Contents for Beams Tested in the Pilot Furnace.

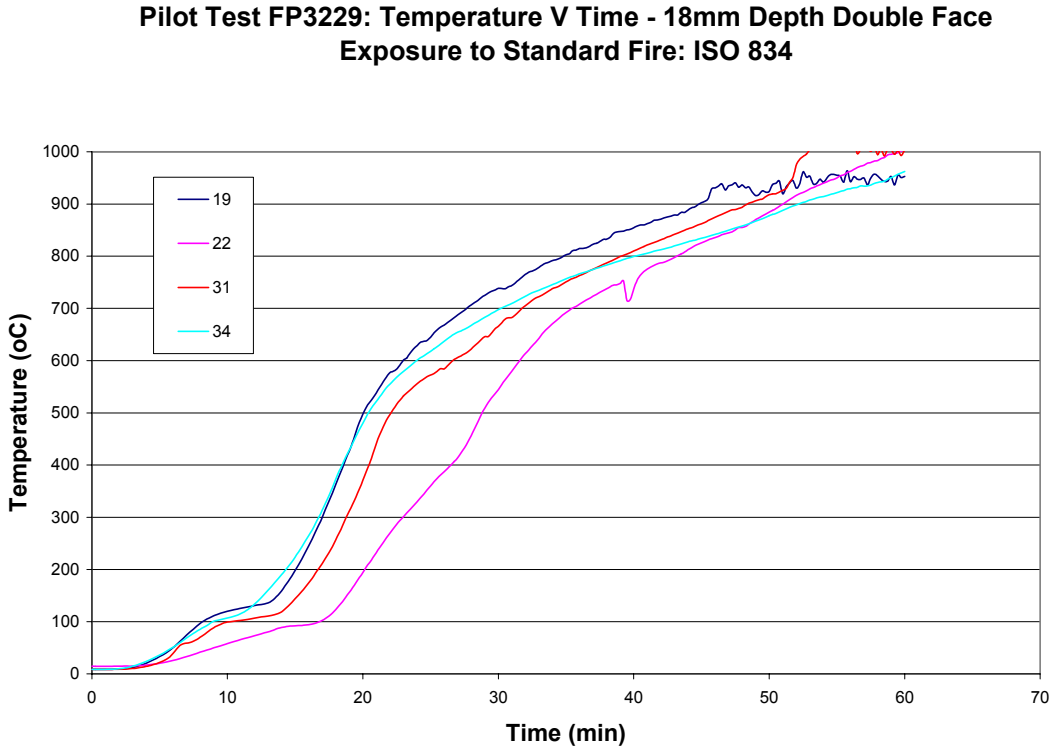

Figure 6.35 Pilot Test No: 1, Double face Exposure – 18 mm Depth

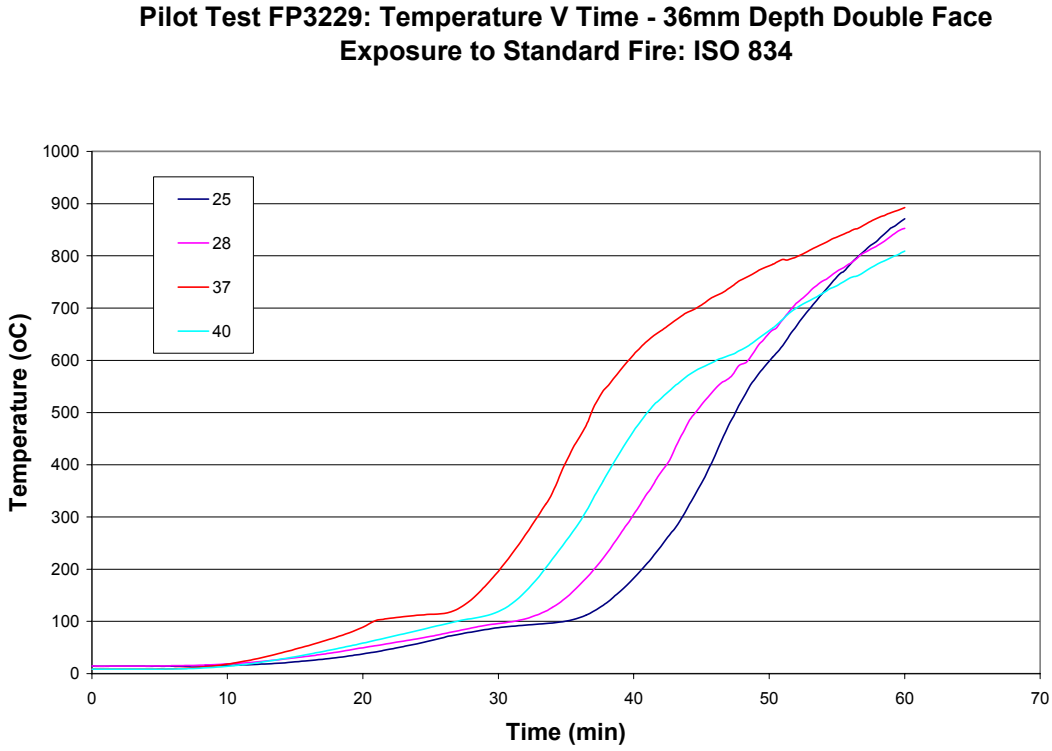

Figure 6.36 Pilot Test No: 1, Double face Exposure – 36 mm Depth

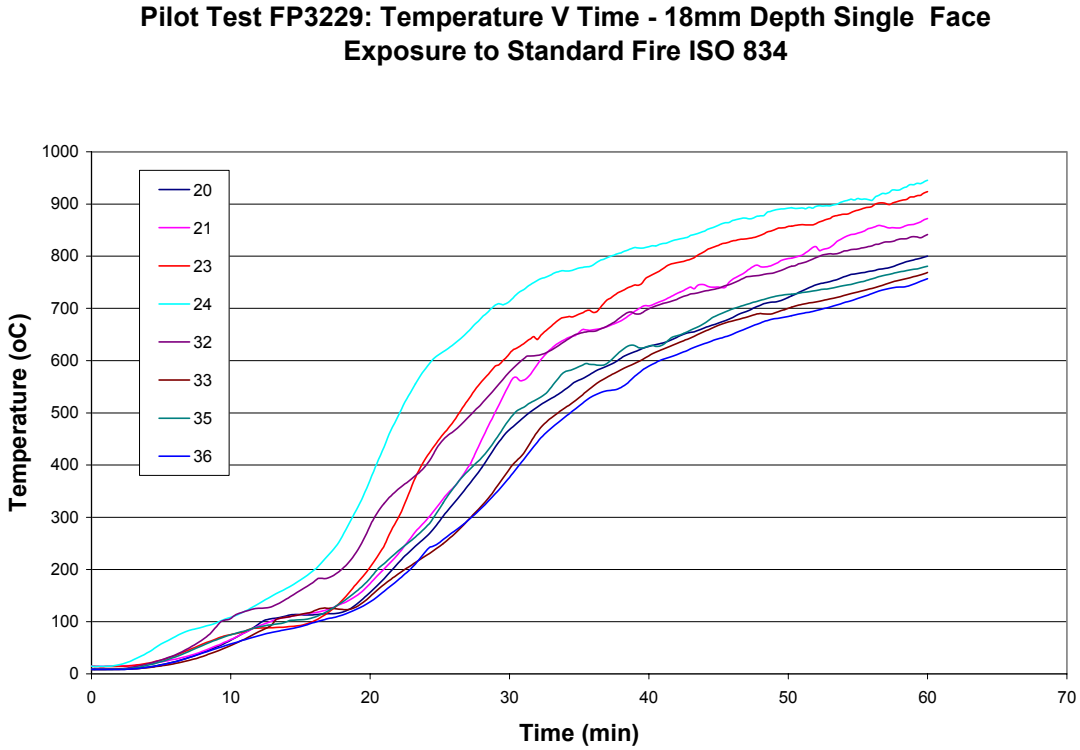

Figure 6.37 Pilot Test No: 1, Single face Exposure – 18 mm Depth

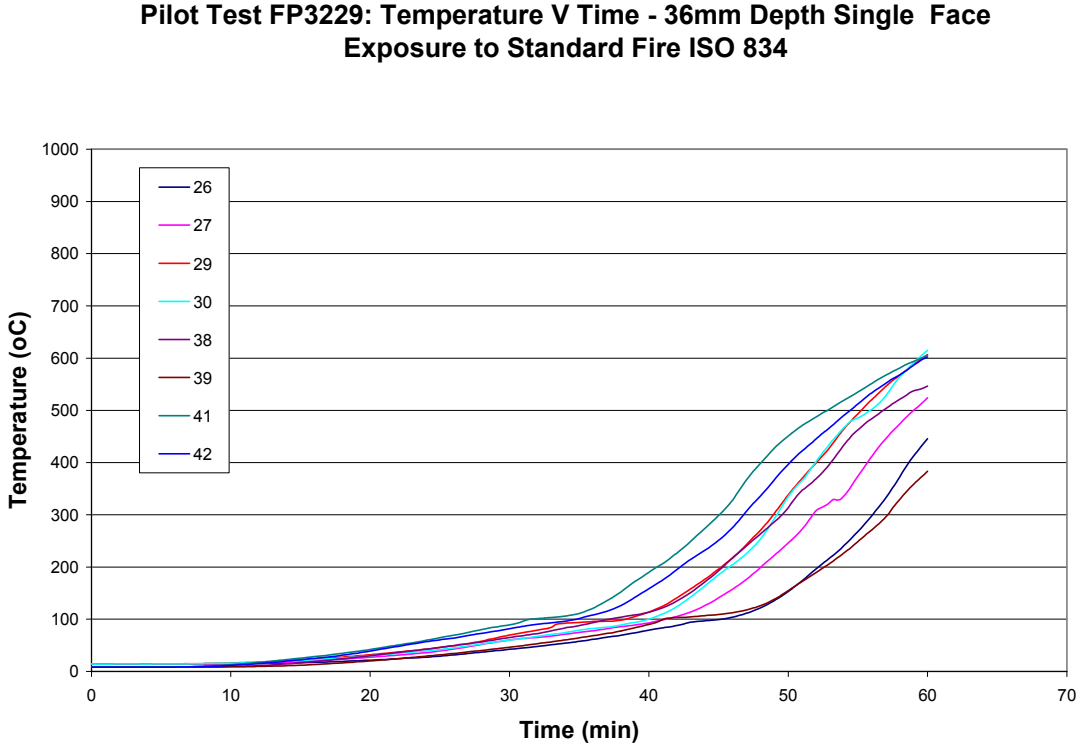

Figure 6.38 Pilot Test No: 1, Single face Exposure – 36 mm Depth

The duration of pilot test No 1 was long enough for the temperature at all thermocouple positions to exceed 300 ^{O}C, and by doing so the time for the char front to reach each thermocouple site was obtained by interpolation of the time – temperature lines in Figures 6.35 – 38.

Graphs similar to Figures 6.35 – 38, for pilot tests No2 and No3, are shown in Appendix D.4.

6.4.2 Pilot Test Variations

Pilot test No 3 was performed on a larger section size (360 x 133 mm) than tests 1 & 2 (300 x 105 mm), and the corresponding times for the thermocouples in Test No 3 to reach the 300 ^{O}C temperature that depicts the char front was marginally slower. For the 18 mm thermocouple depth, 8 of the 12 thermocouples were slower by an average time of up to 13 % and for the 36 mm thermocouple depth, 10 of the 12 thermocouples were slower by an average time of up to 20 % for the worst discrepancy. However even comparing the variations between test No 1 & No 2, variations in comparison times varied from - 8% to + 10 %.

These results tend to indicate that there is a trend for the char rate in larger sections to be slower, however more testing will be required to confirm this, and thus the results of all 3 pilot furnace tests were averaged to provide an overall charring rate for LVL.

6.4.3 Pilot Furnace Test Char Rates

From the results of the pilot furnace tests the time for each thermocouple to reach 300^{O}C was extracted from the information and collated in tables. Refer Table 6.2 & Table 6.3.

TC	Test 1 & 2 Depth X mm	Depth Y mm	Pilot Test 1 Time to 300°C min	300 x 105 Char Rate mm/min	Pilot Test 2 Time to 300°C min	300 x 105 Char Rate mm/min
19*	18	18	17.00	1.06	21.25	0.85
20	18	100	25.20	0.71	27.45	0.66
21	18	200	24.20	0.74	24.90	0.72
22*	18	18	22.95	0.78	20.05	0.90
23	18	100	22.05	0.82	24.65	0.73
24	18	200	18.75	0.96	22.50	0.80
25*	36	36	43.60	0.83	38.65	0.93
26	36	100	56.05	0.64	52.80	0.68
27	36	200	51.75	0.70	45.85	0.79
28*	36	36	39.90	0.90	34.20	1.05
29	36	100	48.95	0.74	42.75	0.84
30	36	200	49.20	0.73	48.00	0.75
31*	18	18	18.80	0.96	19.50	0.92
32	18	100	20.35	0.88	23.90	0.75
33	18	200	27.25	0.66	24.85	0.72
34*	18	18	16.75	1.07	16.80	1.07
35	18	100	24.60	0.73	27.10	0.66
36	18	200	27.30	0.66	23.30	0.77
37*	36	36	32.90	1.09	42.20	0.85
38	36	100	49.55	0.73	55.00	0.65
39	36	200	57.15	0.63	49.85	0.72
40*	36	36	36.25	0.99	35.30	1.02
41	36	100	45.05	0.80	42.00	0.86
42	36	200	46.80	0.77	45.85	0.79

Table 6.2 Time for each Thermocouple to Reach 300°C Temperature Pilot Furnace Tests No 1 & No 2.

Note: TC – Thermocouples marked with * indicates double faced exposure, i.e. located at corners.

TC	Test 3 Depth X mm	Depth Y mm	Pilot Test 3 Time to 300°C	360 x 133 Char Rate mm/min
19*	18	18	18.75	0.96
20	18	120	33.50	0.54
21	18	240	27.25	0.66
22*	18	18	23.75	0.76
23	18	120	28.10	0.64
24	18	240	21.40	0.84
25*	36	36	45.20	0.80
26	36	120	59.10	0.61
27	36	240	57.65	0.62
28*	36	36	44.80	0.80
29	36	120	49.75	0.72
30	36	240	49.40	0.73
31*	18	18	15.50	1.16
32	18	120	26.40	0.68
33	18	240	33.10	0.54
34*	18	18	22.55	0.80
35	18	120	26.55	0.68
36	18	240	28.80	0.63
37*	36	36	46.25	0.78
38	36	120	62.25	0.58
39	36	240	64.55	0.56
40*	36	36	39.00	0.92
41	36	120	51.10	0.70
42	36	240	67.10	0.54

Table 6.3 Time for each Thermocouple to Reach 300°C Temperature Pilot Furnace Test No 3.

Note: TC – Thermocouples marked with * indicates double faced exposure, i.e. located at corners.

From the Tables 6.2 and 6.3 above the average char rates for the thermocouples located at 18 mm and 36 mm respectively were taken for double and single face exposure and graphed. See table 6.4 and refer to Figure 6.39.

Exposure	Single Face	Double Face
Thermocouple Depth mm	Cumulative Char Rate mm/min	Cumulative Char Rate mm/min
18 18 36 36	0.74 0.70 0.71 0.69	0.88 1.00 0.89 0.94

Table 6.4 Average Cumulative Char Rates.

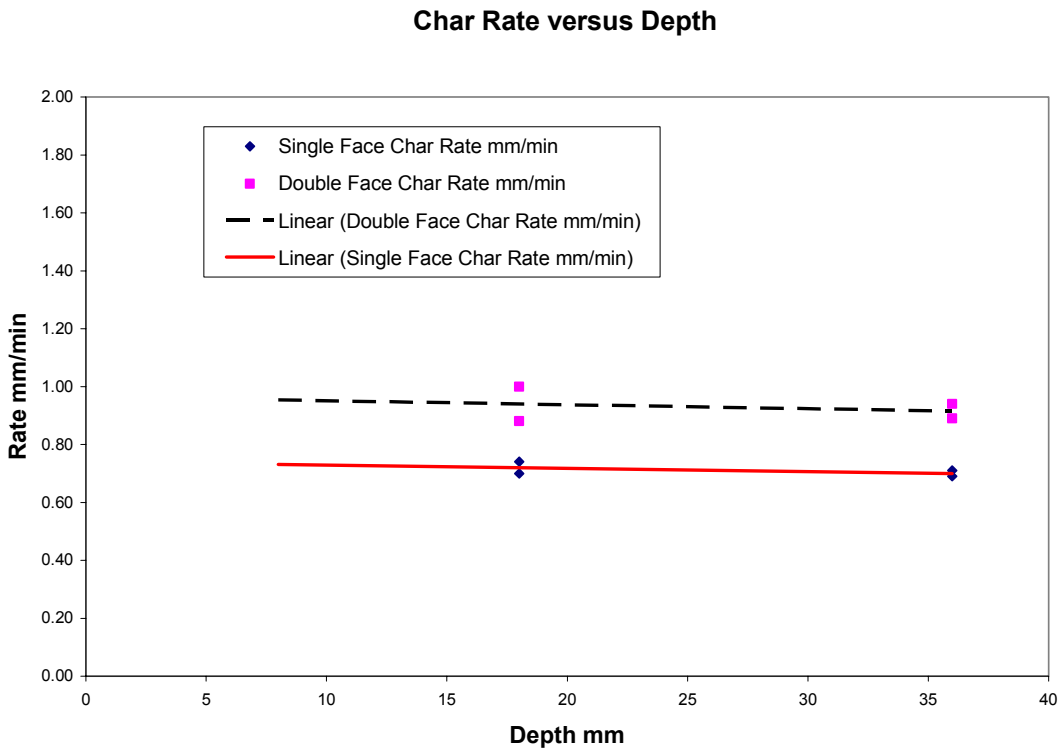

Figure 6.39 Graph Char Rate for Pilot Furnace Tests

Cumulative charring rates for single face exposure from the pilot test, which were subjected to ISO 834 design curve, were calculated and the results averaged for the 18 &

36 mm depths. The average char rate obtained from the 3 pilot tests varied from β = 0.72 mm/min at 18mm depth to β = 0.70 mm/min at 36 mm depth.

Using the rates above for the single face exposure they were superimposed on Figure 5.11; the LVL Char Rate from un-instrumented cone calorimeter test, as shown on Figure 6.40.

The current design charring rate of β = 0.65 mm/min from NZS 3603: 1993 - Code of practice for Timber Design, Standards Association of New Zealand, is also superimposed on Figure 6.40.

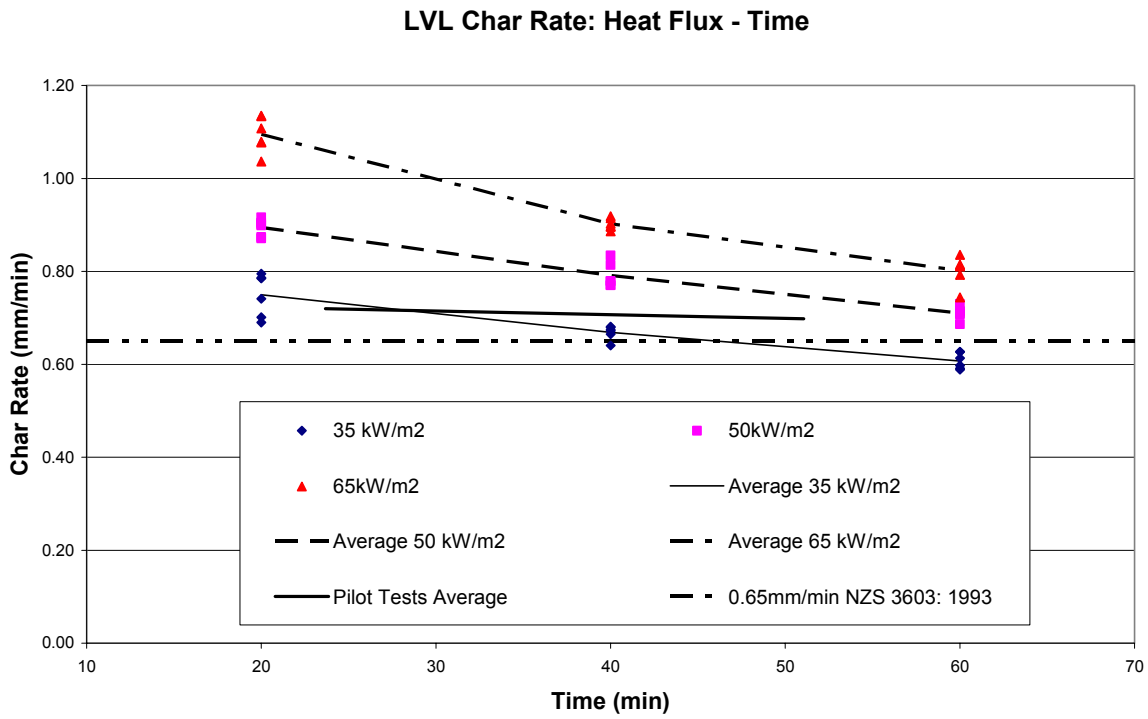

Figure 6.40 LVL Char Rate from un-instrumented cone calorimeter tests, with comparisons to Pilot furnace test exposed to the ISO 834 design curve & NZS 3603: 1993 charring rate.

6.4.4 Pilot Furnace Char Rate Comparison with Cone Calorimeter Char Rates

Comparing the overall char rate obtained from the cone calorimeter at heat fluxes 35, 50 & 65 kW/m^2 and exposure to the ISO 834 Design Fire Curve of the pilot test, it can be

seen that exposure to the ISO 834 curve equates closely to an irradiance of 35 kW/m^2 in the cone calorimeter. Refer to Figure 6.40.

6.4.5 Comparison of White's Char Model to Pilot Furnace Test Char Results

As already discussed in chapter 5, R H White (Refer Appendix F) developed a model for estimating the char depth with time, charring rate and the cumulative charring rate. The model allowed for differing density of timber, moisture content and a factor for the hardness of the timber. In Figure 6.41 White's Model is compared to the single face exposure results from the three pilot tests undertaken on the LVL beams. It can be seen from Figure 6.41 that very good correlation was attained.

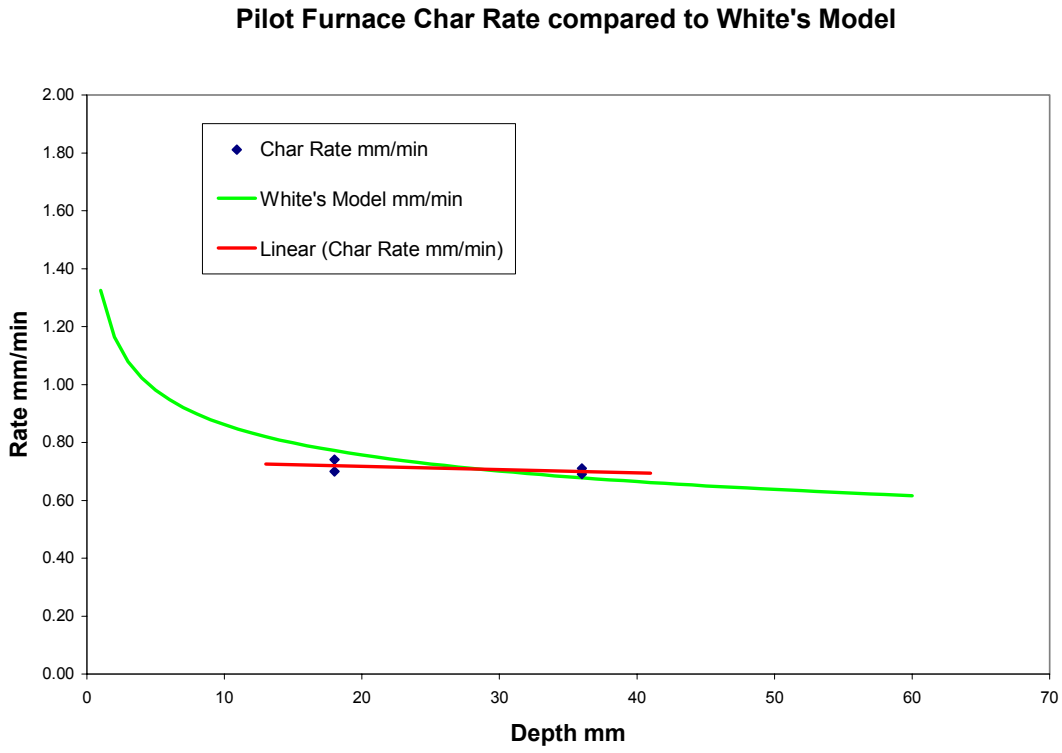

Figure 6.41 Pilot Furnace Char Rate compared to White's Model.

6.4.6 Evaluation of Zero Strength Zone below Charred Surface.

From the pilot test results the time lag at each thermocouple between recording 100^{o}C and 300^{o}C was evaluated. (Refer table H1 – H3, in Appendix H, where the results for each individual thermocouple has been tabulated.)

The lag time was multiplied by the cumulative charring rate for that particular thermocouple to calculate the thickness of LVL at a temperature over 100°C. This layer of material is likely to have reduced mechanical properties because of the elevated temperatures. The estimated thickness of the temperature-affected material varied from 6 to 13 mm, with an average thickness of 9 mm. This information is useful because some design methods require an estimate of the thickness of zero-strength heated wood below the char layer. The Australian timber codes (1990) & (1997) states that a zero-strength layer thickness of 7.5 mm should be used, which is consistent with the findings of this study, recognising that not all of the wood between 100°C and 300°C will have zero strength. Table 6.5 shows a summary of the thickness zero strength zones evaluated.

Zero Strength Zone	**Thickness: Summary Table**			
Test No	**1**	**2**	**3**	**units**
Beam size	300 x 105	300 x 105	360 x 133	mm
18 mm Double Face	5.75	7.67	8.72	mm
36 mm Double Face	8.94	8.38	13.09	mm
18 mm Single Face	7.82	6.65	8.93	mm
36 mm Single Face	8.34	7.49	11.14	mm
Average thickness	7.71	7.55	10.47	mm

Table 6.5 Estimated Zero Strength Zone.

From the results it can be seen that the average estimated zero strength zones for the 105 mm thick beams tested in pilot furnace tests 1 & 2 compared very well. The average estimated zero strength zones for the 133 mm thick beam in pilot test 3 were significantly thicker.

With the beam section in test No 3 being 27% thicker section than the beams in tests No 2 & 3, the corresponding increase in the thickness of the average estimated zero strength zones was 38%. However there was also a variance in the charring rates that may have an effect. For the 36 mm deep thermocouples there was up to a 20% variation in difference in the charring rate between the thicker beam in test No 3 and the smaller beams in tests No's 2 & 3 and for the 18 mm depth thermocouples there was up to 13 % variation. Therefore it appears that the thickness of the zero strength zone located beneath the char base, may be affected by the rate of charring, the thickness of the remaining un-charred wood and the original section size of the beam.

To establish a better understanding of this zero strength zone beneath the char base, further testing will be required to identify the significant factors involved.

Chapter 7 Load Test: Full Size Furnace

In this chapter the charring rate developed from the char testing in the cone calorimeter and the pilot furnace tests is to design a full scale loaded test on a large LVL beam in the full size furnace exposed to the ISO fire curve. The LVL beam tested measured section size of 305 x 400 mm, was simply supported over a span of 4.4 metres and subjected to a central point load of 30kN. Refer to Figures 2.9 – 2.11 in chapter 2 for beam installation into the furnace and the used of the reaction frame to apply the load.

The average char rate obtained from the 3 pilot tests varied from $\beta = 0.72$ mm/min at 18mm depth, to $\beta = 0.70$ mm/min at 36 mm depth. Using this maximum char rate ($\beta = 0.72$ mm/min) the loaded test in the full scale furnace was designed as described below.

7.2 Beam Properties and Design

7.2.1 Modulus of Elasticity

Initially the beam was subjected to a bending test to establish the modulus of elasticity ('E') of the beam as shown in Photo 7.2. The beam was subjected to a known weight and the deflection measured to enable the 'E' value to be calculated. The weight used in the modulus of elasticity ('E') test was a concrete specimen frame from the pilot furnace. The frame was suspended by the BRANZ gantry crane with a load cell fitted above the hook to measure the total weight of the frame and assembly.

Figure 7.1 Load Cell and Deflection Gauge used in 'E' Test

After the weight of the frame was recorded, then the frame was positioned centrally on the LVL beam and the deflection measured with a gauge fitted under the beam, measuring the deflection at midspan relative to the concrete floor as shown on Figure 7.1.

Figure 7.2 Modulus of Elasticity Test on Beam

From the 'E' value calculated (refer to Appendix E1) and using the relationship between mean bending stress and modulus of elasticity as shown in Figure 7.3 which has been derived from two LVL Properties Evaluation Documents supplied by Carter Holt Harvey Ltd (2001) a value for the mean bending strength for the beam being tested was obtained. See Figure 7.1 for graph of mean bending strength against modulus of elasticity.

Using the mean bending stress the ultimate section capacity of the LVL beam was calculated and the test moment applied to the beam was assessed. (Refer Appendix E2)

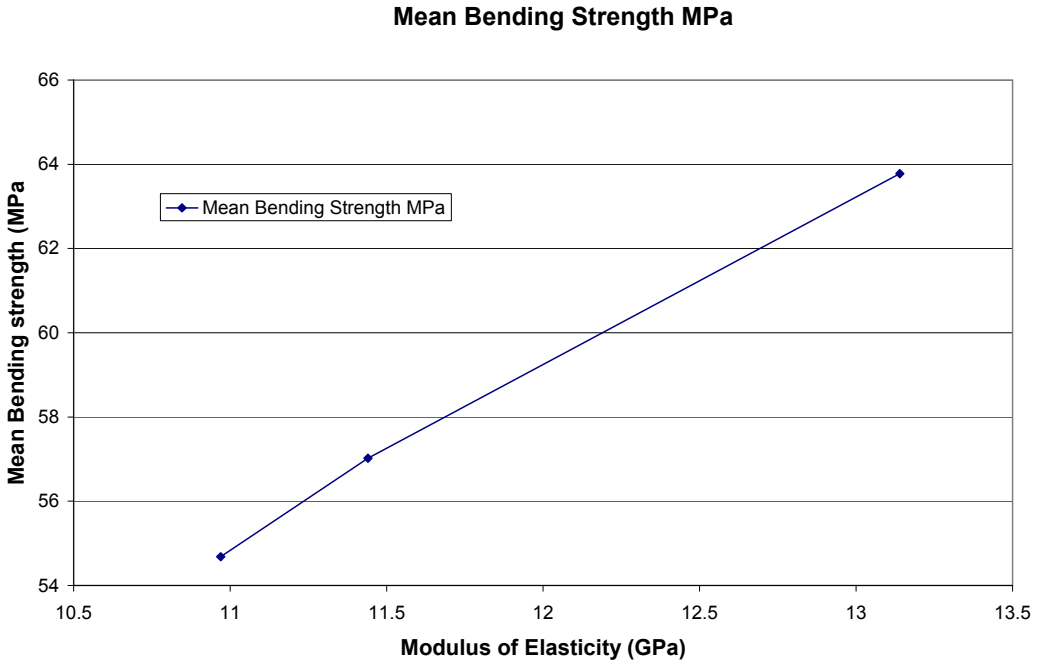

Figure 7.3 Relationships between Mean Bending Stress & Modulus of Elasticity.

7.2.2 Beam Properties

The following beam properties and capacities have been determined and used in assessment of LVL beam design for this load test. (Refer Appendix E2)

Modulus of Elasticity	E	=	11.15	GPa
Mean Bending Strength	f_b	=	55.58	MPa
Ultimate Section Capacity	ϕMn	=	87.5	kNm
Test Moment Applied	Mn	=	34.1	kNm

At this stage using the average char rate obtained from the 3 pilot tests, $\beta = 0.72$ mm/min a time to failure for the beam was calculated.

In the calculation for time to failure, the modified Section Modulus (S) for the charred residual cross section was assessed with time, using corner rounding as specified in NZS

3603: 1993 [4] and then the reducing moment capacity of the section compared to that of the test applied moment.

The calculated time to failure was: **t = 36.6 minutes**

7.2 Test Results.

7.2.1 Deflection

The load of 30kN was applied to the beam for a period of 30 minutes prior to the test commencing, to establish weather any significant creep in the LVL beam would occur. The initial deflection in the beam under full loading was measured and compared to the calculated deflection:

Deflection (calculated)	Δ_c	=	20.2 mm
Deflection (initial)	Δ_i	=	17.1 mm
Deflection (30 minutes)	Δ_{30}	=	17.4 mm

From the deflections listed above it can be seen that reasonable correlations were achieved between calculated and measured and that creep deflection over 30 minutes was not significant.

The small variance between calculated and the initial deflection may be explained by minor inaccuracies in the estimation of building material weights used and the distribution of weight in the construction of the framing and cladding used in the test setup. Care was taken to alleviate any possible load sharing by cutting the 100 x 50 mm framing almost all the way through directly over the loaded beam. (Refer Figure 7.4)
Also minor fluctuations in load pressure may have contributed to this small variation.

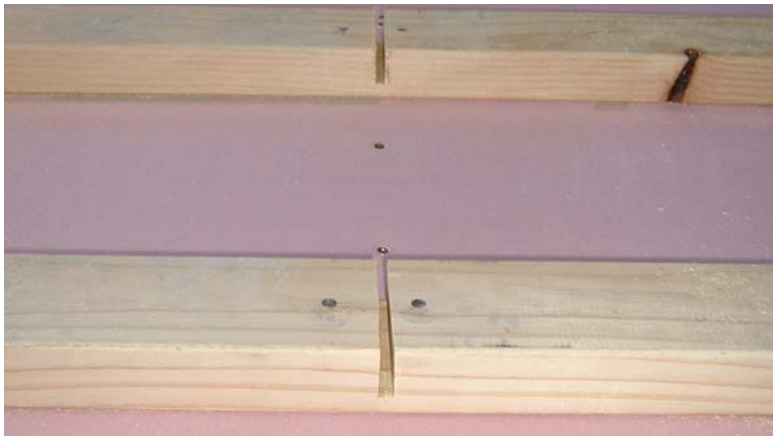

Figure 7.4 Cut framing over Beam to minimised possible Load Sharing.

7.2.2 Load

Once the test commenced and the LVL beam exposed to the ISO 834 standard fire, the load was maintained during the test and the deflection of the beam recorded. The load was maintained by visually monitoring the load pressure gauge and manually controlling the hydraulic oil pressure. Figure 7.2 shows the load and the corresponding deflection.

Figure 7.5 Enclosed beam assembly, prior to placing on furnace.

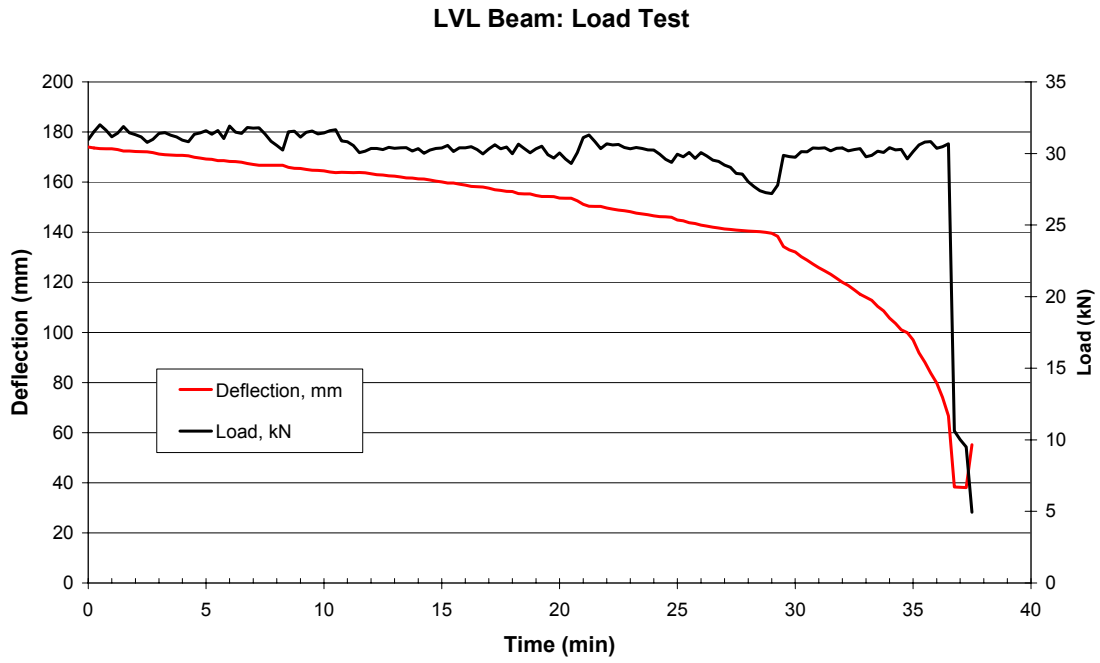

Figure 7.6 Load & Deflection Record for Beam Exposed to ISO 834 Fire Curve.

7.2.3 Time to Failure

Failure of the LVL beam occurred at 36.75 minutes which was a good result, with close comparison to the calculated time of 36.6 minutes using the charring rate of $\beta = 0.72$ mm/min. Measurements of the section after removal from the furnace (approximately 7 minutes) confirmed the section charring rate.

In the graph of load and deflection against the load in Figure 7.6, after 27 minutes the load pressure reduced over a period of 2 minutes and once the pressure was increased to maintain the 30 kN point load the deflection increased more rapidly until failure occurred. Another interesting observation was the fact that once the test started the deflection started to increase immediately, even in the first few minutes when there were little or no effect on the LVL beam due to charring, as the onset of char had not commenced. This increase in deflection is contributed to the elevated temperature producing softening effects in the LVL and on the properties of the LVL, especially the modulus of elasticity.

7.2.4 Modulus of Elasticity

The deflection recorded during the test exceeded that of the calculated deflection, which was expected as no reduction in the modulus of elasticity due to the effects from the fire were taken into account in the calculations.

Using the measured deflection results, and the residual charred section moment of Inertia, estimates of the variation in the modulus of elasticity were calculated and plotted as shown in Figure 7.7. These effects we calculated over 30 minutes and not for the last 6.75 minutes of the test, as the deflection rapidly increased over this period and other effects such as slenderness ratio on the residual section for one, may have been a more dominant effect.

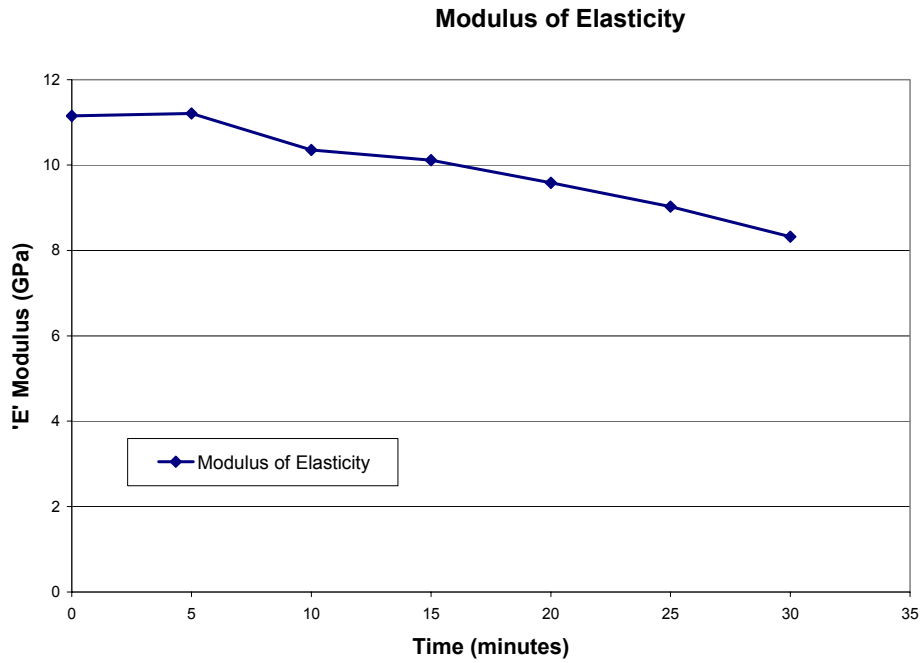

Figure 7.7 Variations in Modulus of Elasticity

7.3 Observations during Test

The following photos, observations and comments were recorded during the test. Figure 7.8 below shows the furnace with the beam in place with the reaction frame over it. The hydraulic jack that applies the load and the load cell are fitted between the steel stub and the reaction frame. The steel stub is screw fixed to the framing attached to the LVL beam. The clock at the end of the furnace has been set at zero ready for the test to commence.

Figure 7.8 Furnace LVL beam and assembly ready to test to commence.

In Figure 7.8 above also shows that access onto the top of the furnace is possible during the test via a LVL plank that spans the length of the furnace, ensuring that it does not influence the test. Access onto the assembly was necessary in order to retrieve the jack and load cell if anything went wrong.

The load to measure the initial deflection has not been applied at this stage as seen in Figure 7.8. The test commenced at 10:20 am on Friday 31st October 2004.
Figure 7.9 shows a view through an observation port at the end of the furnace at the time the furnace was ignited. Figure 7.10 shows a similar view to that in Figure 7.9 after 56 seconds lapsed time, the beam has not blackened or showing any signs of charring.

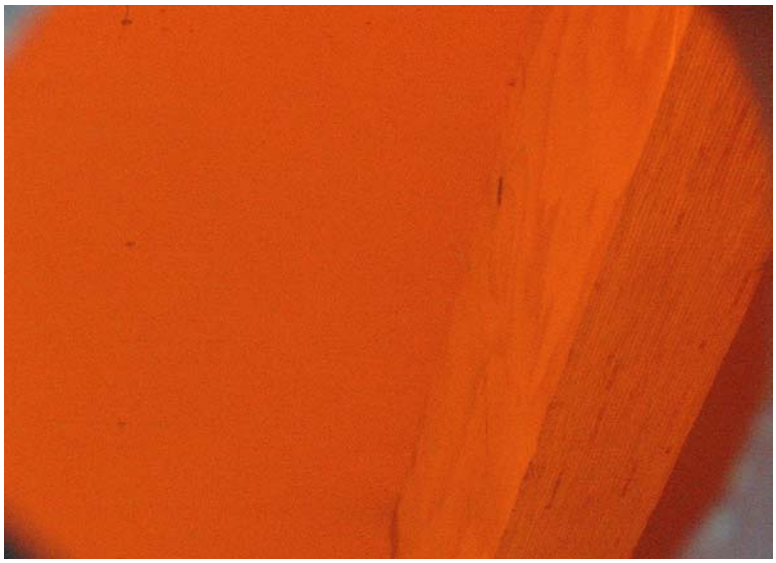

Figure 7.9 View of beam through end observation port at start of test, t = 0.

Figure 7.10 View of beam through end observation port, t = 56 seconds.

Figure 7.11 has been taken transversely across the test assembly to show the deflection in the beam after 5 minutes, and 50 seconds. The deflection at this stage was estimated by eye to be approximately 20 mm; from the electronic data record deflection after 5.75 minutes it was 23 mm. Therefore there had been 6 mm increase in deflection from the initial deflection recorded at the start of the test.

Figure 7.11 View across the central assembly showing the deflection after 5 minutes 50 seconds.

Unfortunately the photo taken through the observation port after 2 minutes was undistinguishable; it would have shown the beam blackened with the onset of charring just commencing.

Figures 7.12 and 7.13 were taken through the end observation ports of the furnace after 17 minutes and 8 seconds for Figures 7.12 and 17 minutes 22 second for Figure 7.13, after the furnace was ignited. Figure 7.12 has been taken from the left side of the beam as viewed from the end of the furnace as shown in Figure 7.8 and Figure 7.13 has been taken from the right side of the beam. Both photos are looking up from under the beam and both show the beam to be well involved in the fire. Surface shrinkage cracking in the charred surface is obvious in both photos and the ash residual of the paper surface from the Gibraltar Board cladding is seen to be hanging down.

Figure 7.12 Left side of beam, after 5 minutes 08 seconds.

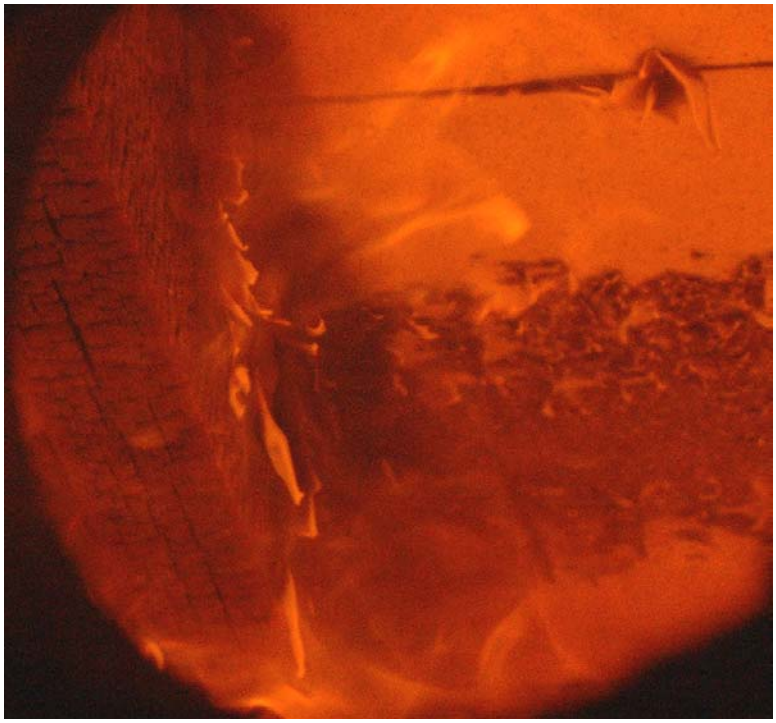

Figure 7.13 Right side of beam, after 5 minutes 22 seconds.

Figure 7.14 Left side of beam, after 23 minutes 24 seconds.

Figure 7.15 Left side of beam, after 24 minutes 08 seconds.

Figures 7.14 and 7.15 were taken through the end observation ports of the furnace after 23 minutes and 24 seconds for Figure 7.14 and 24 minutes 8 second for Figure 7.15, after the furnace was ignited. Both photos in these Figures have been taken from the left side of the beam looking up from under the beam. Again both photos show the beam to be well involved in the fire.

Figure 7.16 End of the furnace showing the observation ports, after 30 minutes 42 seconds.

Figure 7.17 shows the deflection in the beam looking along the beam, note that the contraction cuts sliced into the 100 x 50 mm framing have closed up significantly. The total deflection at this stage was 60.2 mm taken from the electronic data recording from the potentiometer. This was at the stage when the deflection of the beam started to increase more quickly and correspondingly more pressure had to be applied to the hydraulic jack to maintain the 30kN point load.

Figure 7.17 **View along the top of the assembly after 31 minutes and 58 seconds; note increased deflection and the closing up of the contraction cuts placed in the framing over the LVL beam.**

Figure 7.18 **Transverse view across the assembly, after 34 minutes and 42 seconds, note increased deflection of the LVL beam.**

After 36 minutes and 45 seconds there was a distinctive cracking sound from the LVL beam and assembly, indicating that the beam had failed and the test stopped. This cracking sound was accompanied by a significant increase recorded in deflection and a corresponding drop off in load cell pressure. Figure 7.19 shows the same view as in Figure 7.18 after failure.

Figure 7.19 Transverse view across the assembly, after 45 minutes and 18 seconds, test had stopped; note final deflection of the LVL beam.

Figure 7.20 Beam immediately after assembly removed from furnace.

Figure 7.21 Side view of beam immediately after assembly removed from furnace.

Figure 7.22 Beam immediately after assembly removed from furnace, view similar to view of LVL beam in photo 7.4.

Figure 7.23 Beam failure zone with char removed; note tension cracks in tension zone of failure

Figure 7.24 Compression failure zone viewed from top of LVL beam.

Figure 7.25 Char removed from beam, between centre and support.

Figure 7.26 Char removed from beam, viewed from bottom of LVL beam.

Figure 7.27 LVL beam placed on its side on edge of furnace to show permanent deflection after failure.

Chapter 8: Summary and Recommendations

This chapter will provide a summary of the test results found in this project, confirm and/or discuss further those results and comparisons and where appropriate provide recommendations.

8.1 LVL Ignition Results

Generally the time to ignition for the edge grain exposure was longer than for the face grain exposure, for each of the different heat flux levels tested. Correspondingly the amount of surface shrinkage/char depth was greater for the edge grain exposure compared to that for face grain exposure.

Therefore the range of surface ignition temperatures for the edge grain LVL was expected to be greater than that for the face grain LVL samples and correspondingly, the critical heat flux greater for the edge grain LVL compared to that for the face grain LVL. Theses relationships and comparisons have been confirmed in the results for ignition testing in this project. Table 8.1 shows ignition properties determined.

Surface Exposed Face/Edge	Critical Heat Flux q_{cr} (kW/m^2)	Surface Ignition Temperature T_{ig} (^oC)	Thermal Inertia $k\rho c$ $(kW/m2)^2s$
Face	7.66 - 11.97	251 - 341	0.558 - 1.08
Edge	9.9 - 15.47	294 - 380	0.393 - 0.678

Table 8.1 Ignition Properties of LVL

A full summary of the resulting values for the surface ignition temperature (T_{ig}) and the thermal inertia ($k\rho c$) of the LVL samples, along with an estimate of the critical heat flux (q_{cr}) are shown in Table 4.1.

8.1.1 Recommendation

It is recommended that values for ignition properties of LVL from Table 8.1 be used in computer models involving LVL exposure to fire.

8.2 Cone Calorimeter Char Tests

8.2.1 Instrumented Char Tests

The instrumented tests located the 300 O^C isotherm within each sample of LVL at constant irradiances or heat fluxes of 35, 50 & 65 kW/m^2, which in turn identified the char front. From these results an averaged char rate for heat flux and grain exposure was obtained. Table 8.2 is a summary of the instrumented char rates.

Heat flux kW/m^2	**Exposed Surface** Face/Edge	**Char Rate** min/mm
35	Face	0.67
35	Edge	0.68
50	Face	0.75
50	Edge	0.81
65	Face	0.92
65	Edge	0.92

Table 8.2 Instrumented Average Char Rates

These results have been extrapolated from thermocouple temperatures recorded at different depths and then char depth plotted against time for each grain orientation and for

each heat flux. Figure 5.2 shows char depths against time curves for all heat flux levels and grain orientations.

8.2.2 Un-instrumented Char Tests

Un-instrumented LVL blocks were exposed to the same constant heat fluxes as used for the instrumented tests in the Cone Calorimeter, however for these series of tests the time period of exposure was limited to 20, 40 and 60 minutes.

From these test results, cumulative charring rates were calculated, and the average for each heat flux and grain orientations collated and shown in Table 8.3.

Time (min)	Surface Exposure	Char Rates Mm/min		
		35kW/m^2	50kW/m^2	65kW/m^2
20	Face	0.71	0.90	1.12
	Edge	0.79	0.89	1.07
40	Face	0.66	0.79	0.91
	Edge	0.66	0.79	0.91
60	Face	0.61	0.71	0.81
	Edge	0.60	0.71	0.80

Table 8.3 Un-Instrumented Average Char Rates

8.2.3 Comparisons between Instrumented and Un-instrumented Char Tests

Very good correlations between the instrumented and the un-instrumented results where obtained. Refer to Figure 8.1 which shows the instrumented results for each of the heat fluxes and the different grain orientations, together with the un-instrumented results.

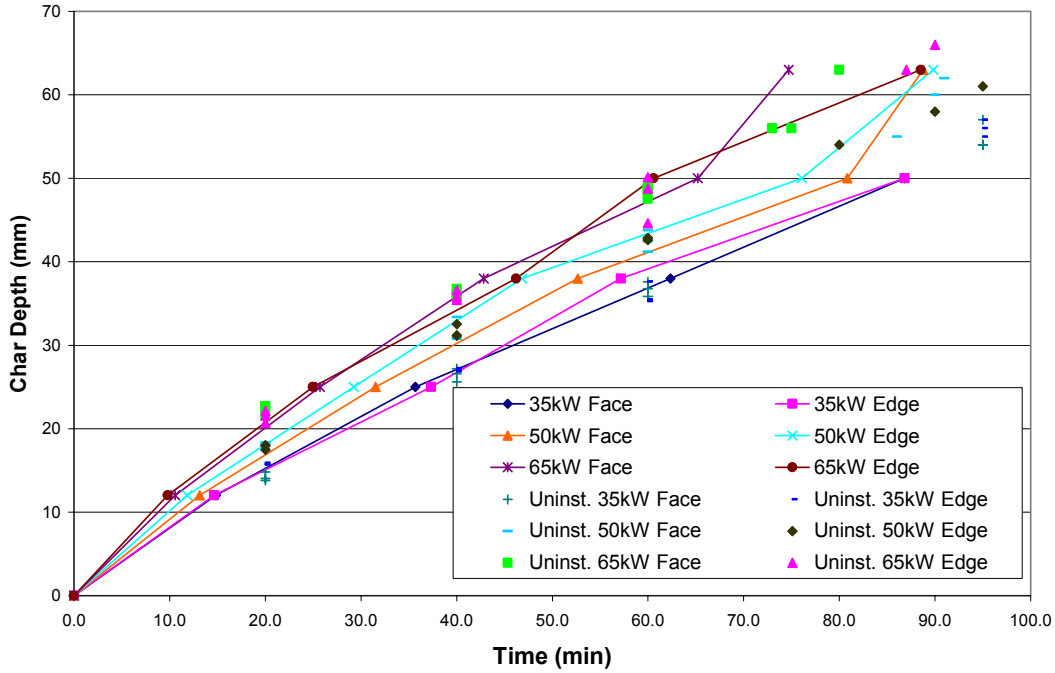

Figure 8.1: Comparisons between Instrumented & Un-instrumented Char Depth results.

The corresponding char rates for the instrumented and the un-instrumented tests are compared in Figure 8.2, for the different heat fluxes tested. Again very good comparisons were achieved between the instrumented and the un-instrumented char rates.

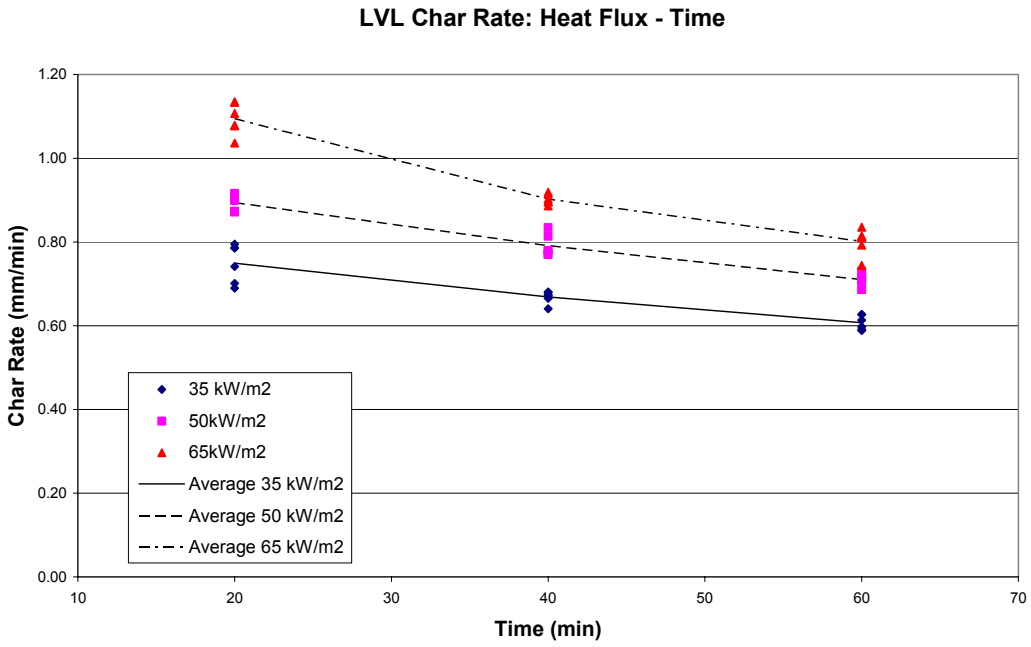

Figure 8.2: LVL Char Rate from un-instrumented cone calorimeter tests.

8.2.4 Transverse Char Rate

The results from the one test inadvertently performed, shown in Figures 5.15 & 5.16, provides an end grain or transverse grain charring rate for LVL of:

Transverse Charring Rate = 0.44 mm/min.

This transverse grain charring rate is 65% of the mean cumulative charring rate found from the instrumented and un-instrumented tests, exposed to 35 kW/m2 heat flux.
Note: this result has been based on only one instrumented char test and results.

8.3 Pilot Furnace Test Char Rates

Cumulative charring rates for single face exposure from the pilot tests, which were subjected to ISO 834 design fire, were measured and the results averaged for the 18 & 36 mm depths. The average char rate obtained from these tests varied from $\beta = 0.72$ mm/min at 18mm depth to $\beta = 0.70$ mm/min at 36 mm depth. Refer Figure 8.3.

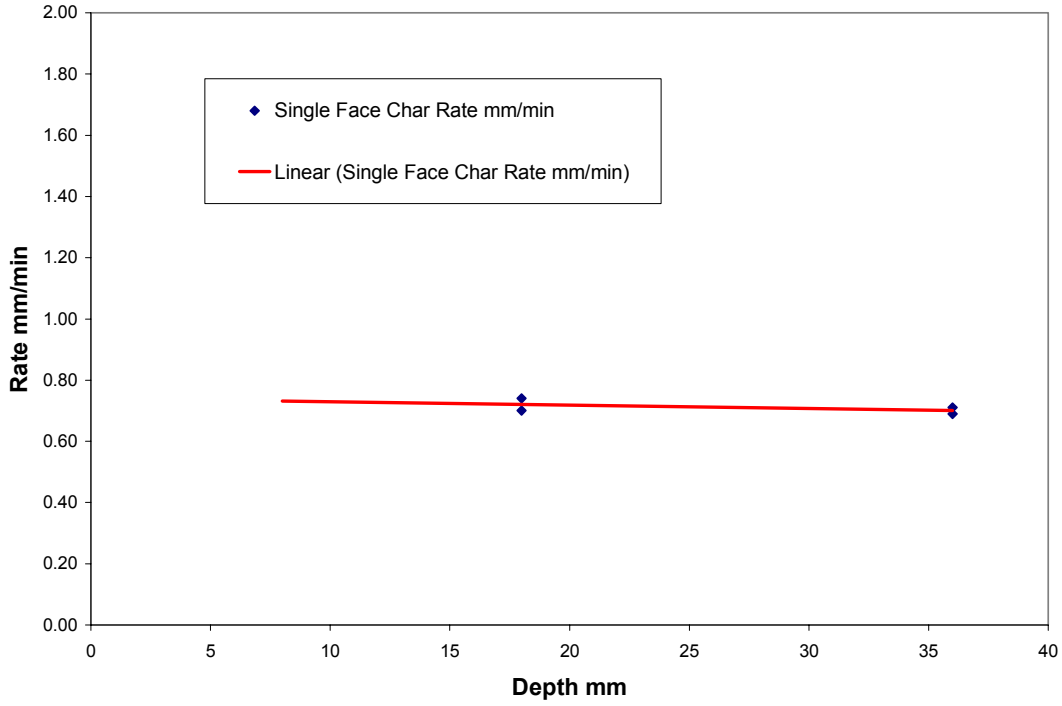

Figure 8.3 Char Rate Versus Depth for Single Face Exposure from Pilot Furnace Tests.

8.3.1 Pilot Furnace Char Rate Comparisons

The single face char rates from the pilot tests subjected to the ISO 834 Design Fire were compared to the un-instrumented char rates from the 35 kW/m^2 cone calorimeter tests and the current design charring rate of β = 0.65 mm/min from NZS 3603 (1993), as shown in Figure 8.4.

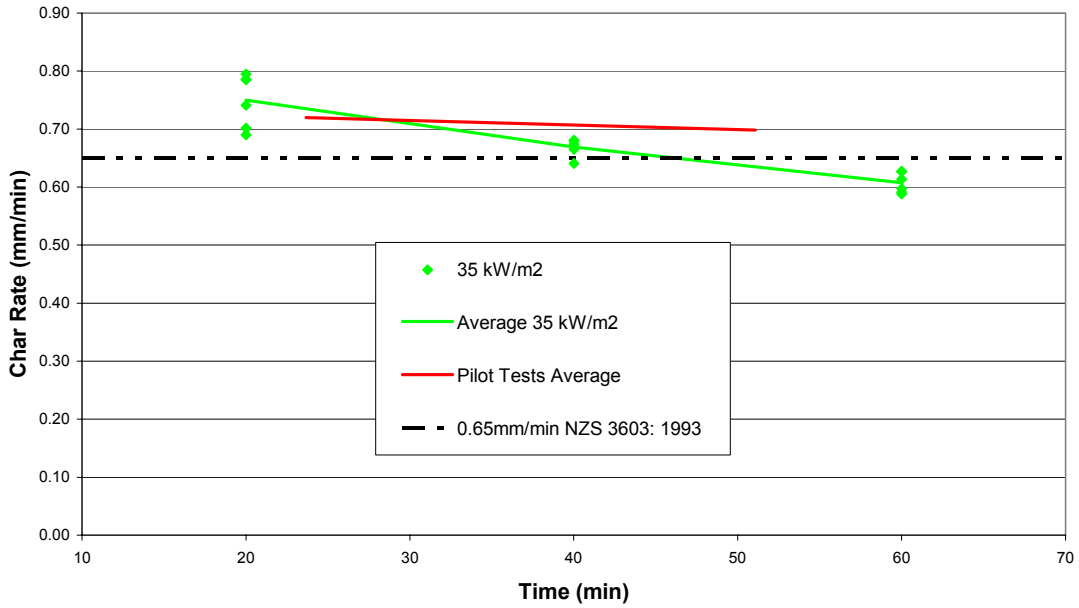

Figure 8.4 LVL Char Rates for 35 kW/m^2 irradiance from Un-instrumented Cone Calorimeter Tests, with comparisons to the Pilot Furnace Tests exposed to the ISO 834 design fire & NZS 3603: 1993 Charring Rate.

From Figure 8.4, it can be seen that exposure to the ISO 834 curve equates closely to an irradiance of 35 kW/m^2 in the cone calorimeter.

8.3.2 Recommendation

It is recommended that the charring rate of β = 0.72 mm/min be adopted for LVL design. This charring rate was used in the design for the subsequent load test.

8.4 White's Char Model

White's model for estimating the char depth, used with test derived values for the oven dried density and moisture content of LVL, with a CCA of 20 mm and a hardness factor for Radiata Pine, produces a char depth –time curve for the LVL that compared very well to the instrumented and un-instrumented char rates, as shown in Figure 5.10.

White's model for the cumulative charring rate of LVL produced a curve that compared remarkably similar to the un-instrumented cone calorimeter tests performed at a heat flux of 35kW/m^2, as shown in Figure 5.12.

In figure 6.41, White's Model is compared to the single face exposure results from the three pilot tests undertaken on the LVL beams. Again a very good correlation is attained.

8.4.1 Recommendation

From this we recommend the use for design of LVL sections of different densities and/or the manufacture of LVL from different species wood that, White's Model may be applicable for preliminary design purposes.

8.7 Zero Strength Zone

From the results of the pilot furnace tests, an estimate of the thickness of the zero strength zones under the char front was attempted. The estimated thickness of the temperature-affected material varied from 6 to 13 mm, with an average thickness of 9 mm. This layer of material is likely to have reduced mechanical properties because of the elevated temperatures.

This information is useful because some design methods require an estimate of the thickness of zero-strength heated wood below the char layer. The Australian timber code AS1720.4-(1990) states that a zero-strength layer thickness of 7.5 mm should be used, which is consistent with the findings of this study, recognising that not all of the wood between 100^{o}C and 300^{o}C will have zero strength.

8.5.1 Recommendation

To establish a better understanding of this zero strength zone beneath the char base, it is recommended that further testing will be required to identify the significant factors involved.

8.8 Load Test Full Size Furnace

The load test used the charring rate developed from the char testing in the cone calorimeter and the pilot furnace tests. This char rate of $\beta = 0.72$ mm/min was now used to design a full scale loaded test on a large LVL beam in the full size furnace exposed to the ISO fire curve. Refer to report section 7.1 for beam properties and design.

8.6.1 Time to Failure

The time to failure was calculated by assessing the modified Section Modulus (S) for the charred residual cross section with time and thus the reducing moment capacity of the section was compared to that test applied moment from the test loading.

The calculated time to failure was 36.6 minutes. The test was a success with failure of the LVL beam occurring after 36.75 minutes which was a very close comparison to the calculated time and a good result. Measurements of the residual section after removed from the furnace (approximately 7 minutes) confirmed the section charring rate.

8.6.2 Deflection

The deflection recorded during the test exceeded that of the calculated deflections, which was expected as no reduction in the modulus of elasticity due to the elevated temperature effects from the fire were considered in the calculations.

8.6.3 Modulus of Elasticity

Using the measured deflection results, and the residual charred section moment of inertia, an estimate of the variation in the modulus of elasticity were calculated and plotted. Refer Figure 7.7.

8.6.4 Recommendation

It is recommended that the design method used for predicting the fire performance of New Zealand manufactured Radiata Pine LVL exposed to post-flashover fires is to use the experimentally found char rate $\beta = 0.72$ mm/min to determine a reduced cross-section, and design using normal temperature properties without considering a heat-affected layer of wood below the char line.

Or

Design using the char rate $\beta = 0.65$ mm/min, complying with NZS 3603 (1993) to calculate a reduced cross section which can be used with normal temperature properties, with an allowance for a 7 mm to 9 mm zero-strength layer of LVL below the char line.

Chapter 9: Conclusions

In relation to the objectives of this report, this chapter concludes that:

- **The ignition properties found in this study are representative for New Zealand manufactured Radiata Pine LVL and are to be used in studies and/or computer models involving LVL exposure to fire.**

- **For New Zealand manufactured Radiata Pine LVL, the experimentally found cumulative char rate of β = 0.72 mm/min be used, and is representative for fire exposure in both grain orientations.**

- **For New Zealand manufactured Radiata Pine LVL, a simple design method be adopted using the char rate β = 0.72 mm/min (found experimentally in this study) to calculate a reduced cross section which can be used with normal temperature properties (characteristic bending stress and modulus of elasticity) with no zero-strength layer of LVL below the char line.**

References

AS1720.1- (1997). Timber Structures Part 1: Design methods, Standards Association Of Australia.

AS 1720.4 - (1990). Standards Association of Australia, 1990. Timber Structures Part 4: Fire Resistance of Structural Timber Members.

AS/NZS 4063 (1992). Timber - Stress graded - In-grade strength and stiffness evaluation, Standards Australia/Standards New Zealand.

AS/NZS 4357 (1995). Structural Laminated Veneer Lumber, Standards Australia/Standards New Zealand.

ASTM (1988) Standard test methods for fire testing of building construction and materials E 119 – 88. American Society for Test and Materials

Babrauskas, V. (2002). Ignition of Wood: A Review of the State of the Art. Fire Science and Technology Inc., Issaquah, WA. Journal of Fire Protection Engineering, Vol. 12, No. 3, 163-189, August 2002.

Buchanan A. H. (2001), Chapter 10 Timber Structures, "Structural Design for Fire Safety." John Wiley & Sons Ltd.

BS 476: Part 13 (1987) Fire Tests on Building Materials and Structures, Part 13: Method of measuring the ignitability of products subjected to thermal irradiance, British Standard BS 476, 1987.

Chu Kang NGU (2001), Ignition Properties of New Zealand of Timber, Research Report 2001/5, University of Canterbury, Christchurch, New Zealand.

Collier P. C. R. (1992). Charring Rates of Timber, BRANZ Study Report No. 42. Building Research Association of New Zealand

Collins M. J. (1983), Density Conversions for Radiate Pine, FRI Bulletin No. 49. Forest Research Institute, Rotorua New Zealand.

Delichatsios, M.A., Panagiotou, TH., and Kiley, F. (1991). The Use of Time to Ignition Data for Characterizing the Thermal Inertia and the Minimum (Critical) Heat Flux for Ignition or Pyrolysis., Combustion and Flame, Vol. 84, 323-332, 1991.

Forest Research Institute (1988). New Zealand Radiata Pine, a Technical Bulletin of produce, processes and uses, F.R.I. Pamphlet, Rororua, New Zealand: (Figure 8)

HYSPAN & TRUFORM LVL (2001) Product testing for Carter Holt Harvey, Commercial report, July 2001.

Jannsens M. L. (1994), Thermo-physical Properties of for Wood Pyrolysis. Models, Proceedings of the Pacific Timber Engineering Conference, Gold Coast Australia , pp 607-618.

Janssens, M.L. (1991). Fundamental Thermophysical Characteristics of Wood and their role in Enclosure Fire Growth., PhD Dissertation, University of Gent, Belgium, 1991.

Knudson R. M. and Schneiwind A. P. (1975), Performance of Wood Structural Member Exposed to Fire, Forest products Journal, 25, 2, pp 23-32.

Konig J. and Walleij L. (1999), One Dimensional Charring of timber Exposed to Standard and parametric fires in, initially Unprotected and Protected Situations. Report No I 9908029. Tratek; Swedish Institute for Wood Technology Research, Stockholm, Sweden.

Mikkola, E. (1990). Charring of Wood. VTT-Technical Research Center of Finland, Espoo. VTT Research Reports 689; Project PAL7003.
Mikkola, E. and Wichman I.S (1989). On the Thermal Ignition of Combustible Materials. Fire and Materials, Vol. 14, 87-96, 1989.

Njankouo J. M., Dotreppe J. C. and Franssen J. M. (2004) Experimental study of the charring rate of tropical hardwoods. Fire and Materials. 2004; 28: 15 – 24.

NZS 3603 (1993), Timber Design Code, NZS 3603:1993, Standards New Zealand.

Shields, T.J., Silcock, G.W.H., & Murray, J.J. (1994). Evaluating Ignition Data Using the Flux Time Product., Fire and Materials, Vol. 18, 243-254, 1994.

White R. H. (1988). Charring Rates of Different Wood Species. A thesis submitted in partial fulfilment of the requirements for the degree of Doctor of Philosophy (Forestry), University of Wisconsin, Madison, USA.

White R. H. (2002), Section 4/Chapter 11 The SFPE Handbook of Fire Protection Engineering. Third Edition: Analytical Methods for Determining Fire Resistance of Timber Members.

White, R H. (2003). Fire resistance of engineered wood rim board products. Res. Pap. FPL-RP-610. Madison, WI: U.S. Department of Agri-culture, Forest Service, Forest Products Laboratory.

List of Appendices

Appendix C Char Rate Comparison Instrumented / Un-Instrumented

Appendix D Pilot Test Results

Appendix E: LVL Load Test: Beam Calculations

Appendix F: Notes on the application of White's model.

Appendix G: Ignition Tests Samples Photos

Appendix H: Zero Strength Zone: Pilot Test Results

Appendix A Density Tests

Table A.1 Sample Densities: Cone Calorimeter Testing

Density of Samples:				Enviroment/Green Density						
Sample No	Thickness t mm	Length l mm	Width w mm	Volume V m^3	Weight wt_g Enviro/ Green kg	Density D_g Enviro/ Green kg/m^3	Moisture m Meter %	Weight wt_{od} Oven Dry kg	Density $D_{b,x}$ Basic kg/m^3	Moisture x Oven Dry %
M1	85.30	101.10	100.20				13.50			
	84.90	101.20	100.40				13.20			
	85.60	101.10	100.20				14.60			
	85.10	100.70	99.90				13.60			
							12.70			
							14.40			
Average	**85.23**	**101.03**	**100.18**	**0.000862**	**0.525**	**608.70**	**13.67**	**0.475**	**550.73**	**10.53%**
M2	85.10	101.20	100.70				14.50			
	85.00	101.50	100.00				12.00			
	84.90	101.00	100.20				14.50			
	85.10	101.00	100.70				14.10			
							14.50			
							13.00			
Average	**85.03**	**101.18**	**100.40**	**0.000864**	**0.525**	**607.86**	**13.77**	**0.478**	**553.44**	**9.83%**
M3	51.00	100.80	98.70				14.20			
	50.50	101.10	98.90				14.00			
	50.90	101.10	99.30				13.60			
	50.80	101.10	99.50				14.00			
							13.70			
							13.00			
Average	**50.80**	**101.03**	**99.10**	**0.000509**	**0.315**	**619.36**	**13.75**	**0.290**	**570.21**	**8.62%**
M4	51.50	101.20	98.90				14.50			
	51.30	101.10	98.80				12.70			
	51.10	101.40	99.30				13.20			
	51.40	101.30	99.10				13.80			
							12.60			
							14.70			
Average	**51.33**	**101.25**	**99.03**	**0.000515**	**0.305**	**592.69**	**13.58**	**0.282**	**548.00**	**8.16%**
						607.16	**13.69%**		**555.60**	**9.28%**

Table A.1 Sample Densities: Cone Calorimeter Testing (cont.)

	Density of samples:			**Oven Dry**		
Sample No	Weight wt_{od} Oven Dry kg	Thickness t_{od} Oven Dry mm	Length l_{od} Oven Dry mm	Width w_{od} Oven Dry mm	Volume V_{od} Oven Dry m3	Density D_{od} Oven Dry kg/m3
M1		83.6	101	98.6		
		83.7	101.1	97.3		
		83.9	101.2	97.4		
		83.1	100.2	98.9		
Average	**0.475**	**83.575**	**100.875**	**98.05**	**0.000827**	**574.63**
Shrinkage		1.9%	0.1%	2.1%		
M2		83.6	101.1	98.8		
		83.3	101.1	98.8		
		83.2	101.7	97.7		
		83.4	101	97.9		
Average	**0.478**	**83.375**	**101.225**	**98.3**	**0.000830**	**576.17**
Shrinkage		1.9%	0.0%	2.1%		
M3		49.6	100.7	97.8		
		49.7	100.1	97.8		
		49.9	101	97.6		
		49.8	101.1	97.5		
Average	**0.290**	**49.75**	**100.725**	**97.675**	**0.000489**	**592.49**
Shrinkage		2.1%	0.3%	1.4%		
M4		50.1	101	96.6		
		50.1	101.1	97.4		
		50.4	101.1	96.9		
		50.4	100.9	97.2		
Average	**0.282**	**50.25**	**101.025**	**97.025**	**0.000493**	**572.53**
Shrinkage		2.1%	0.2%	2.0%		
				Overall	**Average**	**578.96**

Table A.2 Sample Densities: Pilot Furnace Testing

Pilot Tests					**Density of samples**		**Un-Dried Densities**		
Sample	Width	Depth	Length	Volume	Weight Green	Density Green	Weight Oven	Density $D_{b,x}$	Moisture Oven/
	w	d	l	V_g	wt_g	D_g		Basic	Dry
	mm	mm	mm	m^3	kg	kg/m^3	kg	kg/m^3	x %
Pilot 1	105.00	300.00	50.00						
Sample 1	105.00	300.00	48.00						
	105.00	300.00	50.00						
	105.00	300.00	48.00						
Average	**105.00**	**300.00**	**49.00**	**0.001544**	**0.944**	**611.60**	**0.844**	**546.81**	**11.85%**
Pilot 1	105.00	300.00	99.00						
Sample 2	105.00	300.00	95.00						
	105.00	300.00	99.00						
	105.00	300.00	95.00						
Average	**105.00**	**300.00**	**97.00**	**0.003056**	**1.824**	**596.96**	**1.639**	**536.41**	**11.29%**
Pilot 2	105.00	300.00	99.00						
Sample 1	105.00	300.00	97.00						
	105.00	300.00	99.00						
	105.00	300.00	97.00						
Average	**105.00**	**300.00**	**98.00**	**0.003087**	**1.824**	**590.86**	**1.634**	**529.32**	**11.63%**
Pilot 2	105.00	300.00	97.00						
Sample 2	105.00	300.00	101.00						
	105.00	300.00	99.00						
	105.00	300.00	102.00						
Average	**105.00**	**300.00**	**99.75**	**0.003142**	**1.858**	**591.32**	**1.661**	**528.62**	**11.86%**
Pilot 3	67.00	360.00	96.00						
Sample 1	67.00	360.00	96.00						
	67.00	360.00	96.00						
	67.00	360.00	96.00						
Average	**67.00**	**360.00**	**96.00**	**0.002316**	**1.402**	**605.48**	**1.245**	**537.68**	**12.61%**
Pilot 3	66.00	362.00	97.00						
Sample 2	66.00	362.00	97.00						
	66.00	362.00	97.00						
	66.00	362.00	97.00						
Average	**66.00**	**362.00**	**97.00**	**0.002318**	**1.46**	**629.98**	**1.297**	**559.65**	**12.57%**

Table A.2 Sample Densities: Pilot Furnace Testing (cont.)

Pilot Tests			Density of samples				Oven-Dried Densities	
Sample	Weight Oven Dry kg	Density $D_{b,x}$ Basic kg/m3	Moisture Oven x %	Width Oven mm	Depth Oven mm	Length Oven mm	Volume Oven V_d m3	Density D_{od} kg/m3
Pilot 1				105.0	293.0	50.0		
Sample 1				105.0	293.0	47.0		
				105.0	293.0	50.0		
				105.0	293.0	48.0		
Average	**0.844**	**546.81**	**11.85%**	**105.0**	**293.0**	**48.8**	**0.00150**	**562.74**
Shrinkage				0.0%	2.3%	0.5%		
Pilot 1				105.0	294.0	98.0		
Sample 2				105.0	294.0	95.0		
				105.0	294.0	99.0		
				105.0	294.0	94.5		
Average	**1.639**	**536.41**	**11.29%**	**105.0**	**294.0**	**96.6**	**0.00298**	**549.48**
Shrinkage				0.0%	2.0%	0.4%		
Pilot 2				105.0	293.0	99.0		
Sample 1				105.0	293.0	97.0		
				105.0	293.0	98.0		
				105.0	293.0	97.0		
Average	**1.634**	**529.32**	**11.63%**	**105.0**	**293.0**	**97.8**	**0.00301**	**543.35**
Shrinkage				0.0%	2.3%	0.3%		
Pilot 2				105.0	293.0	97.0		
Sample 2				105.0	294.0	100.0		
				105.0	294.0	98.0		
				105.0	293.0	102.0		
Average	**1.661**	**528.62**	**11.86%**	**105.0**	**293.5**	**99.3**	**0.00306**	**543.05**
Shrinkage				0.0%	2.2%	0.5%		
Pilot 3				67.0	354.0	96.0		
Sample 1				67.0	354.0	95.5		
				67.0	353.0	95.0		
				67.0	354.0	96.0		
Average	**1.245**	**537.68**	**12.61%**	**67.0**	**353.8**	**95.6**	**0.00227**	**549.32**
Shrinkage				0.0%	1.7%	0.4%		
Pilot 3				66.0	355.0	97.0		
Sample 2				66.0	356.0	96.0		
				66.0	355.0	96.5		
				66.0	354.0	96.5		
Average	**1.297**	**559.65**	**12.57%**	**66.0**	**355.0**	**96.5**	**0.00226**	**573.64**
Shrinkage				0.0%	1.9%	0.5%		

Table A.3 Sample Density: Load Test - Full Scale Furnace.

Test	**Load Test**	
Date	28-Nov-03	
Dimensions		
Width	105	mm
Length	95	mm
Depth	300	mm
Weights		
Undried	1820.1	gms
Dried	1618.8	gms
Time	19	days
Moisture Content	12.4	%
Volumn	0.0030	kg
Density		
Test	**608.2**	**kg/m^3**
Dried	**541.0**	**kg/m^3**

Appendix B: Instrumented Char Tests

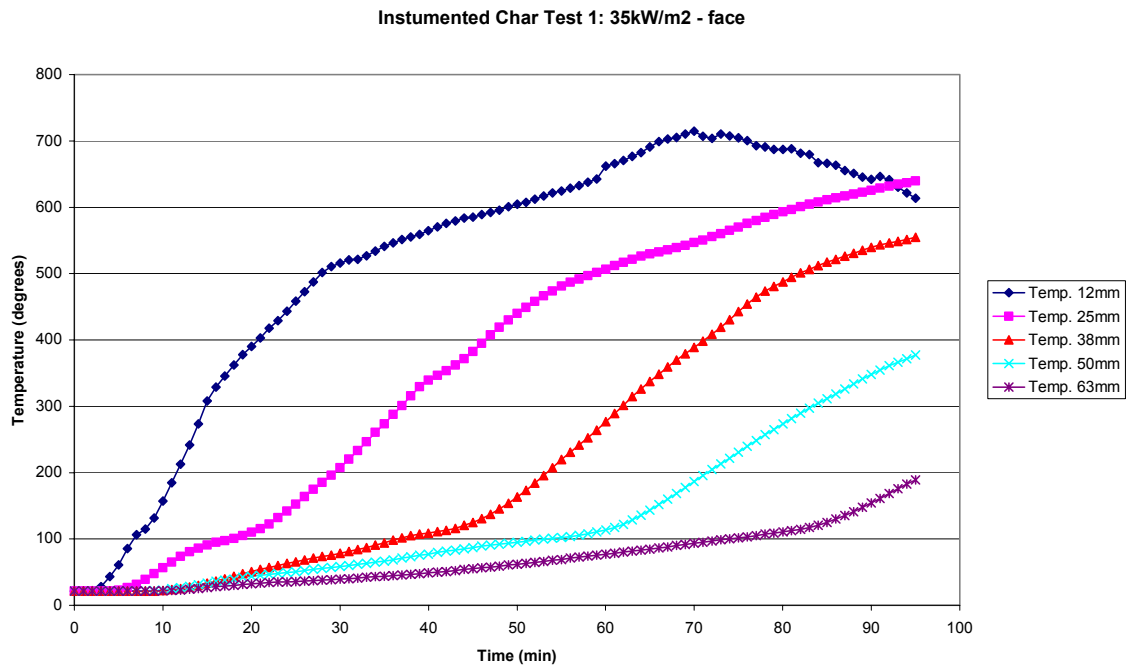

Figure B1: Instrumented Char Test 1 - 35 kW/m^2, Face Grain

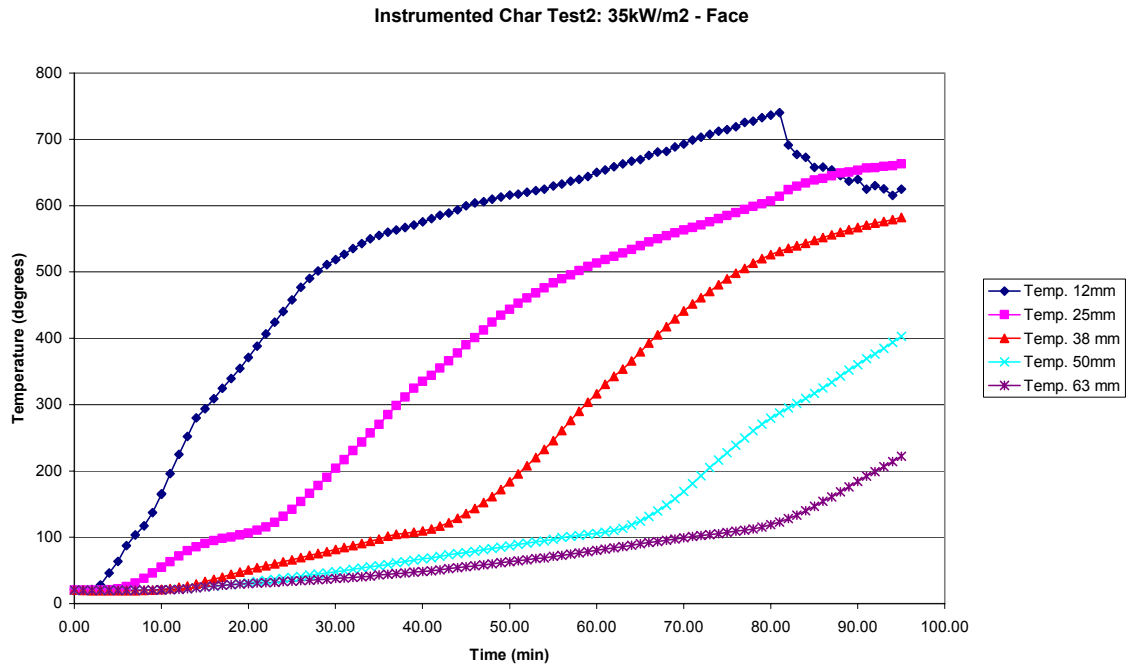

Figure B2: Instrumented Char Test 2 - 35 kW/m^2, Face Grain

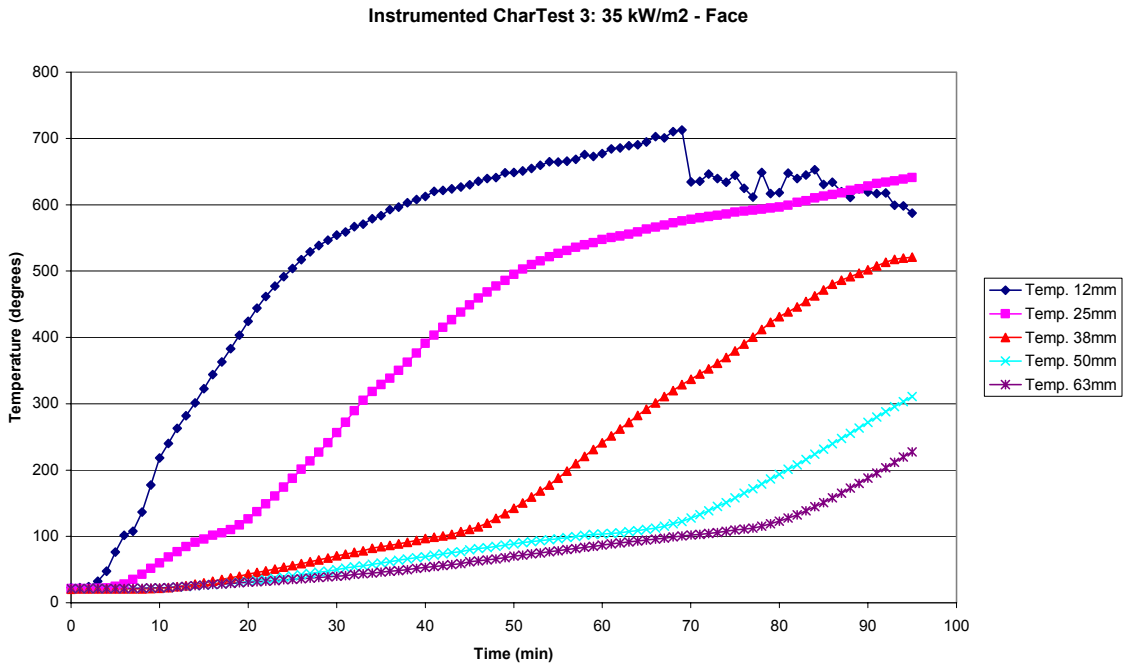

Figure B3: Instrumented Char Test 3 - 35 kW/m^2, Face Grain

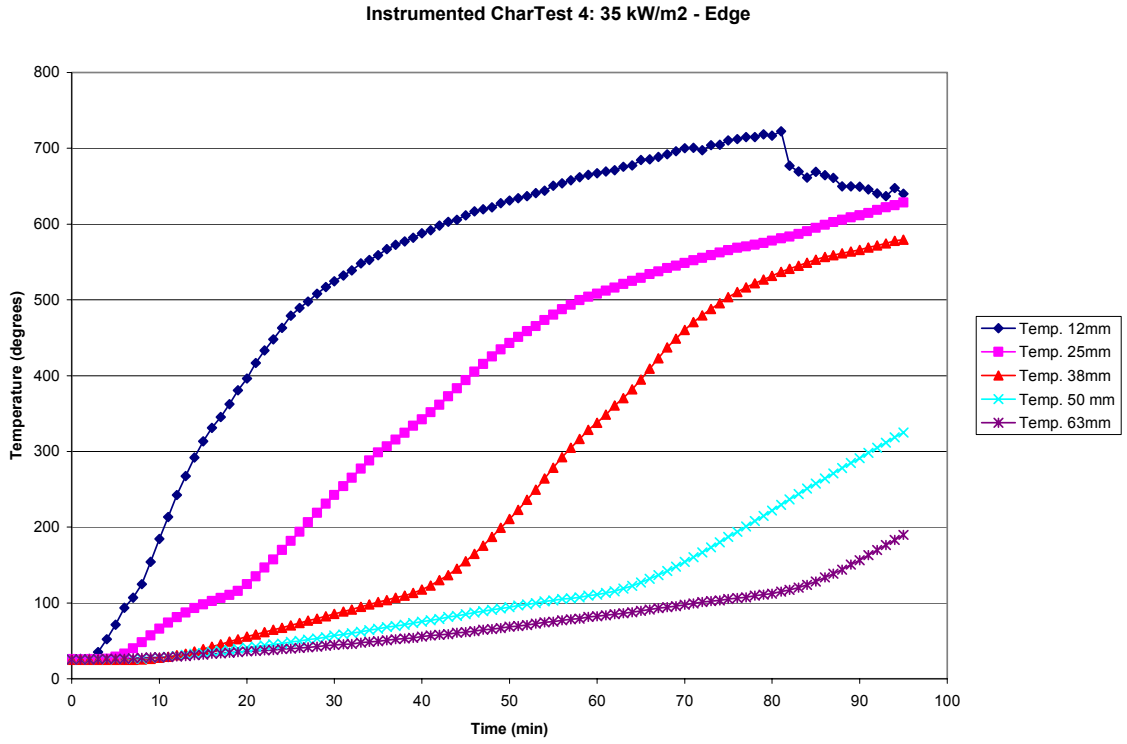

Figure B4: Instrumented Char Test 4 - 35 kW/m^2, Edge Grain

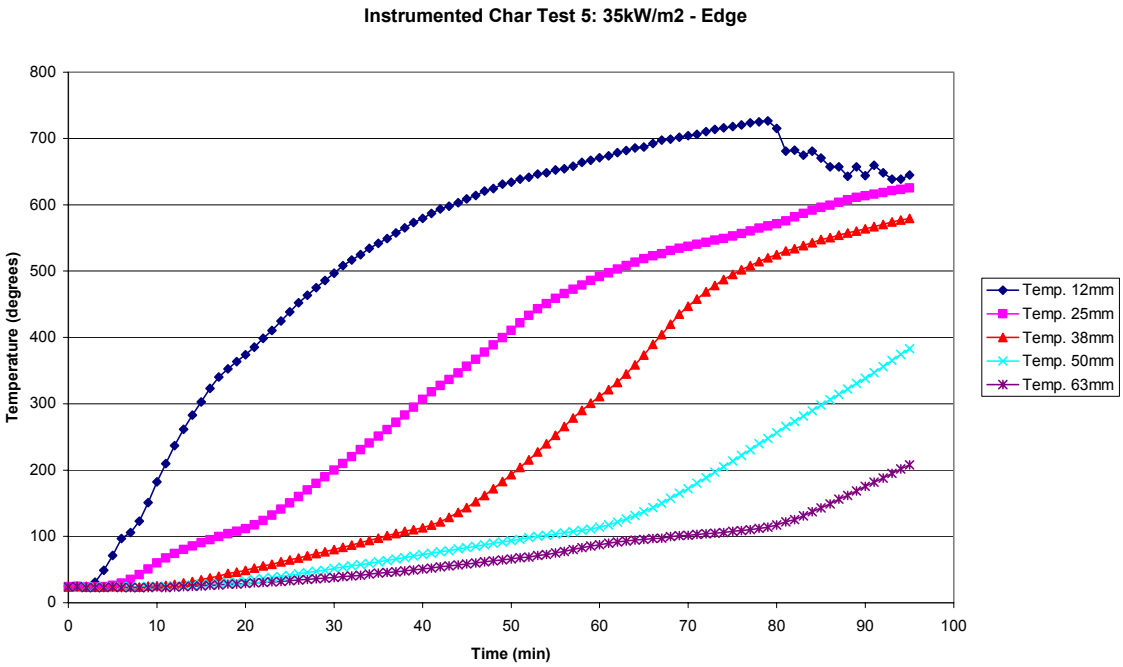

Figure B5: Instrumented Char Test 5 - 35 kW/m^2, Edge Grain

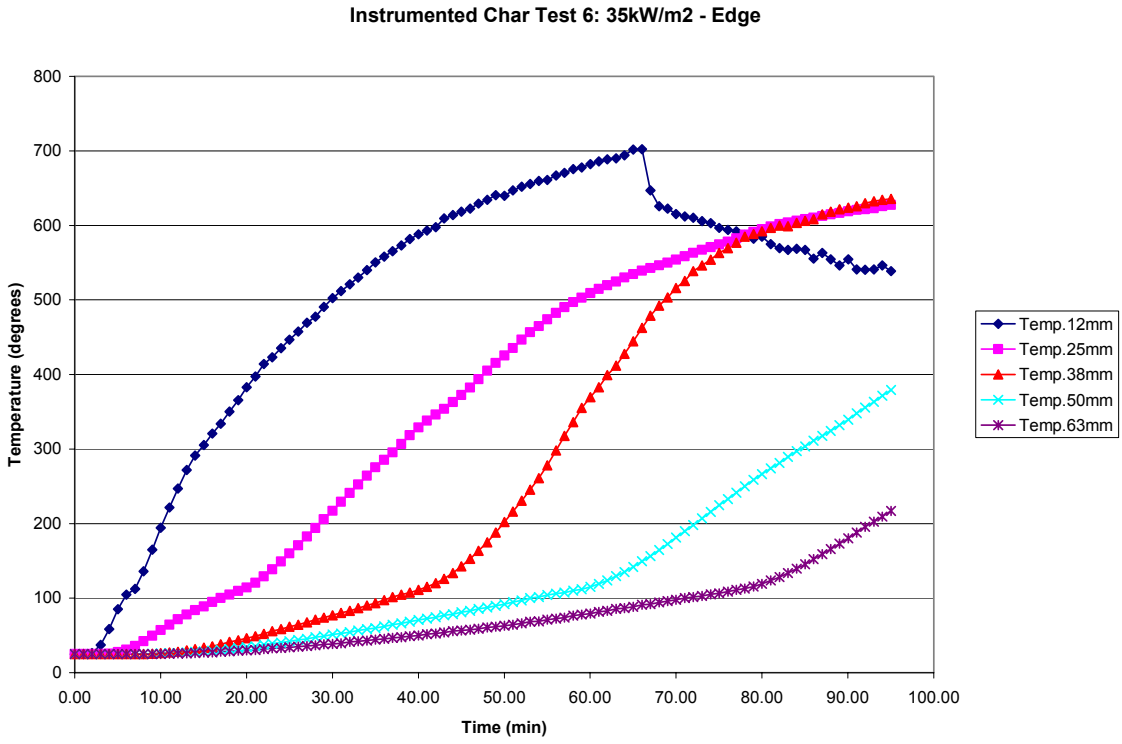

Figure B6: Instrumented Char Test 6 - 35 kW/m^2, Edge Grain

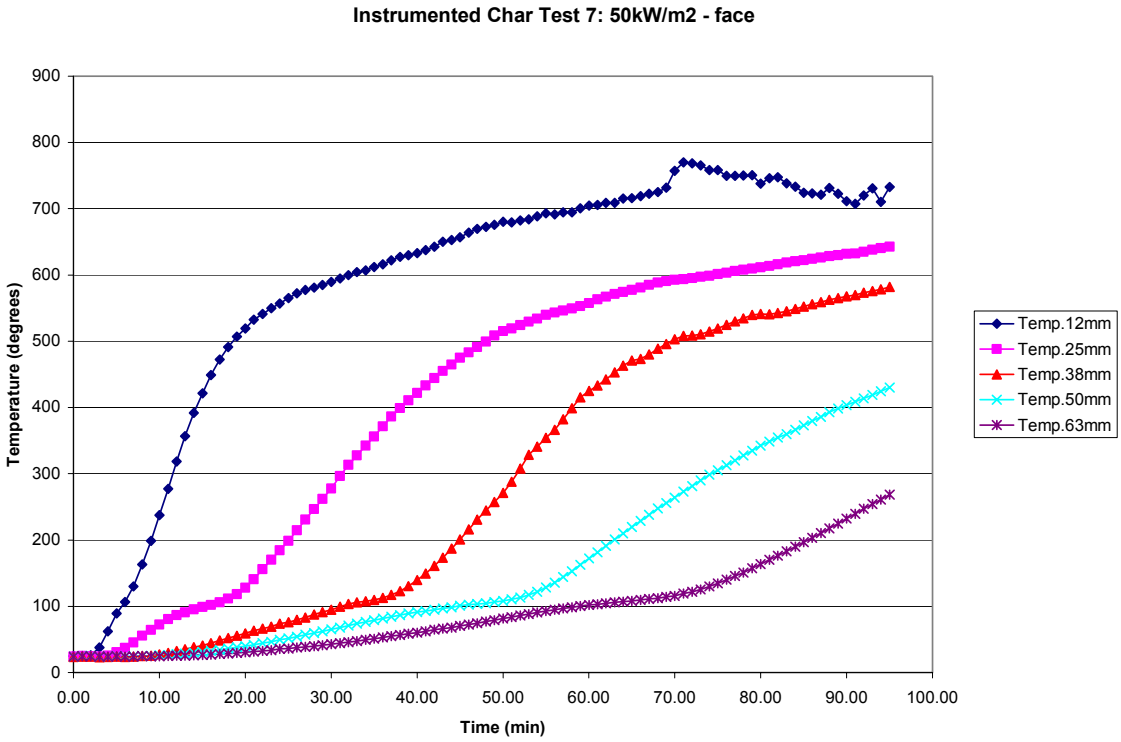

Figure B7: Instrumented Char Test 7 - 50 kW/m^2, Face Grain

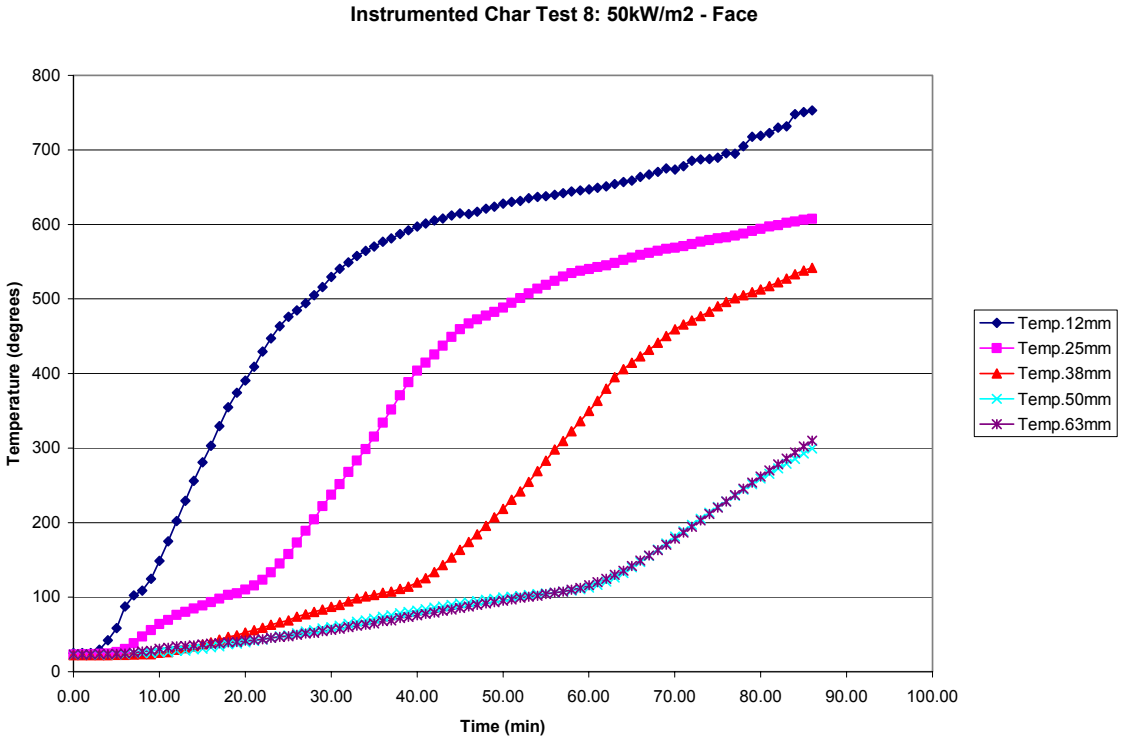

Figure B8: Instrumented Char Test 8 - 50 kW/m^2, Face Grain

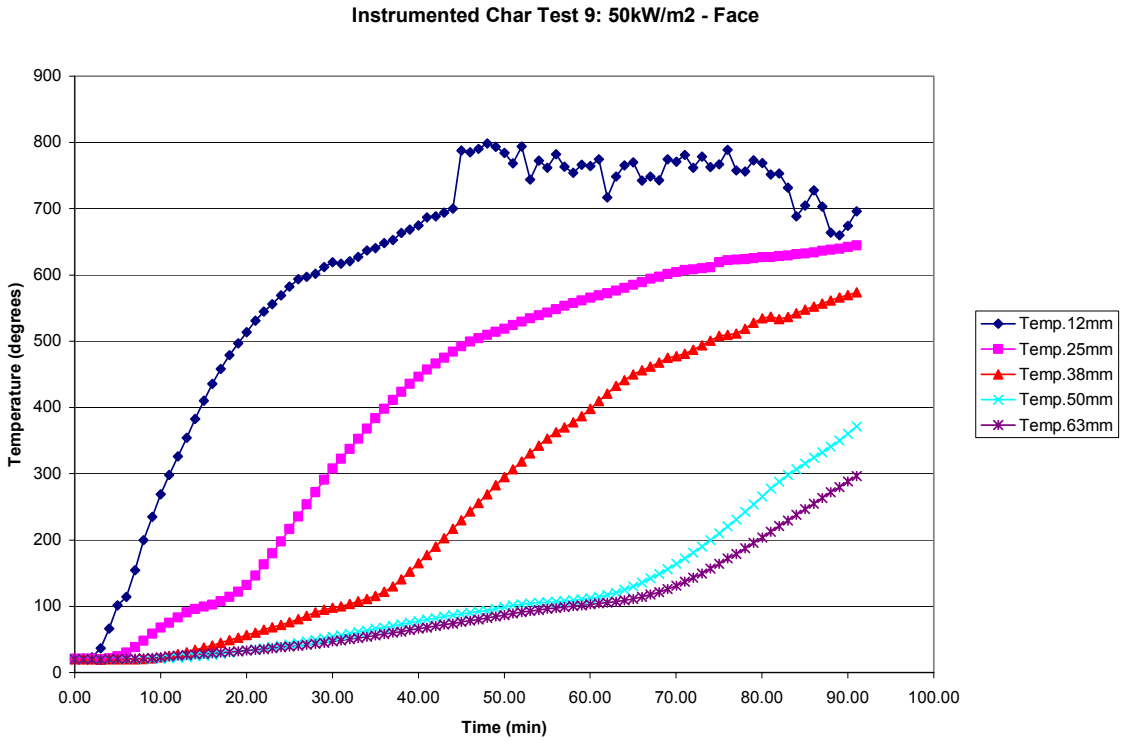

Figure B9: Instrumented Char Test 9 - 50 kW/m^2, Face Grain

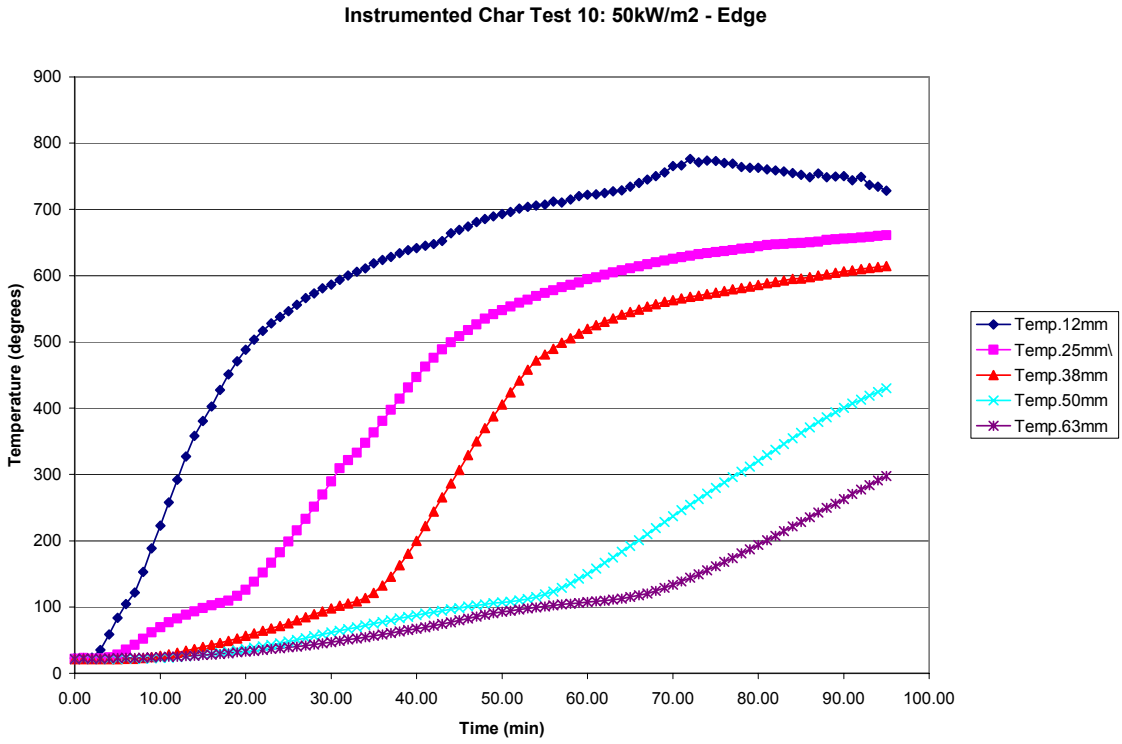

Figure B10: Instrumented Char Test 10 - 50 kW/m^2, Edge Grain

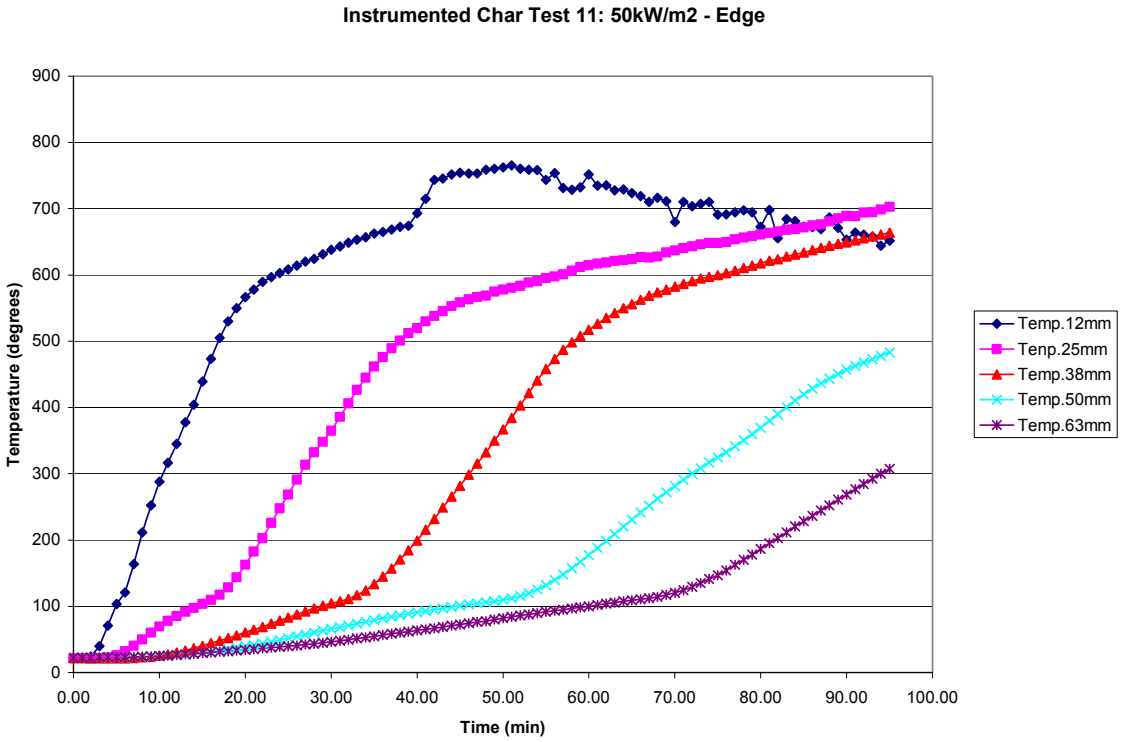

Figure B11: Instrumented Char Test 11 - 50 kW/m^2, Edge Grain

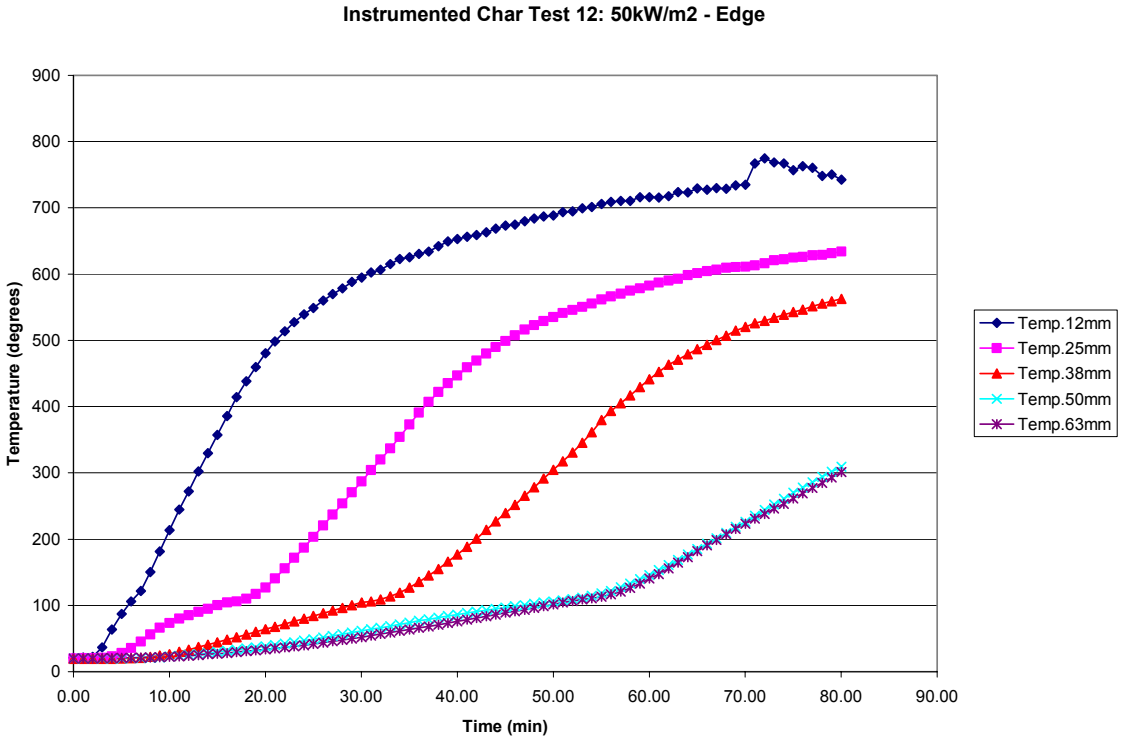

Figure B12: Instrumented Char Test 12 - 50 kW/m^2, Edge Grain

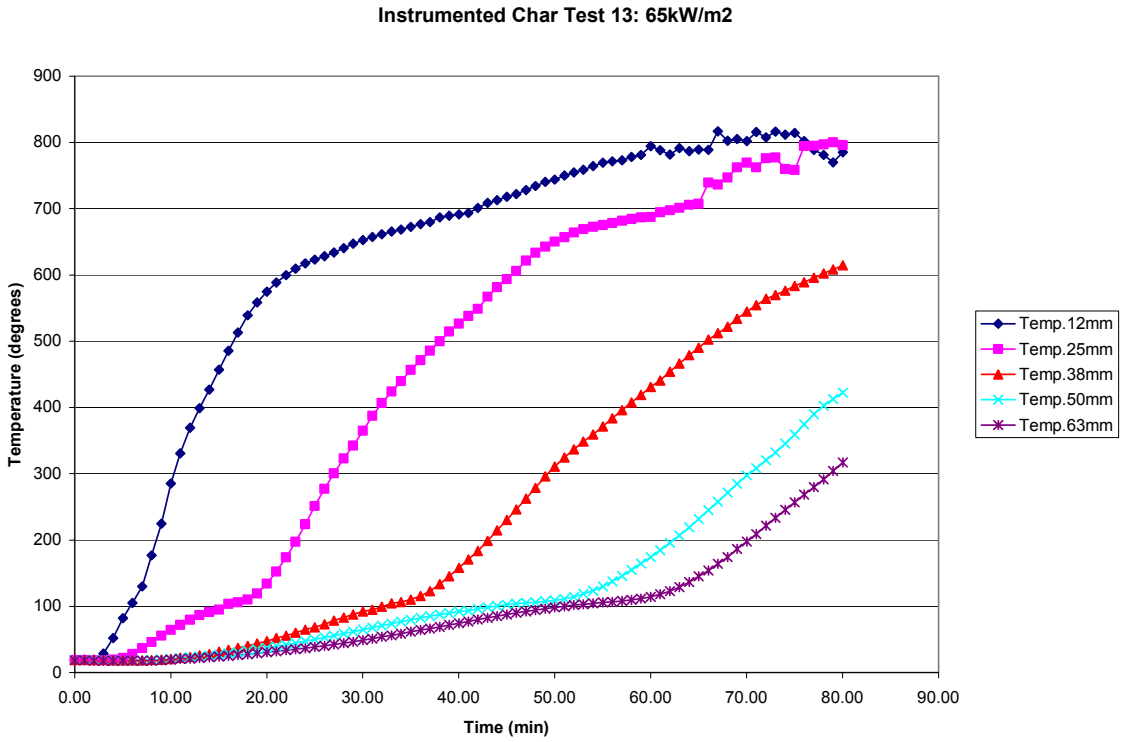

Figure B13: Instrumented Char Test 13 - 65 kW/m^2, Face Grain

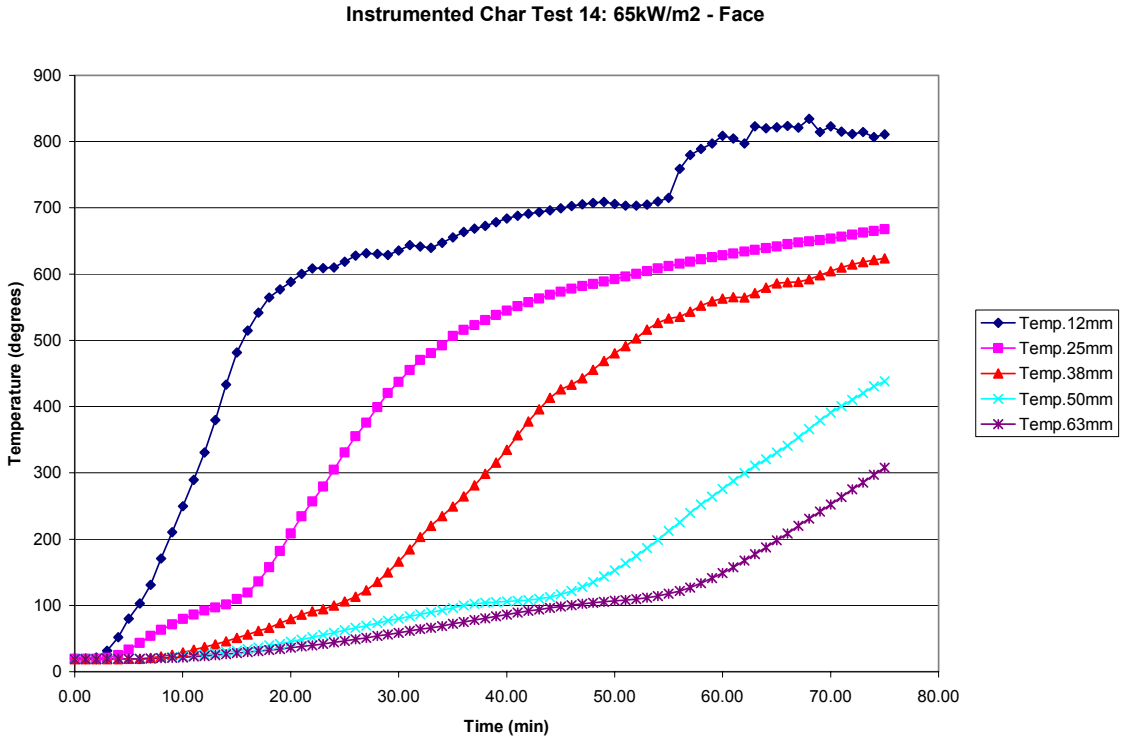

Figure B14: Instrumented Char Test 14 - 65 kW/m^2, Face Grain

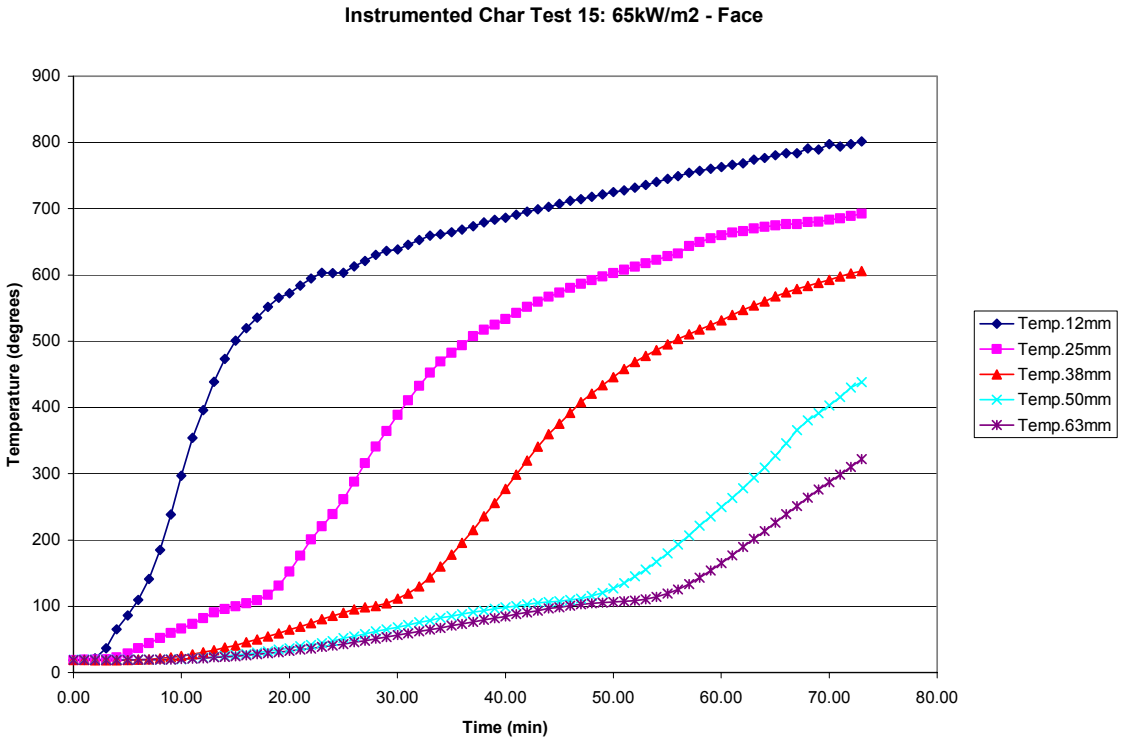

Figure B15: Instrumented Char Test 15 - 65 kW/m^2, Face Grain

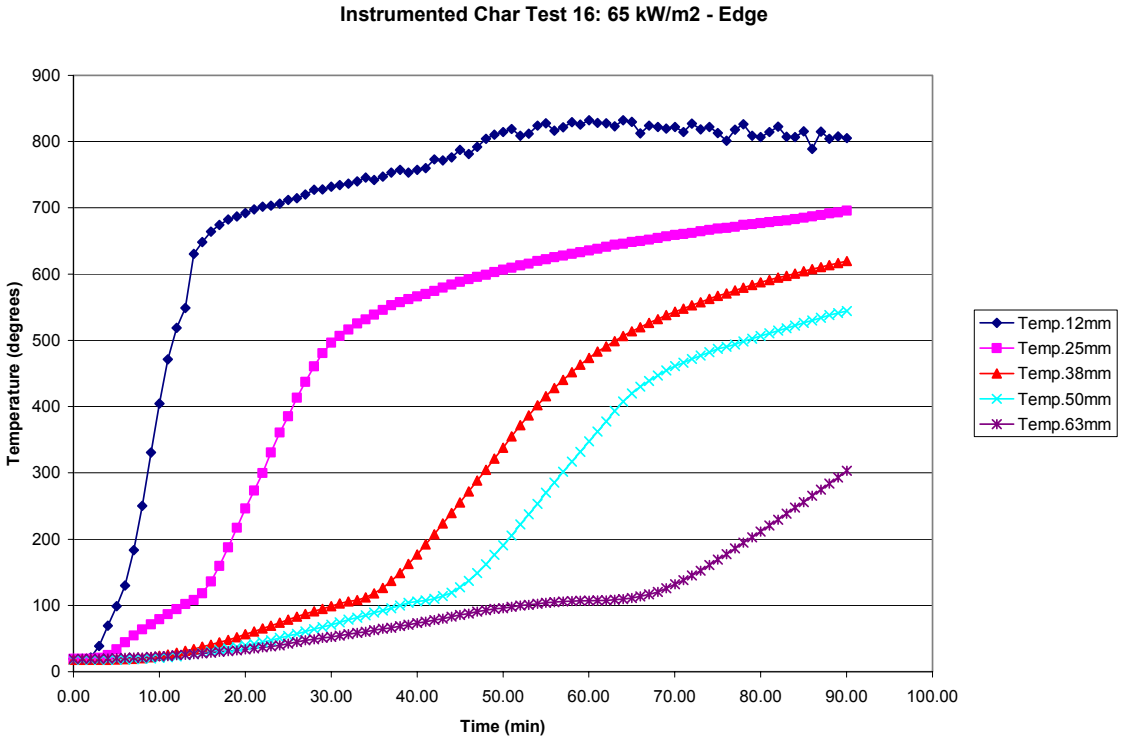

Figure B16: Instrumented Char Test 16 - 65 kW/m^2, Edge Grain

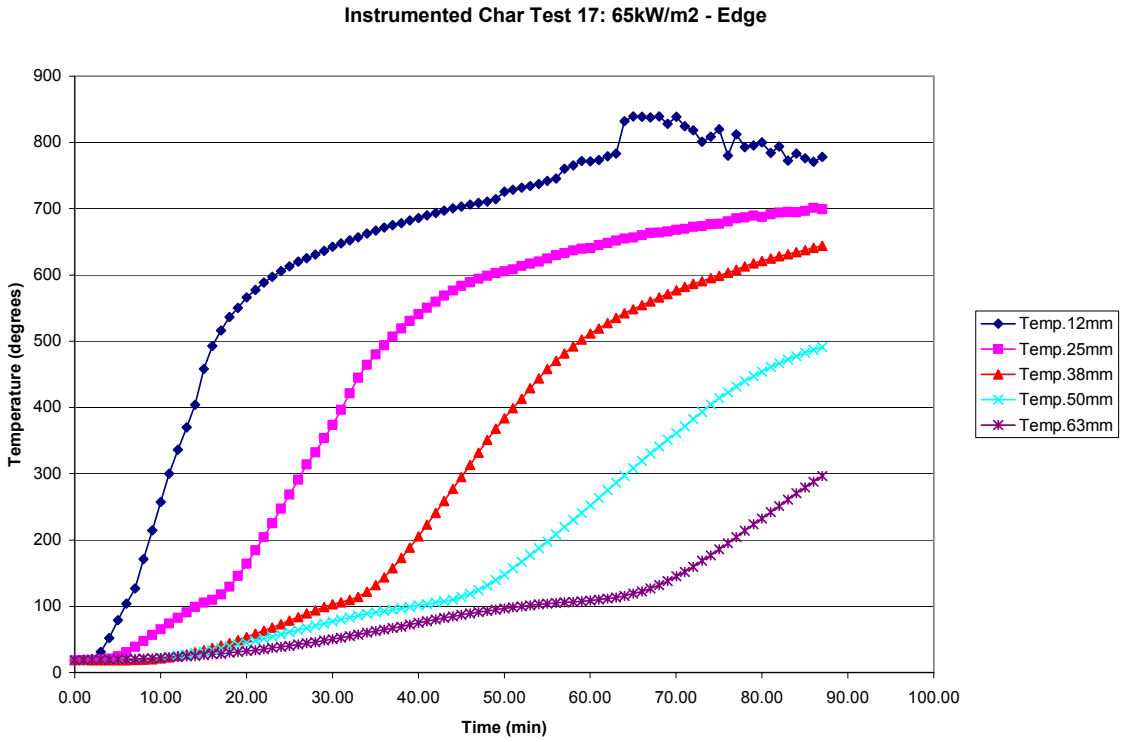

Figure B17: Instrumented Char Test 17 - 65 kW/m^2, Edge Grain

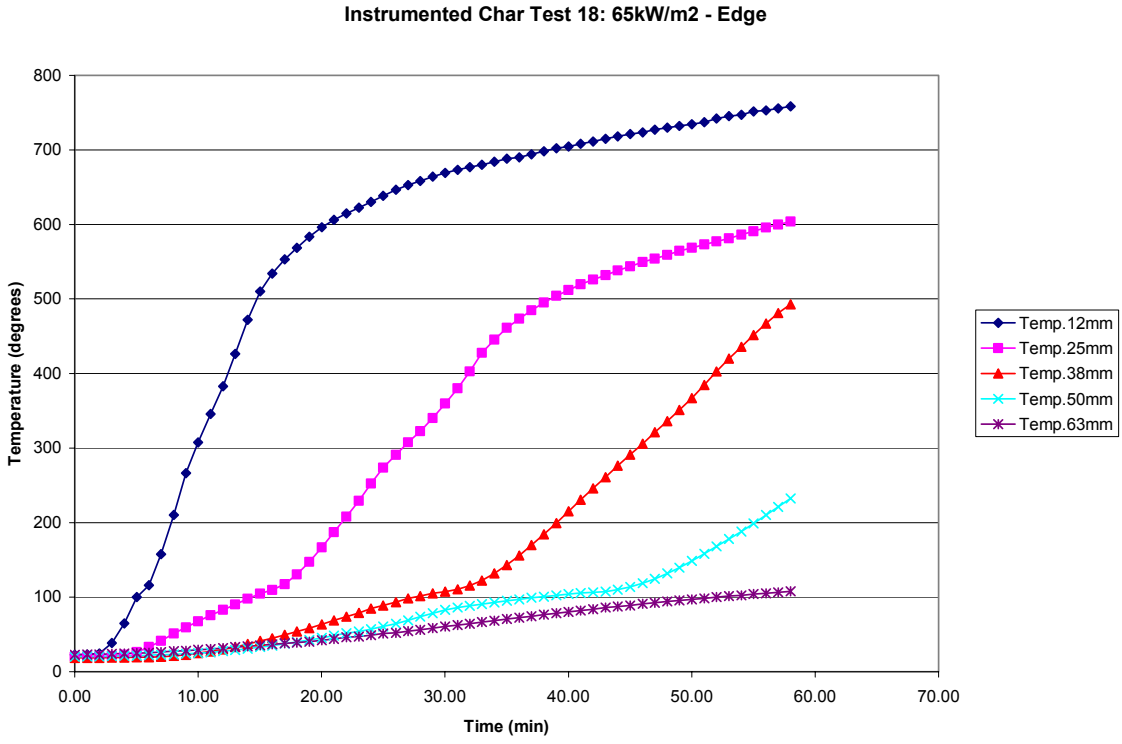

Figure B18: Instrumented Char Test 18 - 65 kW/m^2, Edge Grain

Appendix C Char Rate Comparison Instrumented / Un-Instrumented

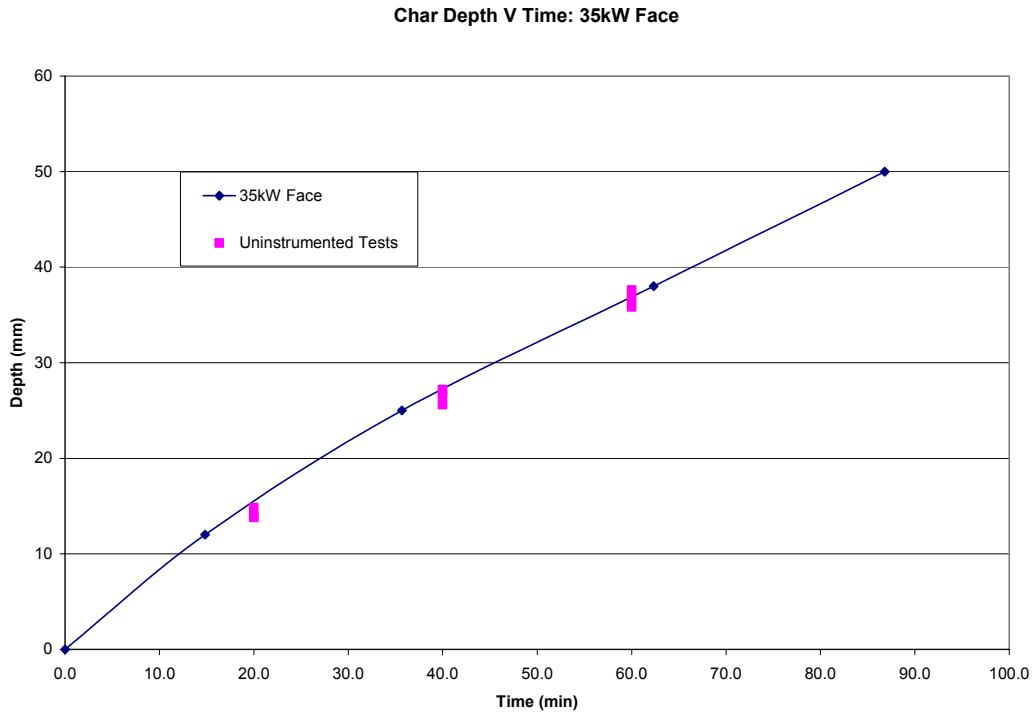

Figure C1: Char Depth Comparisons - 35 kW/m^2, Face Grain

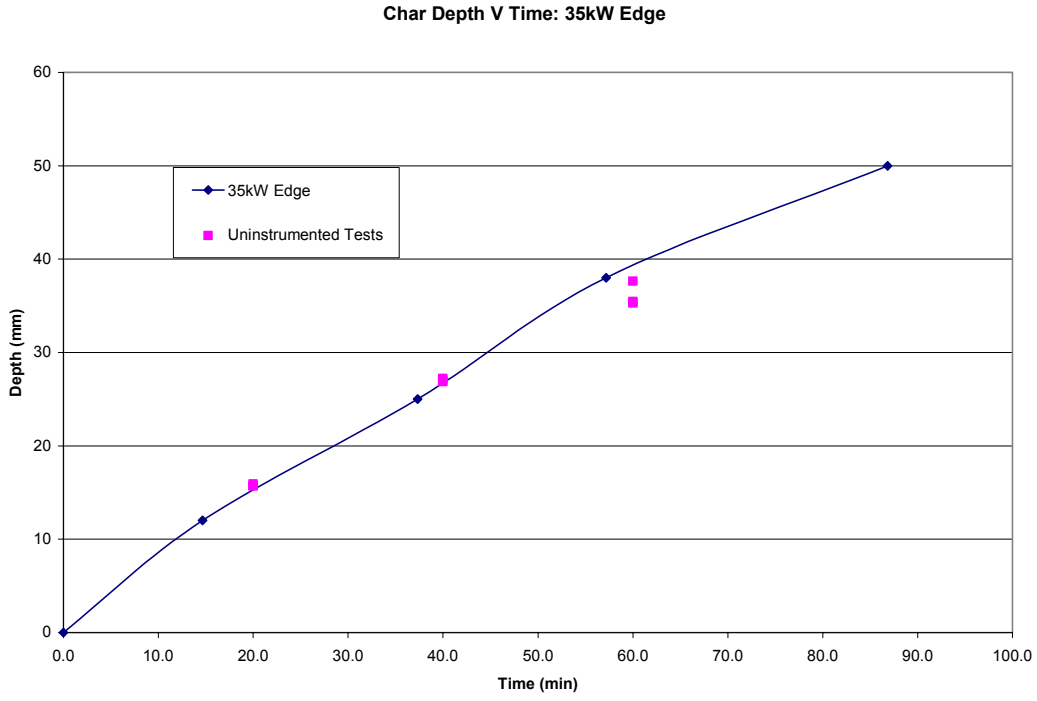

Figure C2: Char Depth Comparisons - 35 kW/m^2, Edge Grain

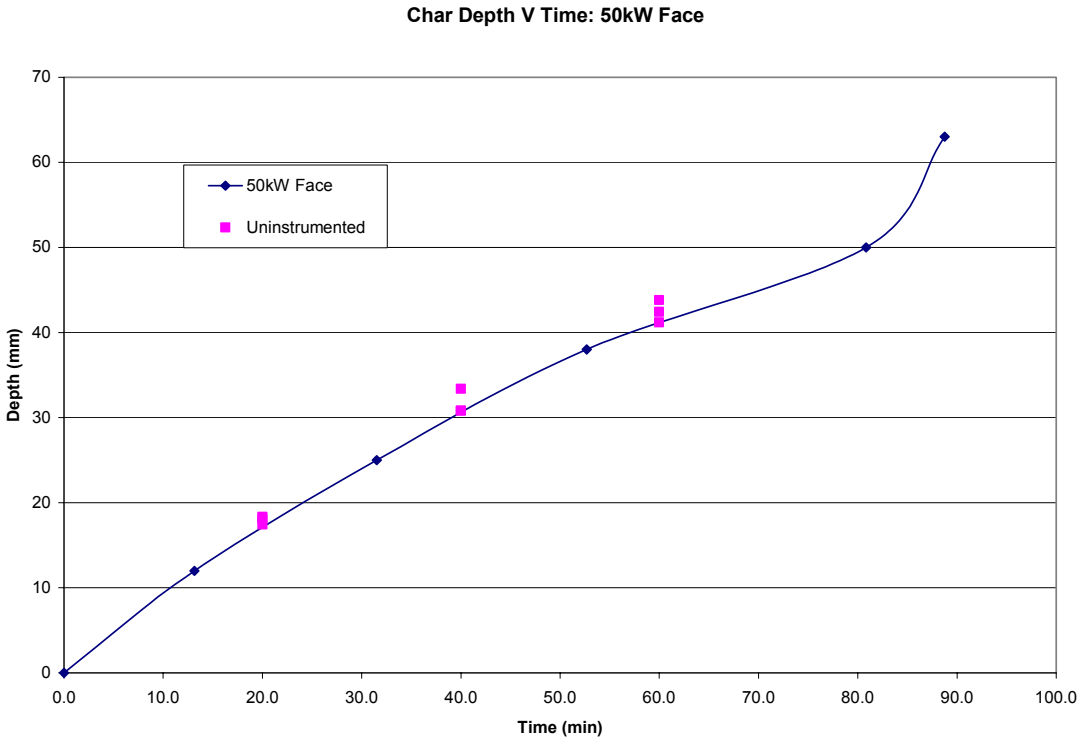

Figure C3: Char Depth Comparisons - 50 kW/m^2, Face Grain

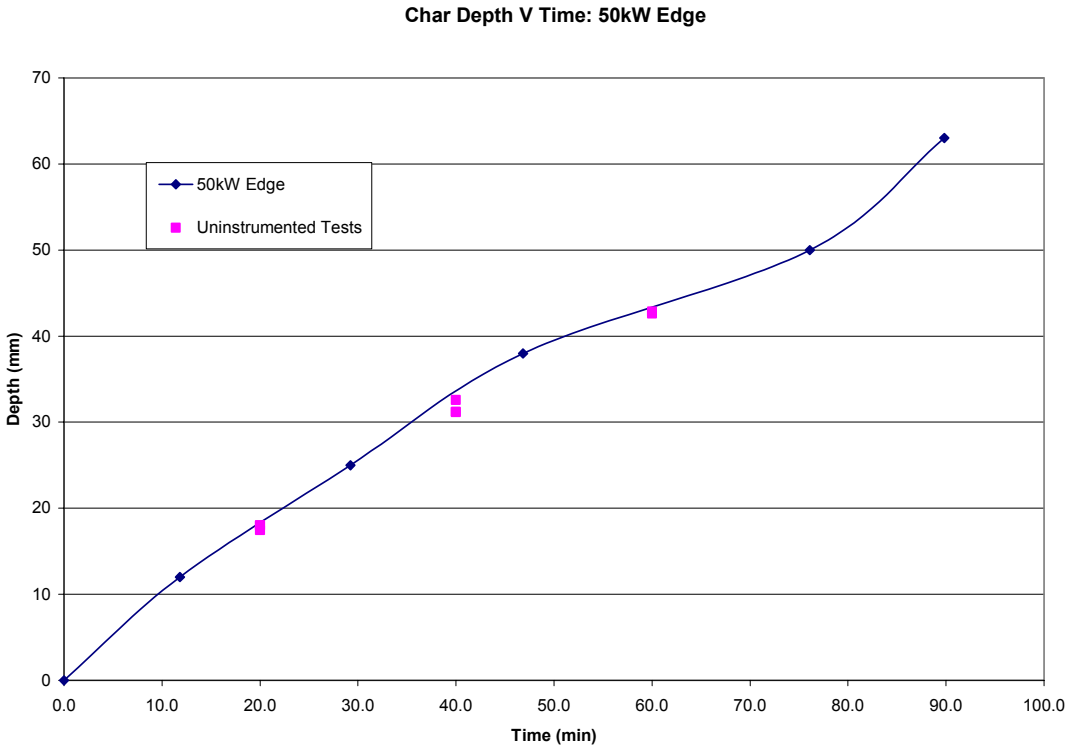

Figure C4: Char Depth Comparisons - 50 kW/m^2, Edge Grain

Appendix C Char Rate Comparison Instrumented / Un-Instrumented

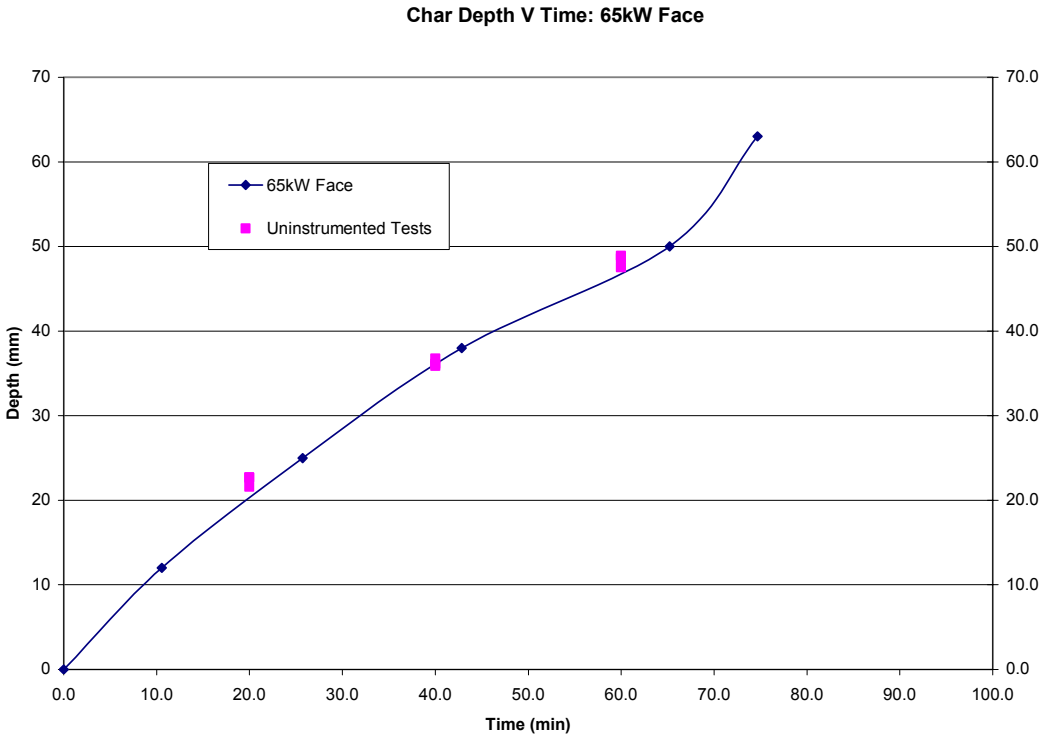

Figure C5: Char Depth Comparisons - 65 kW/m^2, Face Grain

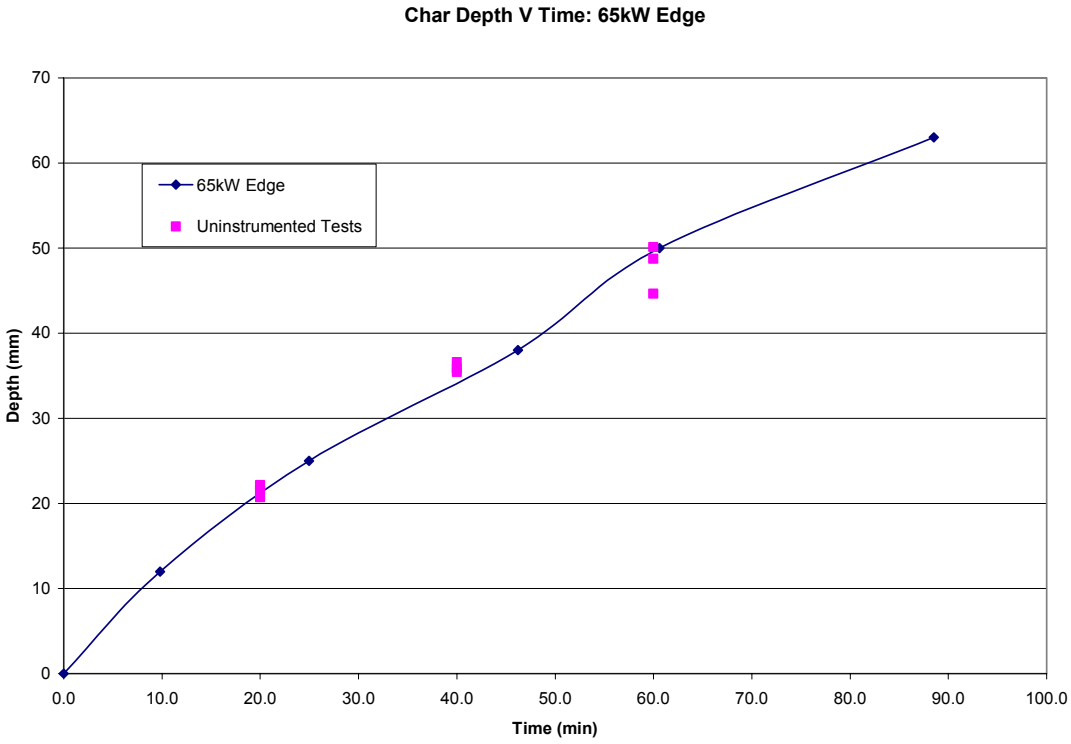

Figure C6: Char Depth Comparisons - 65 kW/m^2, Edge Grain

Appendix D Pilot Test Results

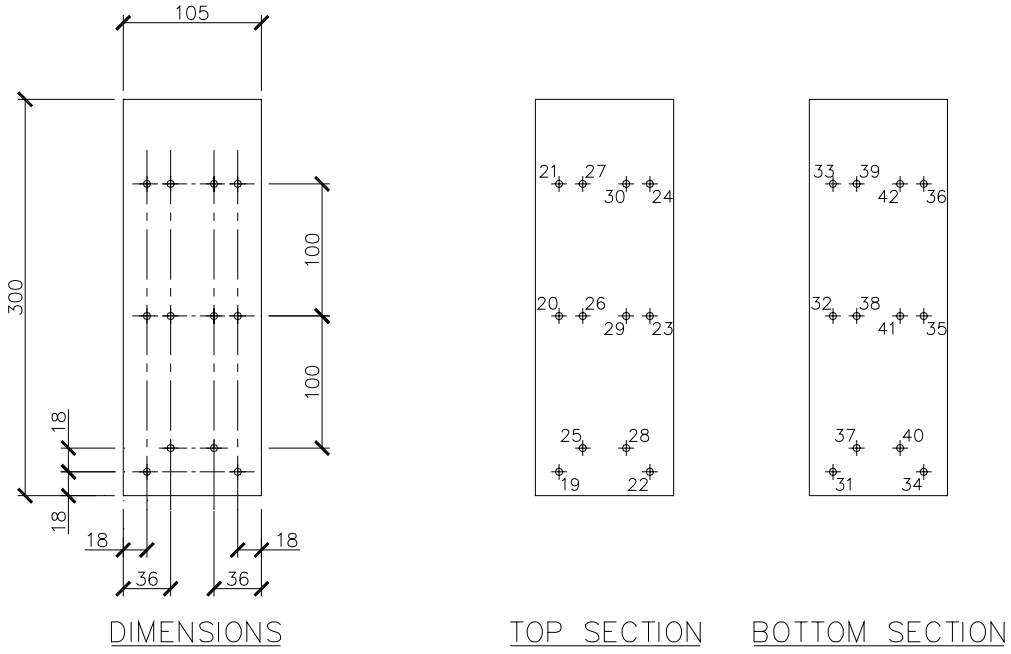

Figure D.1 Thermocouple Layout & Dimensions for Tests 1 & 2

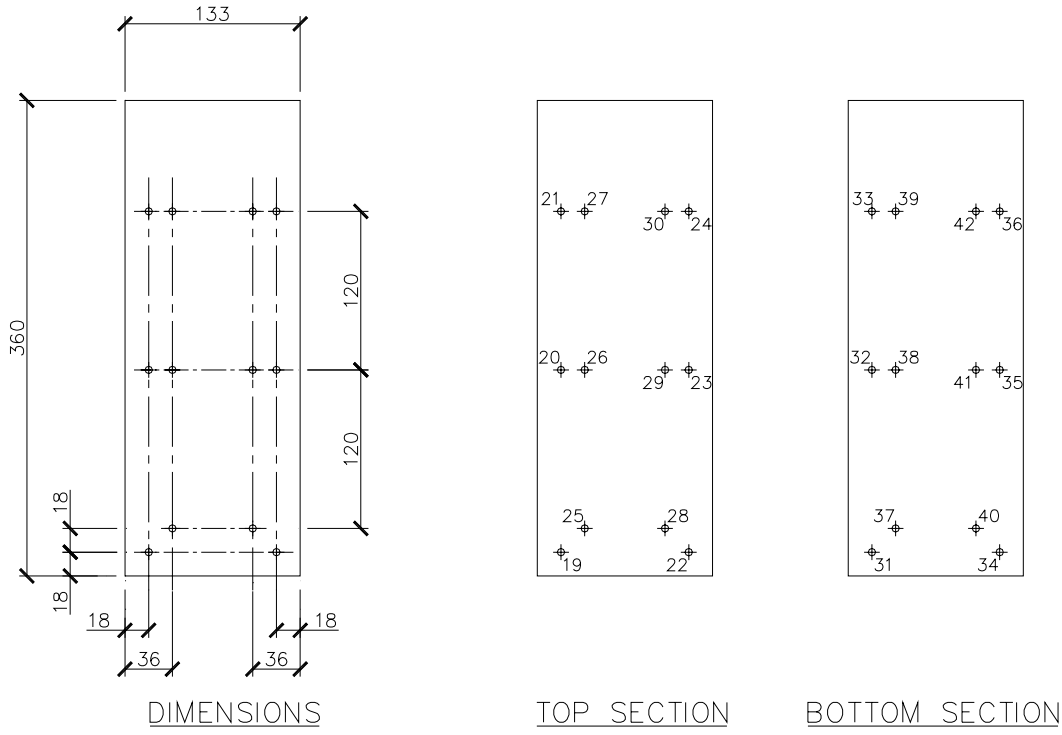

Figure D.2 Thermocouple Layout & Dimensions for Tests 3

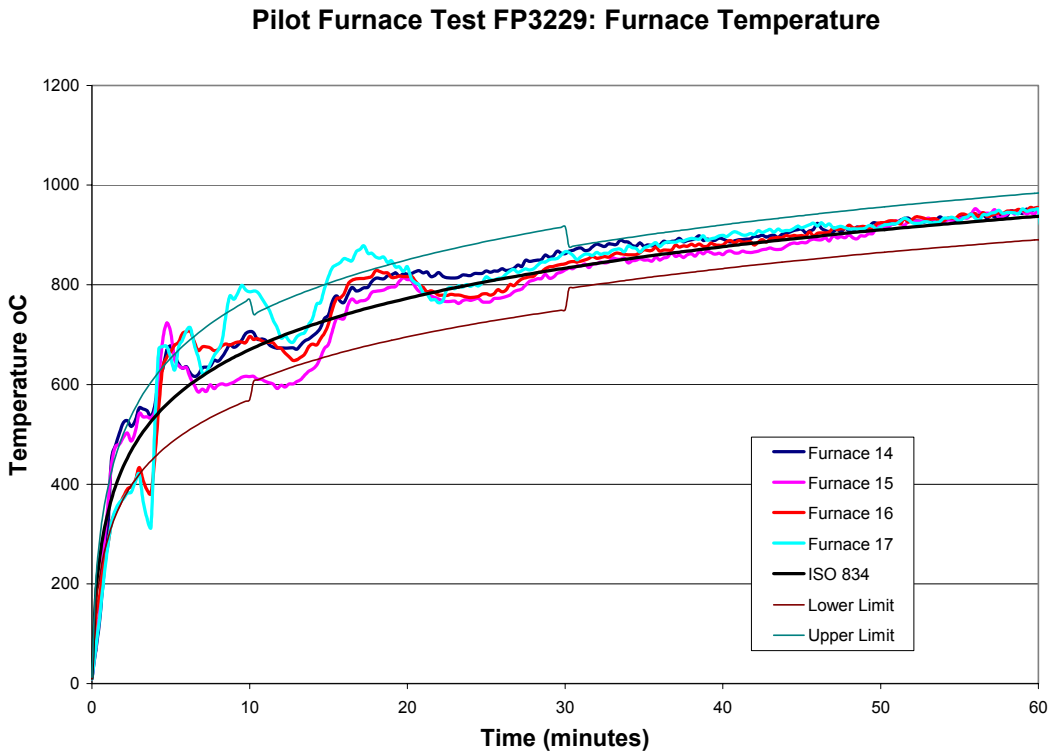

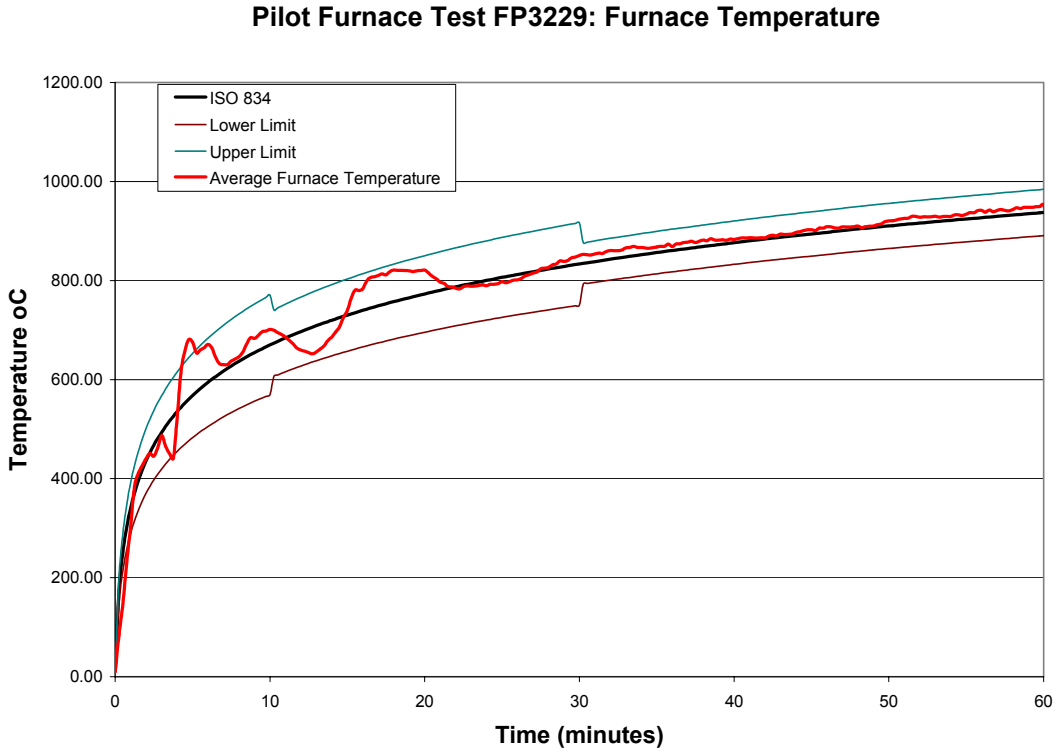

Figure D.3 Pilot Test 1: Furnace Temperature Graphs

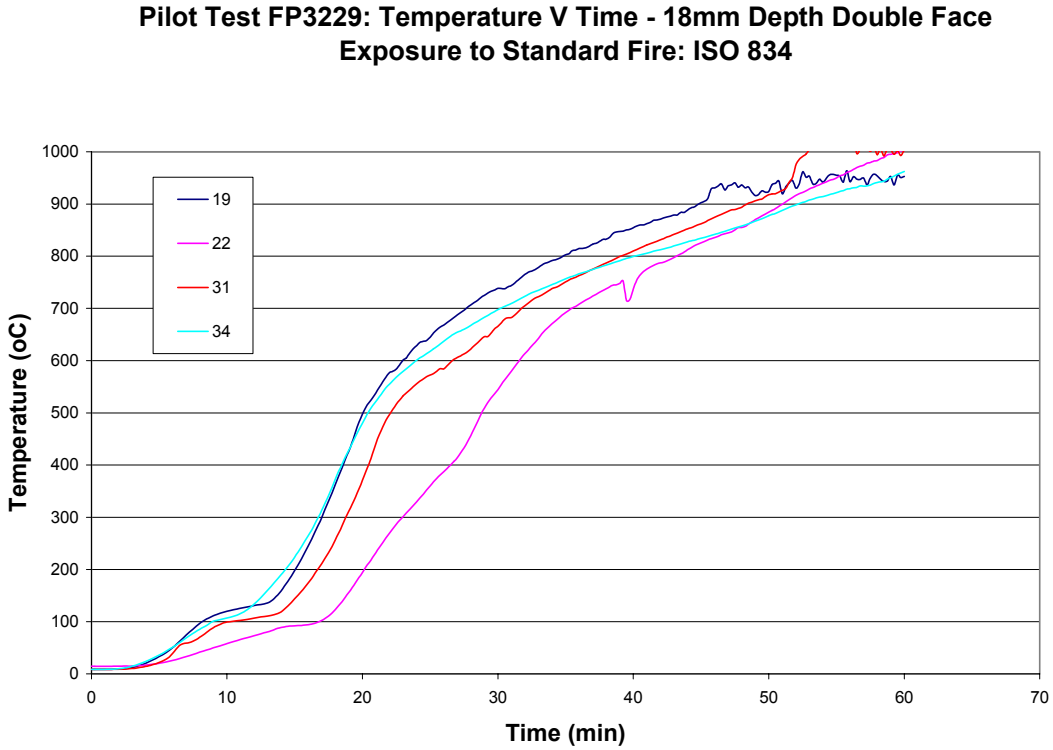

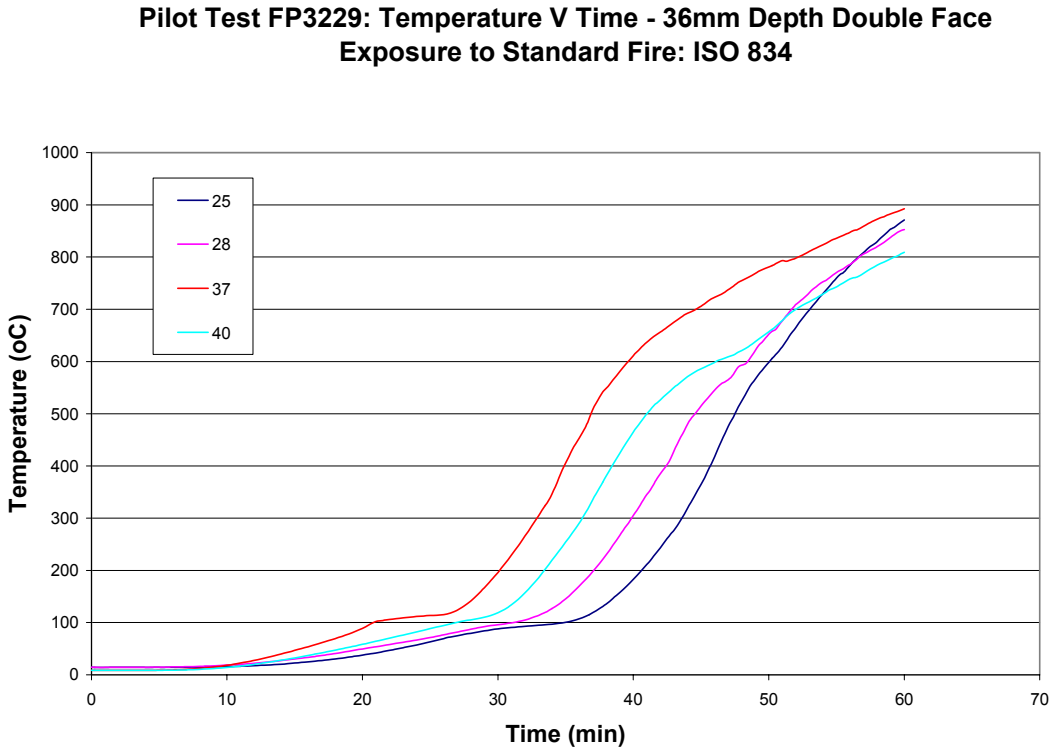

Figure D.4 **Pilot Test 1: Thermocouple Temperature – Time Graphs Double Face Exposure**

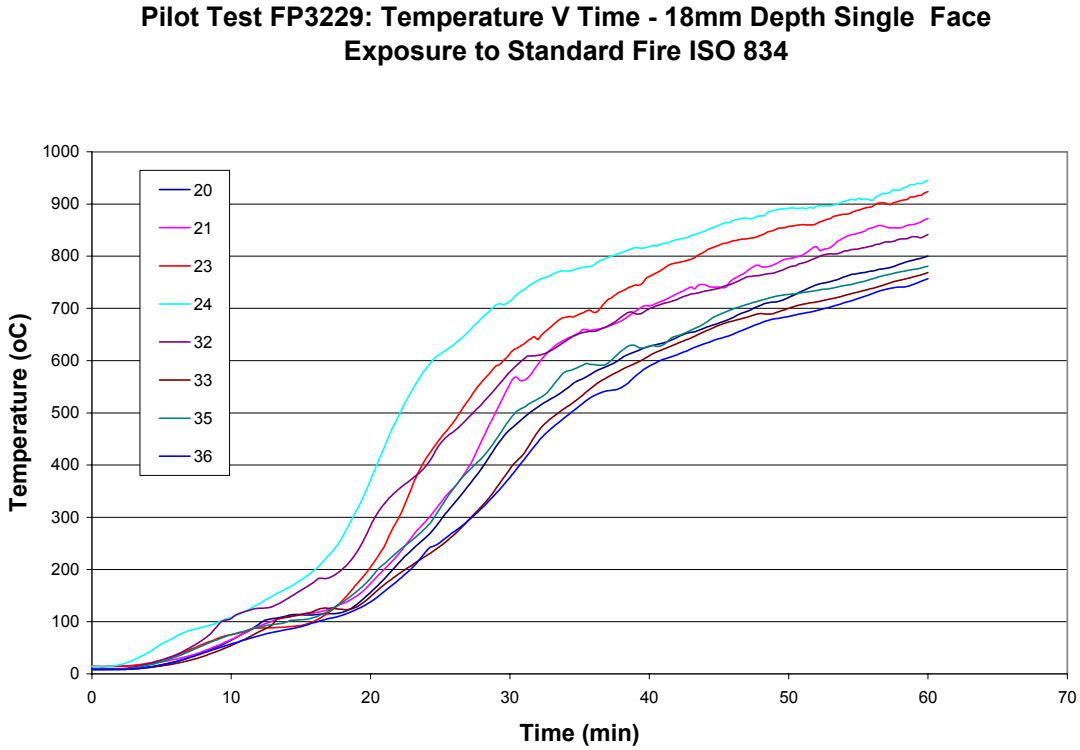

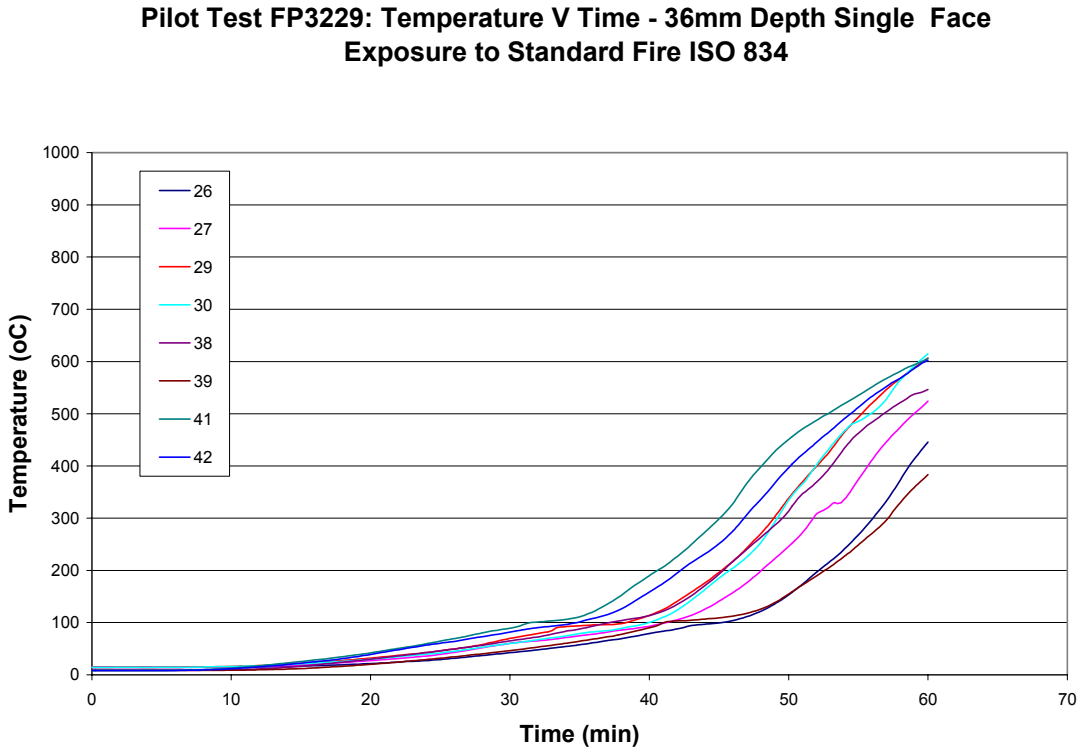

Figure D.5 **Pilot Test 1: Thermocouple Temperature – Time Graphs Single Face Exposure**

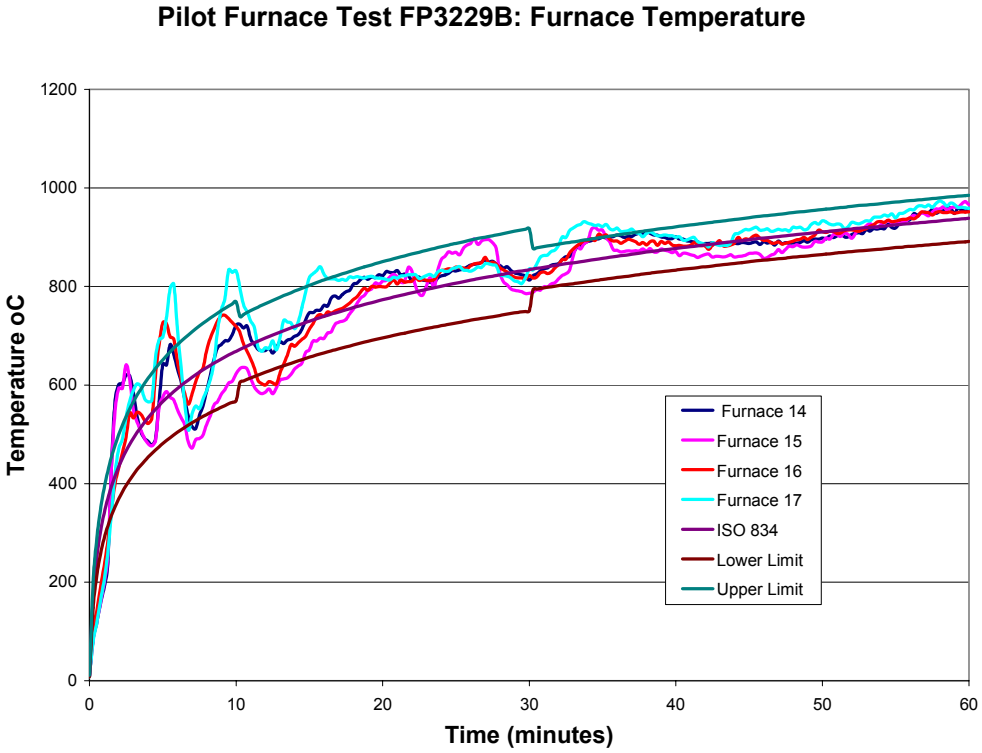

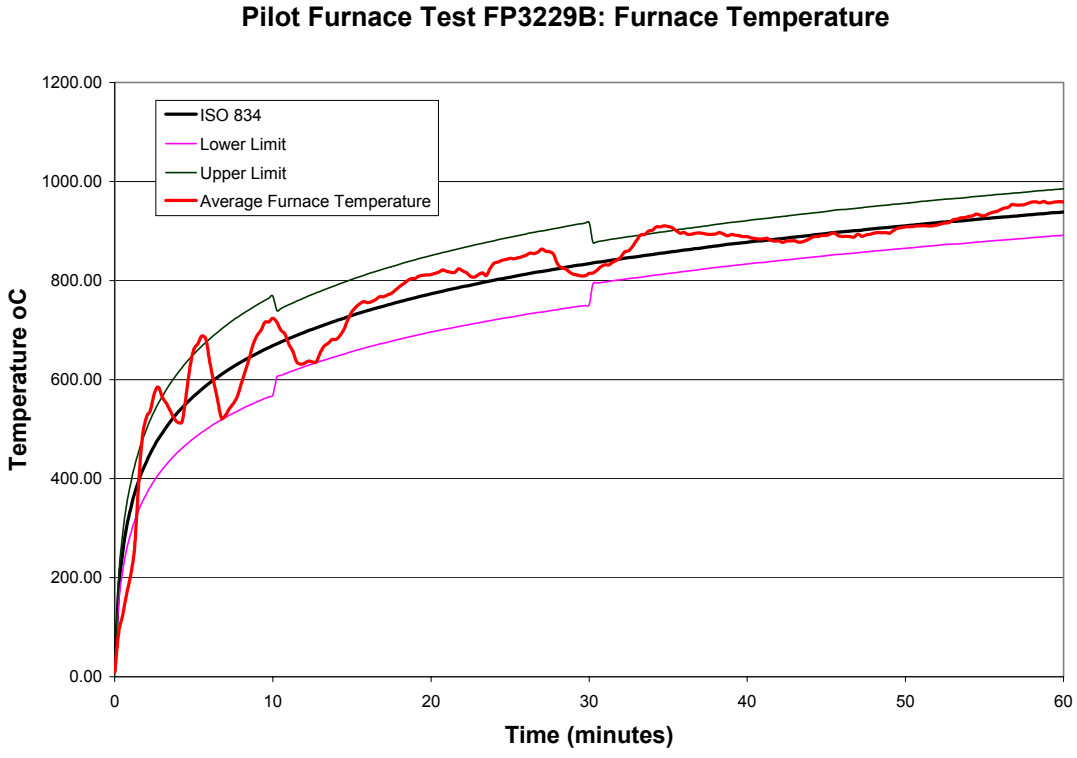

Figure D.6 **Pilot Test 2: Furnace Temperature Graphs**

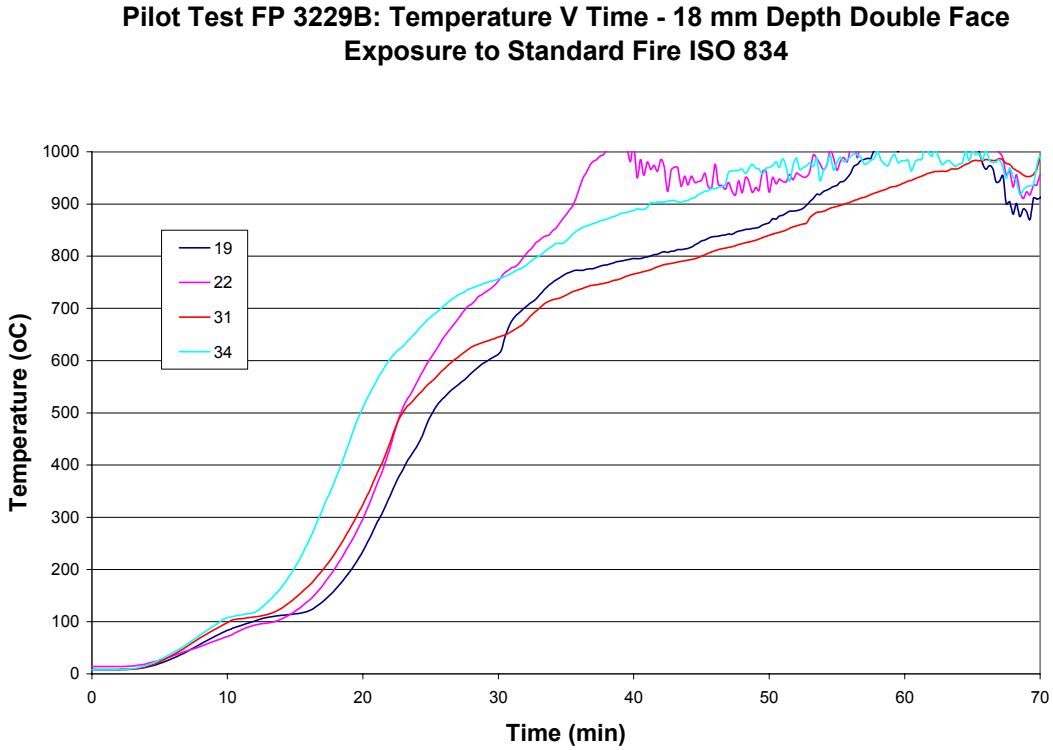

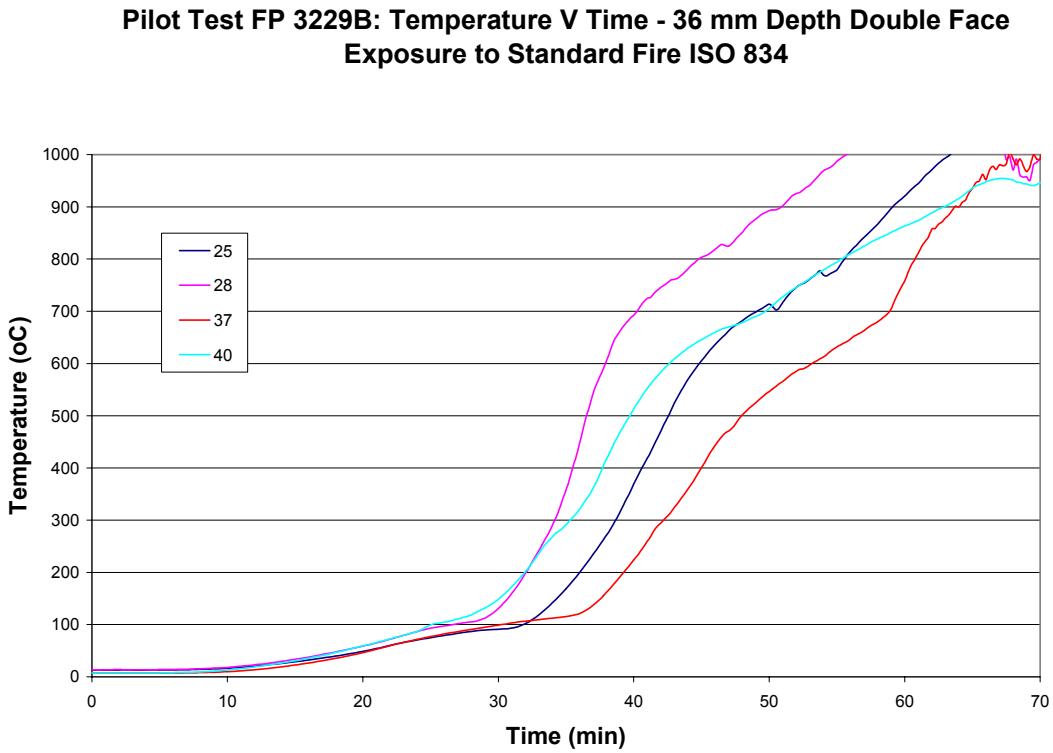

Figure D.7 **Pilot Test 2: Thermocouple Temperature – Time Graphs Double Face Exposure**

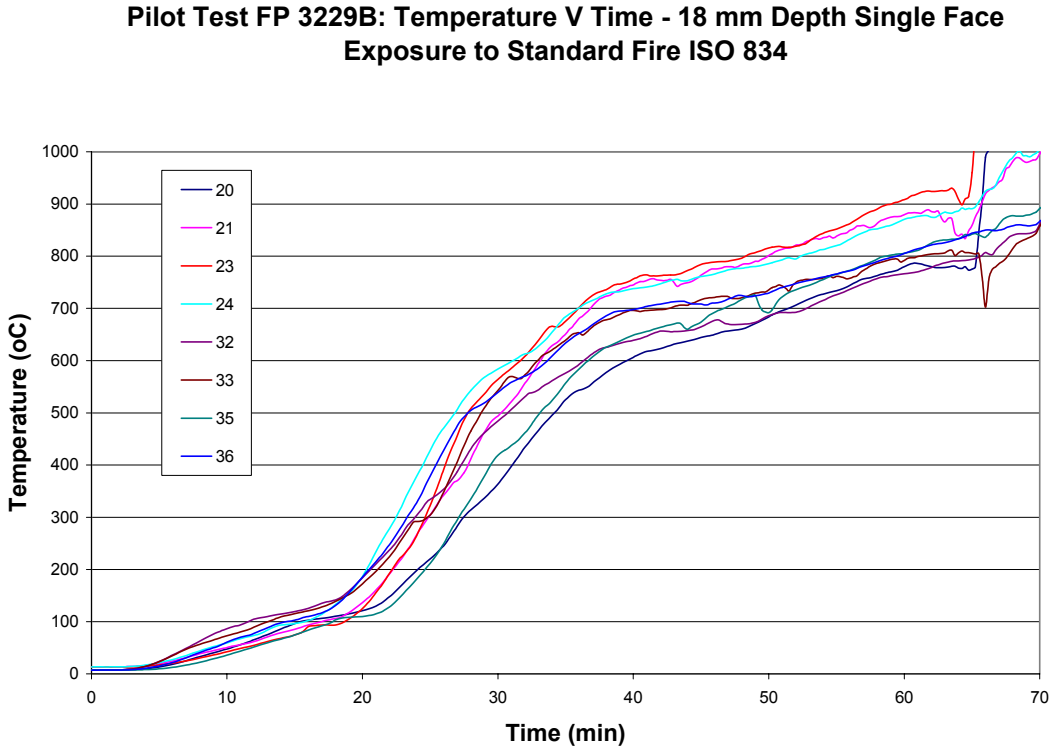

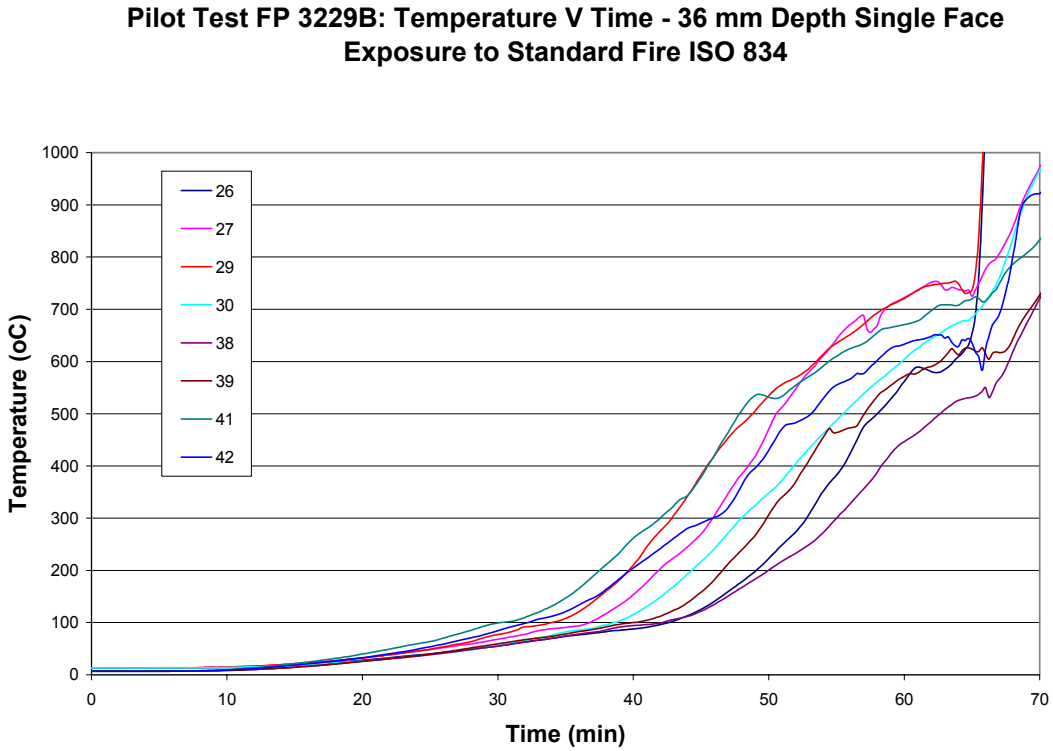

Figure D.8 **Pilot Test 2: Thermocouple Temperature – Time Graphs Single Face Exposure**

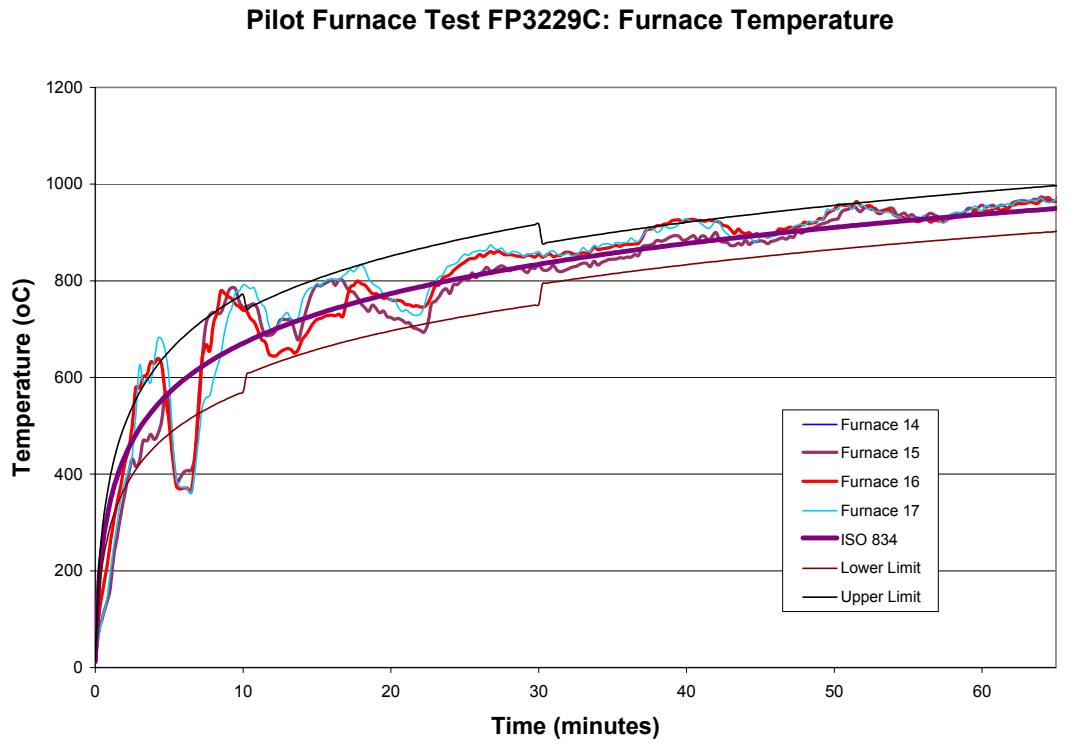

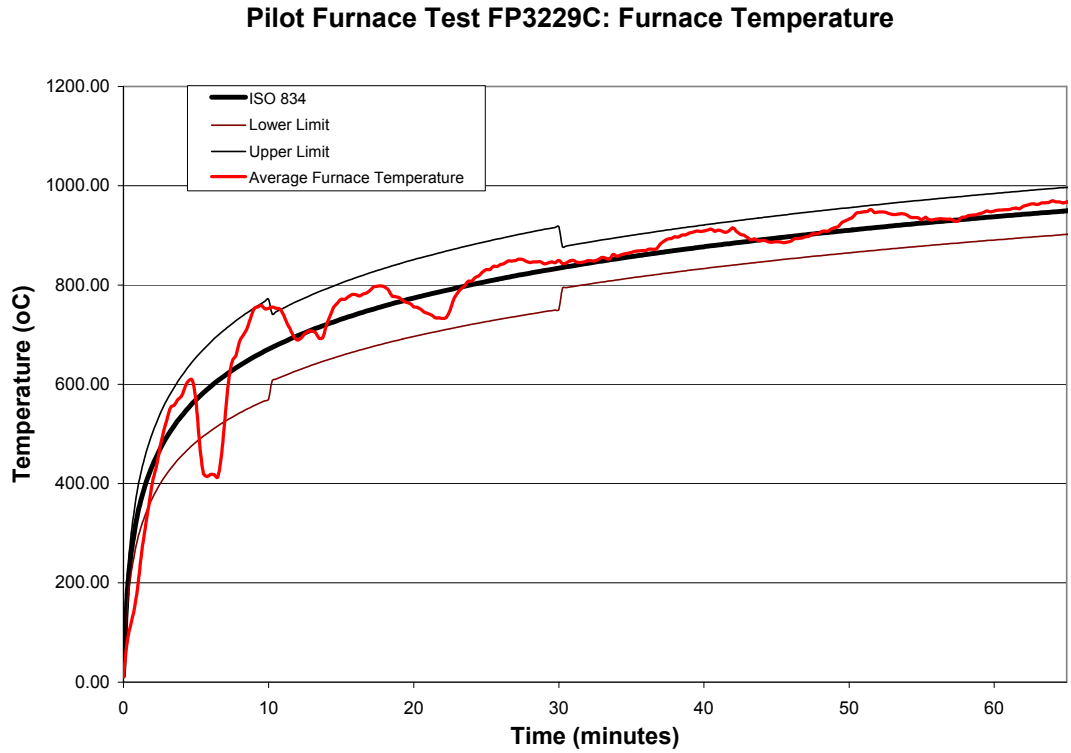

Figure D.9 **Pilot Test 3: Furnace Temperature Graphs**

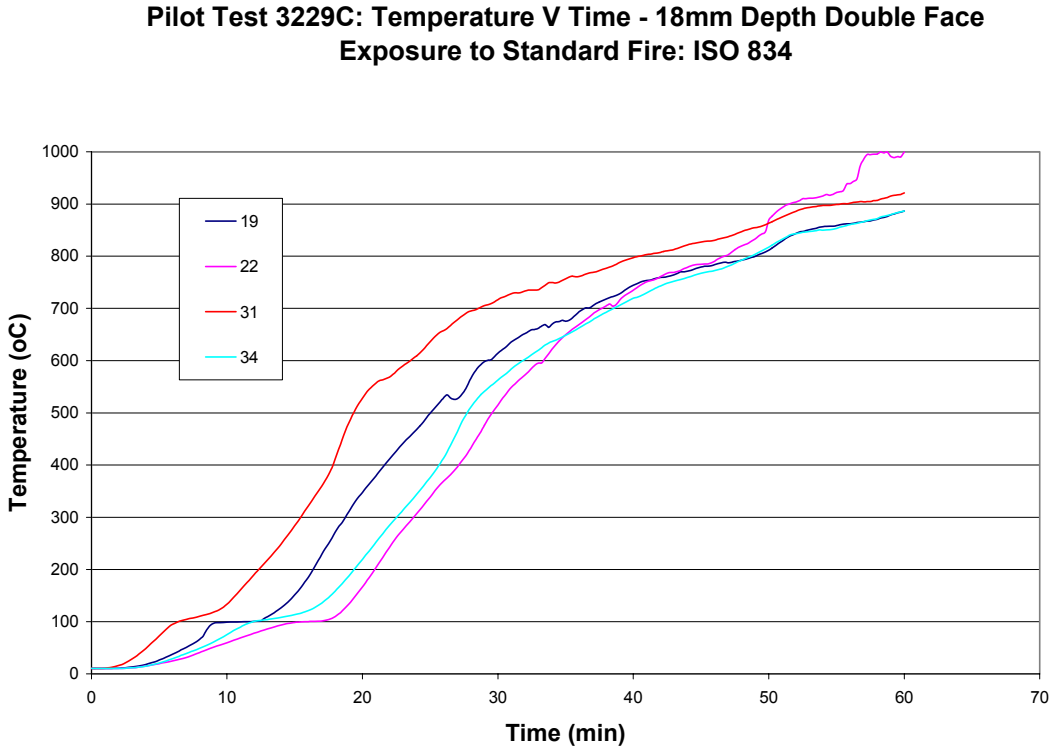

Figure D.10 **Pilot Test 3: Thermocouple Temperature – Time Graphs Double Face Exposure**

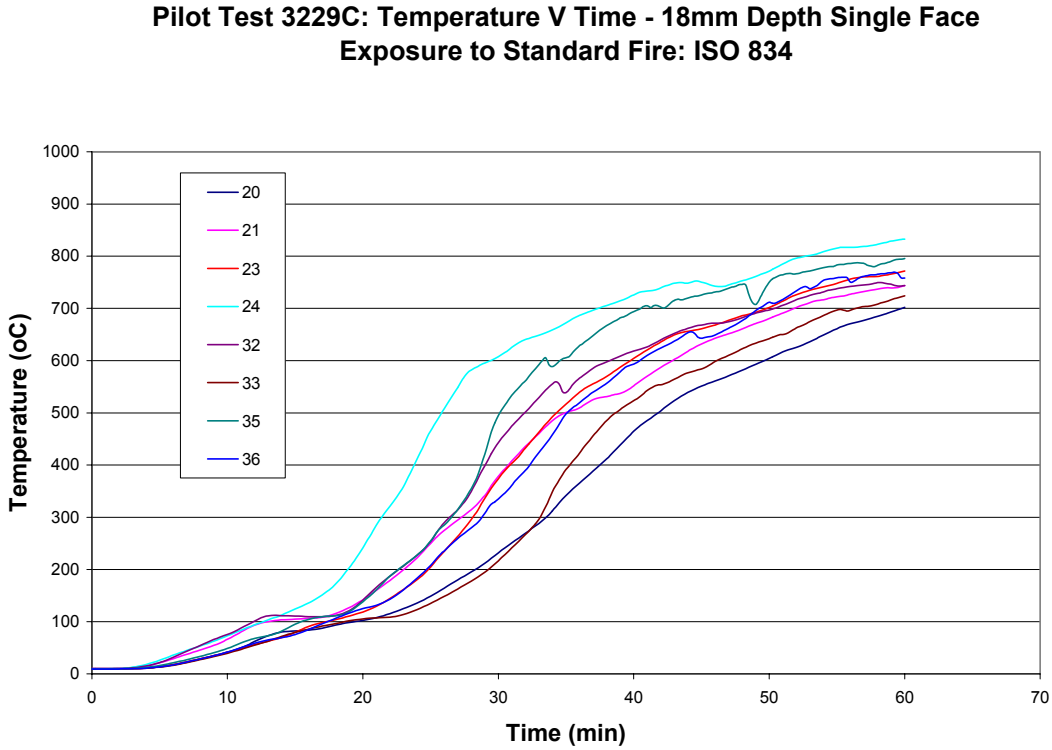

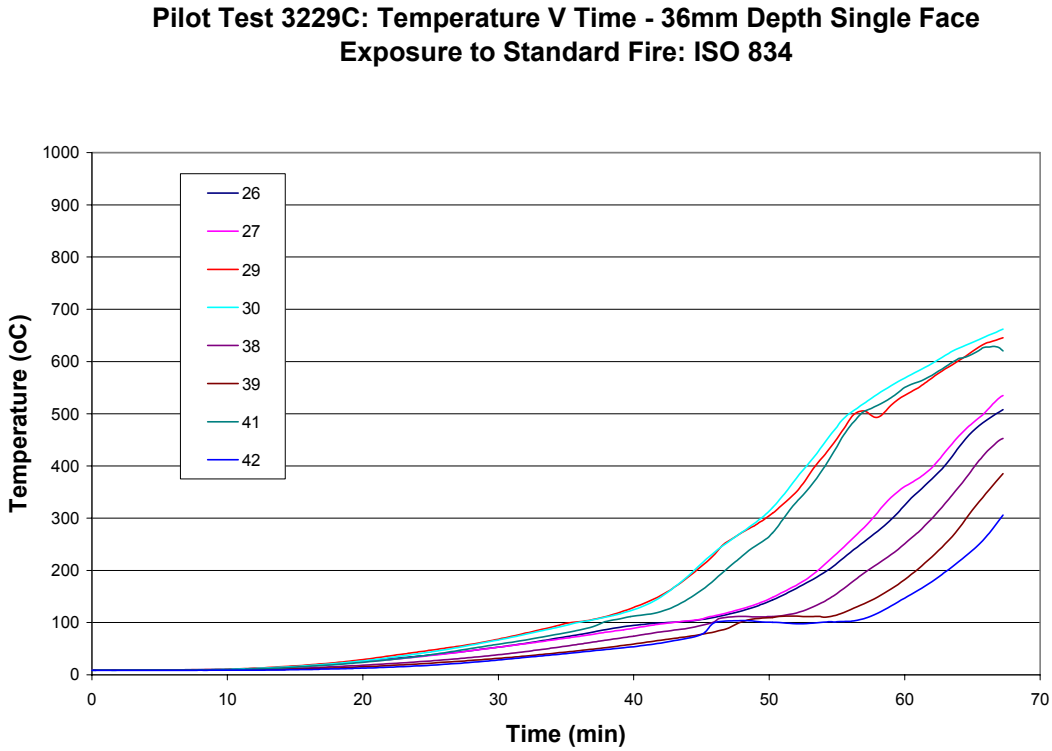

Figure D.11 **Pilot Test 3: Thermocouple Temperature – Time Graphs Single Face Exposure**

Appendix E: LVL Load Test: Beam Calculations

Appendix E1 Modulus of Elasticity Calculations

Modulus of Elasticity Test on Sample

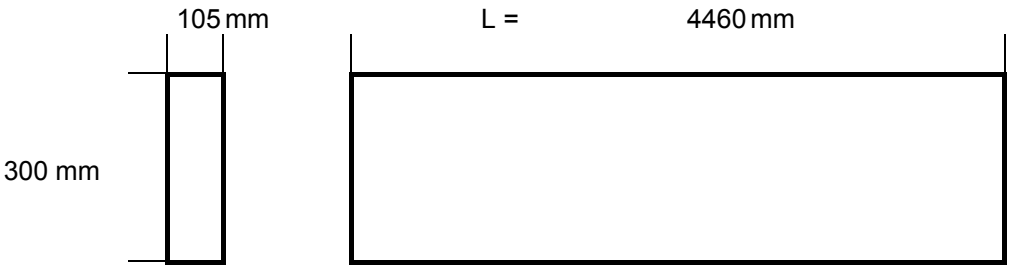

Width	b =		105	mm
Depth	d =		300	mm
	I =		236250000	mm^4
Load cell	P =		7.67	kN
Deflection	Δ =		5.38	mm
now	Δ =	P x L^3/48EI		mm
therefore	**E =**		**11.15**	**GPa**

Appendix E2 LVL beam Properties & Design Calculations

LVL Properties			**Hyspan**	**Truform**	**Truform**	
Section Size			95 x 45	95 x 77	95 x 65	mm
Mean Modulus of Elasticity			13.14	11.44	10.97	GPa
Mean Bending Strength			63.78	57.02	54.68	MPa
			Values taken from:		LVL Properties Evaluation Documents	
Beam Modulus of Elasticity					11.15	GPa
Beam Bending Strength					55.58	MPa
				MOE	Assessed from 'E' Test	
Beam Strength:			**Original:**			
	Width	b	105	mm		
	Depth	d	300	mm		
	Moment of Inertia	I	236250000	mm^4		
	Section Modulus	Z	1575000	mm^3		
Moment Capacity		Mn	**87.54**	KNm		
Loading	Width		1.5	m		
	Gib		9.00	KN/m^3		
	Gib Thick.		26	mm		
	Framing		5.00	KN/m^3		
	Spacing		0.4	mm		
	Framing		0.06	Kpa		
	Gib		0.23	Kpa		
	UDL Assembly		**0.30**	**Kpa**		
Applied Moment						
	Span	L	4400	mm		
	Load	P	30	KN		
Test Point load	Moment	PL/4	33	KNm		
	UDL	w	0.44	KN/m		
UDL Assembly Load	Moment	$wL^2/8$	1.08	KNm		
Total Moment			**34.1**	**KNm**		

Appendix E2 LVL beam Properties & Design Calculations (cont.)

Load Test					**Predicted**	**Measured**	
Pilot Test	Char Rate	β	0.72	0.72	0.72	0.72	mm/min
	Time	t	30	40	**36.6**	44	min
	Char Depth	c	21.6	28.8	26.352	31.68	mm
	Width b_f	b_f	61.8	47.4	52.296	41.64	mm
	Depth d_f	d_f	278.4	271.2	273.648	268.32	mm
	Ixx		111125805	78789102	89302591	67032993	mm^4
	Zxx		798318	581041	652682	499650	mm^3
Corner Rounding	r	βt	22	29	26	32	mm
(r = c)	A	$0.215r^2$	100	178	149	216	mm^2
	y	$0.223r$	5	6	6	7	mm
	Zc	$0.0097r^2$	5	8	7	10	mm^3
	Zr		771348	534952	613567	444781	mm^3
Moment Capacity			**42.9**	**29.7**	**34.1**	**24.7**	**KNm**
	Ic	$0.0075r^4$	1632.6	5159.8	3616.7	7554.4	mm^4
	Ixx_r		107499560	72827263	84175121	60046834	mm^4
Deflection	Δr	$PL^3/48EI_r$	44.4	65.6	56.7	79.5	mm

Appendix F: Notes on the application of White's model.

A time location model expressed as:

$$\mathbf{t = m x_c^{1.23}}$$

$$\mathbf{or \quad \ln t = 1.23 \ln x_c + \ln m}$$

and is based on fire exposure conditions according to ASTM E 119

where: t = time of exposure min
x_c = depth of char layer mm
m = charring rate parameter

$$\ln m = 1.3349\, p - 0.009887\, p\, d + 0.1176\, c - 0.003887\, c\, d + 0.01717\, u - 1.2521$$

and p = density of timber in gm/cm^3 (oven dried)
u = moisture content (%)
d = depth of CCA penetration in mm (transport property)
c = Hardwood or softwood classification
(1 for softwood or -1 for hardwood)

Attempts to measure CCA penetration were unsuccessful, and a figure of 20 mm was assessed for Radiate pine, on the basis of White's report, and CCA treatment information on Radiata pine and other species (FRI, 1988).

By assigning the following values C= 1 and d = 20 an expression for ln m is obtained as follows:

$$\ln m = 1.13716\, p + 0.01717\, u - 1.21224 \quad \text{for Radiata pine.}$$

By substituting the value for m obtained into the expression,

$$\mathbf{t = m x_c^{1.23}}$$

The time taken for the char to reach a specified depth, and hence the mean charring for that period of exposure can be obtained.

For the LVL as tested in this report, the physical parameters were:

Density (oven dried) d = 0.555 gm/cm^3
Moisture Content m = 13.7 %,

ln m was determined using the expression for Radiata pine above:

	ln m	=	1.13716 p + 0.01717 u – 1.21224
therefore	ln m	=	- 0.34589
and then	m	=	exp(-0.34589)
		=	0.707592

Hence for a char depth of 18 mm the mean cumulative charring rate form White's model for the LVL tested is 0.77 mm/min, and for 36 mm char depth 0.68mm/min. Refer table F.1 and Figure F.1 below.

Considering the pilot test results (Refer Fig 6.4.5 single face exposure), for thermocouples at 18 mm and 36 mm the mean results of the cumulative charring rate for each depth was found to be 0.72 and 0.70 mm/min respectively, which compares very well with White's model.

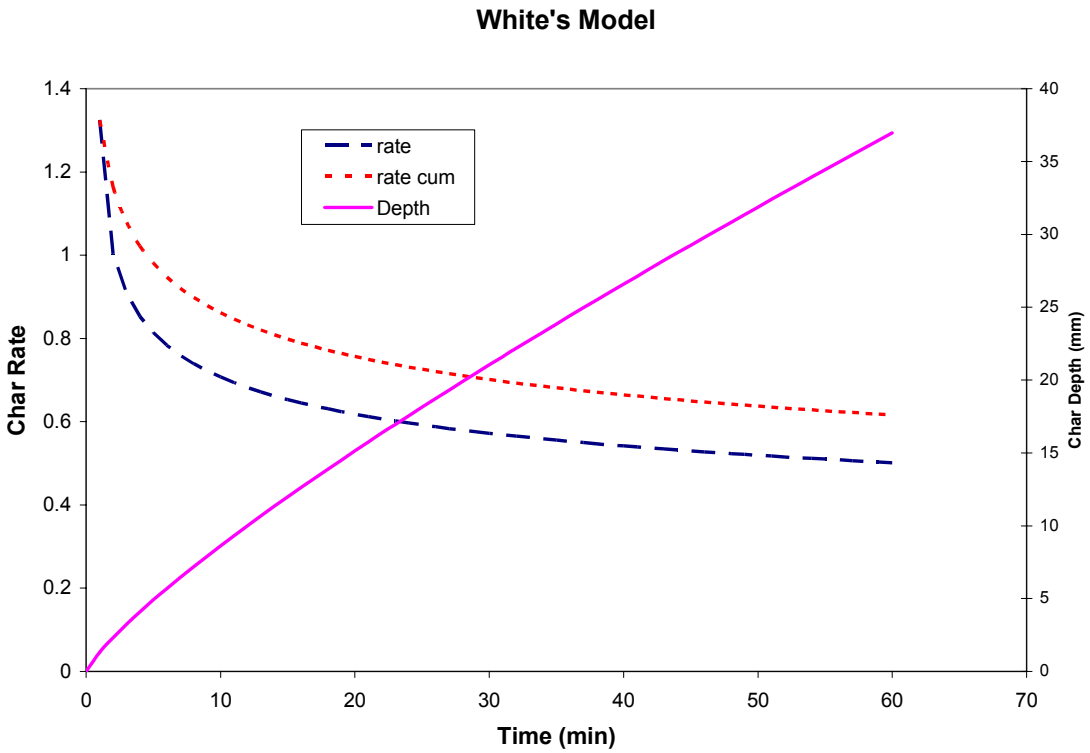

Figure F1 White's Model applied to LVL test parameters.

White's model.

A time location model expressed as: $\mathbf{t = mx_c^{1.23}}$

Time	Depth	rate	rate cum			
0	0.00			Density	555	gm/cm^3
1	1.32	1.3247	1.3247	Moist con	13.7	%
2	2.33	1.0026	1.1637	depth CCA pen	20	
3	3.24	0.9088	1.0787	Hardwood or softwood	1	
4	4.09	0.8527	1.0222			
5	4.90	0.8133	0.9805	ln m	-0.34589	
6	5.69	0.7833	0.9476	m	0.707592	
7	6.44	0.7591	0.9207			
8	7.18	0.7390	0.8980			
9	7.91	0.7219	0.8784			
10	8.61	0.7070	0.8613			
11	9.31	0.6939	0.8460			
12	9.99	0.6822	0.8324			
13	10.66	0.6716	0.8200			
14	11.32	0.6620	0.8087			
15	11.98	0.6532	0.7984			
16	12.62	0.6451	0.7888			
17	13.26	0.6376	0.7799			
18	13.89	0.6307	0.7716	Pilot Test	Comparison	
19	14.51	0.6241	0.7639			
20	15.13	0.6180	0.7566			
21	15.74	0.6123	0.7497			
22	16.35	0.6068	0.7432			
23	16.95	0.6017	0.7370			
24	17.55	0.5968	0.7312			
25	18.14	0.5922	0.7256			
26	18.73	0.5878	0.7203			
27	19.31	0.5836	0.7153			
28	19.89	0.5795	0.7104			
29	20.47	0.5757	0.7058			
30	21.04	0.5720	0.7013			
31	21.61	0.5684	0.6970			
32	22.17	0.5650	0.6929			
33	22.73	0.5617	0.6889			
34	23.29	0.5585	0.6851			
35	23.85	0.5555	0.6814			
36	24.40	0.5525	0.6778	Pilot Test	Comparison	
37	24.95	0.5497	0.6744			
38	25.50	0.5469	0.6710			
39	26.04	0.5442	0.6677			
40	26.58	0.5416	0.6646			

Appendix G: Ignition Tests Samples Photos

Figure G1: Photos of samples, 30 kW/m^2 Heat Flux

Figure G2: Photos of samples, 25 kW/m^2 Heat Flux

Figure G3: Photos of samples, 20 kW/m^2 Heat Flux

Figure G4: Photos of samples, 15 kW/m^2 Heat Flux

Figure G5: Photos of samples, 10 kW/m^2 Heat Flux

Appendix H Zero Strength Zone: Pilot Test Results

Table H1 Pilot Test 3229 Zero Strength Zone: LVL beam 300 x 105 mm

18 mm Double Face	Time (min)							
Thermocouple No:	19	22	31	34				
Time to 100^{O}C	15.05	16.80	10.25	8.95				
Time to 300^{O}C	17.00	22.95	18.80	16.75				
Time Diff. (min)	1.95	6.15	8.55	7.80				
Char Rate (mm/min)	0.94	0.94	0.94	0.94				
Zero Strength (mm)	1.83	5.78	8.04	7.33			**Average**	**5.75**
36 mm Double Face	Time (min)							
Thermocouple No:	25	28	37	40				
Time to 100^{O}C	34.90	31.15	20.80	26.90				
Time to 300^{O}C	43.60	39.85	32.90	36.25				
Time Diff. (min)	8.70	8.70	12.10	9.35				
Char Rate (mm/min)	0.92	0.92	0.92	0.92				
Zero Strength (mm)	8.00	8.00	11.13	8.60			**Average**	**8.94**
18 mm Single Face	Time (min)							
Thermocouple No:	20	21	23	24	32	33	35	36
Time to 100^{O}C	12.25	12.85	15.85	9.15	9.30	13.15	14.00	16.20
Time to 300^{O}C	25.20	24.20	22.05	18.75	20.30	27.25	24.55	27.30
Time Diff. (min)	12.95	11.35	6.20	9.60	11.00	14.10	10.55	11.10
Char Rate (mm/min)	0.72	0.72	0.72	0.72	0.72	0.72	0.72	0.72
Zero Strength (mm)	9.32	8.17	4.46	6.91	7.92	10.15	7.60	7.99
							Average	**7.82**

36 mm Single Face	Time (min)							
Thermocouple No:	26	27	29	30	38	39	41	42
Time to 100^{O}C	45.20	41.20	38.30	40.00	37.15	41.05	31.50	34.80
Time to 300^{O}C	56.05	51.75	48.95	49.20	49.55	57.15	45.05	46.80
Time Diff. (min)	10.85	10.55	10.65	9.20	12.40	16.10	13.55	12.00
Char Rate (mm/min)	0.70	0.70	0.70	0.70	0.70	0.70	0.70	0.70
Zero Strength (mm)	7.60	7.39	7.46	6.44	8.68	11.27	9.49	8.40
							Average	**8.34**

Table H2 **Pilot Test 3229B Zero Strength Zone: LVL beam 300 x 105 mm**

18 mm Double Face	Time (min)							
Thermocouple No:	19	22	31	34				
Time to 100^{O}C	11.90	13.45	10.15	9.45				
Time to 300^{O}C	21.25	20.05	19.50	16.80				
Time Diff. (min)	9.35	6.60	9.35	7.35				
Char Rate (mm/min)	0.94	0.94	0.94	0.94				
Zero Strength (mm)	8.79	6.20	8.79	6.91			**Average**	**7.67**
36 mm Double Face	Time (min)							
Thermocouple No:	25	28	37	40				
Time to 100^{O}C	31.85	26.65	30.25	25.15				
Time to 300^{O}C	38.65	34.20	42.20	35.30				
Time Diff. (min)	6.80	7.55	11.95	10.15				
Char Rate (mm/min)	0.92	0.92	0.92	0.92				
Zero Strength (mm)	6.26	6.95	10.99	9.34			**Average**	**8.38**
18 mm Single Face	Time (min)							
Thermocouple No:	20	21	23	24	32	33	35	36
Time to 100^{O}C	15.25	16.95	18.70	15.50	13.05	13.15	17.80	14.35
Time to 300^{O}C	27.45	24.90	24.65	22.50	23.90	24.85	27.10	23.30
Time Diff. (min)	12.20	7.95	5.95	7.00	10.85	11.70	9.30	8.95
Char Rate (mm/min)	0.72	0.72	0.72	0.72	0.72	0.72	0.72	0.72
Zero Strength (mm)	8.78	5.72	4.28	5.04	7.81	8.42	6.70	6.44
							Average	**6.65**

36 mm Single Face	Time (min)							
Thermocouple No:	26	27	29	30	38	39	41	42
Time to 100^{O}C	42.55	36.75	34.00	38.60	42.15	40.05	30.20	32.20
Time to 300^{O}C	52.80	45.85	42.75	48.00	55.00	49.85	42.00	45.85
Time Diff. (min)	10.25	9.10	8.75	9.40	12.85	9.80	11.80	13.65
Char Rate (mm/min)	0.70	0.70	0.70	0.70	0.70	0.70	0.70	0.70
Zero Strength (mm)	7.18	6.37	6.13	6.58	9.00	6.86	8.26	9.56
							Average	**7.49**

Table H3 **Pilot Test 3229C Zero Strength Zone: LVL beam 360 x 133 mm**

18 mm Double Face	Time (min)							
Thermocouple No:	19	22	31	34				
Time to 100^{O}C	11.25	15.75	6.40	11.95				
Time to 300^{O}C	18.75	23.75	15.50	22.55				
Time Diff. (min)	7.50	8.00	9.10	10.60				
Char Rate (mm/min)	0.94	0.94	0.94	0.94				
Zero Strength (mm)	7.05	7.52	8.55	9.96			**Average**	**8.27**
36 mm Double Face	Time (min)							
Thermocouple No:	25	28	37	40				
Time to 100^{O}C	30.25	32.35	30.25	25.50				
Time to 300^{O}C	45.20	44.80	46.25	39.00				
Time Diff. (min)	14.95	12.45	16.00	13.50				
Char Rate (mm/min)	0.92	0.92	0.92	0.92				
Zero Strength (mm)	13.75	11.45	14.72	12.42			**Average**	**13.09**
18 mm Single Face	Time (min)							
Thermocouple No:	20	21	23	24	32	33	35	36
Time to 100^{O}C	19.40	13.00	17.30	12.65	11.95	18.70	15.45	17.40
Time to 300^{O}C	33.50	27.25	28.10	21.40	26.40	33.10	26.55	28.80
Time Diff. (min)	14.10	14.25	10.80	8.75	14.45	14.40	11.10	11.40
Char Rate (mm/min)	0.72	0.72	0.72	0.72	0.72	0.72	0.72	0.72
Zero Strength (mm)	10.15	10.26	7.78	6.30	10.40	10.37	7.99	8.21
							Average	**8.93**

36 mm Single Face	Time (min)							
Thermocouple No:	26	27	29	30	38	39	41	42
Time to 100^{O}C	42.35	42.80	35.35	35.85	45.80	47.80	37.70	45.95
Time to 300^{O}C	59.10	57.65	49.75	49.40	62.25	64.55	51.10	67.10
Time Diff. (min)	16.75	14.85	14.40	13.55	16.45	16.75	13.40	21.15
Char Rate (mm/min)	0.70	0.70	0.70	0.70	0.70	0.70	0.70	0.70
Zero Strength (mm)	11.73	10.40	10.08	9.49	11.52	11.73	9.38	14.81
							Average	**11.14**